NASA/TP—2017–219406

Curved Displacement Transfer Functions for Geometric Nonlinear Large Deformation Structure Shape Predictions

William L. Ko, and Van Tran Fleischer
Armstrong Flight Research Center, Edwards, California

Shun-Fat Lung
Jacobs Technology, Edwards, California

TECHNOLOGY PROTECTION NOTICE

NASA is currently seeking patent protection on the methods described in this NASA technical publication. Therefore, those interested in using the methods should contact the NASA Technology Transfer Office, NASA Armstrong Flight Research Center, Edwards, California for more information.

March 2017

NASA STI Program ... in Profile

Since its founding, NASA has been dedicated to the advancement of aeronautics and space science. The NASA scientific and technical information (STI) program plays a key part in helping NASA maintain this important role.

The NASA STI program operates under the auspices of the Agency Chief Information Officer. It collects, organizes, provides for archiving, and disseminates NASA's STI. The NASA STI program provides access to the NASA Aeronautics and Space Database and its public interface, the NASA Technical Reports Server, thus providing one of the largest collections of aeronautical and space science STI in the world. Results are published in both non-NASA channels and by NASA in the NASA STI Report Series, which includes the following report types:

- TECHNICAL PUBLICATION. Reports of completed research or a major significant phase of research that present the results of NASA Programs and include extensive data or theoretical analysis. Includes compilations of significant scientific and technical data and information deemed to be of continuing reference value. NASA counter-part of peer-reviewed formal professional papers but has less stringent limitations on manuscript length and extent of graphic presentations.

- TECHNICAL MEMORANDUM. Scientific and technical findings that are preliminary or of specialized interest, e.g., quick release reports, working papers, and bibliographies that contain minimal annotation. Does not contain extensive analysis.

- CONTRACTOR REPORT. Scientific and technical findings by NASA-sponsored contractors and grantees.

- CONFERENCE PUBLICATION. Collected papers from scientific and technical conferences, symposia, seminars, or other meetings sponsored or co-sponsored by NASA.

- SPECIAL PUBLICATION. Scientific, technical, or historical information from NASA programs, projects, and missions, often concerned with subjects having substantial public interest.

- TECHNICAL TRANSLATION. English-language translations of foreign scientific and technical material pertinent to NASA's mission.

Specialized services also include organizing and publishing research results, distributing specialized research announcements and feeds, providing information desk and personal search support, and enabling data exchange services.

For more information about the NASA STI program, see the following:

- Access the NASA STI program home page at http://www.sti.nasa.gov

- E-mail your question to help@sti.nasa.gov

- Fax your question to the NASA STI Information Desk at 757-864-6500

- Phone the NASA STI Information Desk at 757-864-9658

- Write to:
  NASA STI Program
  Mail Stop 148
  NASA Langley Research Center
  Hampton, VA 23681-2199

NASA/TP—2017–219406

Curved Displacement Transfer Functions for Geometric Nonlinear Large Deformation Structure Shape Predictions

William L. Ko, and Van Tran Fleischer
Armstrong Flight Research Center, Edwards, California

Shun-Fat Lung
Jacobs Technology, Edwards, California

National Aeronautics and
Space Administration

Armstrong Flight Research Center
Edwards, CA 93523-0273

March 2017

Available from:

NASA STI Program
Service Mail Stop 148
NASA Langley Research Center
Hampton, VA 23681-2199

National Technical Information
5285 Port Royal Road
Springfield, VA 22161
703-605-6000

This report is also available in electronic form at http://www.sti.nasa.gov/ and http://ntrs.nasa.gov/

TABLE OF CONTENTS

ABSTRACT

For shape predictions of structures under large geometrically nonlinear deformations, Curved Displacement Transfer Functions were formulated based on a curved displacement, traced by a material point from the undeformed position to deformed position. The embedded beam (depth-wise cross section of a structure along a surface strain-sensing line) was discretized into multiple small domains, with domain junctures matching the strain-sensing stations. Thus, the surface strain distribution could be described with a piecewise linear or a piecewise nonlinear function. The discretization approach enabled piecewise integrations of the embedded-beam curvature equations to yield the Curved Displacement Transfer Functions, expressed in terms of embedded beam geometrical parameters and surface strains. By entering the surface strain data into the Displacement Transfer Functions, deflections along each embedded beam can be calculated at multiple points for mapping the overall structural deformed shapes. Finite-element linear and nonlinear analyses of a tapered cantilever tubular beam were performed to generate linear and nonlinear surface strains and the associated deflections to be used for validation. The shape prediction accuracies were then determined by comparing the theoretical deflections with the finite-element-generated deflections. The results show that the newly developed Curved Displacement Transfer Functions are very accurate for shape predictions of structures under large geometrically nonlinear deformations.

NOMENCLATURE

c	depth factor (vertical distance from neutral axis to bottom surface of uniform embedded beam), in
$c(s)$	$= c(x)$, depth factor, vertical distance from neutral axis to bottom surface of in-extensional ($s = x$) nonuniform embedded beam, in
c_i	$= c(x_i)$, depth factor at $x = x_i$, in
$\overline{c}_i$	$= h_i - c_i$, depth factor at $x = x_i$ for upper surface, in
c_j	$= c(x_j)$, depth factor at $x = x_j$, in
c_0	value of c_i at embedded beam root $x = x_0 = 0$, in
c_n	value of c_i at embedded beam tip $x = x_n = l$, in
d	math symbol—differential
E	Young's modulus, lb/in^2
h_i	embedded beam depth at $x = x_i$, in
h_0	value of h_i at embedded beam root $x = x_0 = 0$, in
h_n	value of h_i at embedded beam tip $x = x_n = l$, in
l	length of embedded beam, in
n	index for the last span-wise strain-sensing station (or number of domains)
P	applied load, lb
$R(s)$	radius of curvature, in
s	curved axial coordinate along elastic curve of deformed embedded beam, in
x, y	Cartesian coordinates (x in beam axial direction y in lateral direction), in
s_i	deformed curved axial coordinate of strain-sensing station at $s_i (= x_i)$, in
t	tubular beam wall thickness, in
u_i	magnitude of displacement along x-axis of deformed material point at s_i, in
x_i	x coordinate of the i-th strain-sensing station

y_i straight deflection at axial location $x = x_i$, in

$(y_i)_{NL}$ value of y_i calculated from Nastran linear analysis, in

$\hat{y}(x)$ curved deflection (curved distance traced by a material point from its initial un-deformed position to its final deformed position), in

$\hat{y}_i$ $\equiv \hat{y}(x_i) = \hat{y}(s_i)$, curved deflection at axial location $x = x_i$, in

$(\hat{y}_i)_{NN}$ value of $\hat{y}_i$ calculated from Nastran nonlinear analysis, in

y_n beam-tip $(i = n)$ vertical deflection, in

$\hat{y}_n$ beam-tip $(i = n)$ curved deflection, in

Δl $\equiv (x_i - x_{i-1}) = (s_i - s_{i-1}) = l/n$, domain length (strain-sensing stations separation distance), in

$\varepsilon(s)$ surface strain at curved axial location *s*, in/in

$\varepsilon(x)$ surface strain at *x*-location, in

ε_i lower surface strain at *i*-th strain-sensing station, in/in

$\overline{\varepsilon}_i$ upper surface strain at *i*-th strain-sensing station, in/in

ε_s axial strain in *s*-direction, in/in

$\theta(s)$ beam slope angle in reference to *s*-system, rad or deg

$\theta(x)$ beam slope in reference to *x*-system, rad or deg

θ_i $\equiv \theta(s_i)\ [= \theta(x_i)]$, slope angle at *i*-th strain-sensing station, rad or deg

θ_0 $\equiv \theta(s_0)\ [= \theta(x_0)]$, slope angle at 0-th (beam root) strain-sensing station, rad or deg

θ_n $\equiv \theta(s_n)\ [= \theta(x_n)]$, slope angle at *n*-th (beam tip) strain-sensing station, rad or deg

$\hat{\theta}_i$ slope angle of a straight line connecting origin and deformed material point s_i on elastic curve of deformed embedded beam, rad or deg

ν Poisson's ratio

ξ $\equiv x - x_{i-1}$, shifted axial coordinate, in

INTRODUCTION

After the Helios prototype with a wing span 247 ft (fig. 1) broke-up in mid-air at an altitude of 2,800 ft under very large wing dihedral deformation with a wing tip deflection reaching 40 ft (fig. 2), there was a need to develop a new technology for monitoring the deformations of highly flexible aircraft for feedback control and flight safety. A new technology has been developed that can convert distributed surface strain data into structure deformed shapes.

Strain sensors can only measure surface strains and not the structure deformed shape. However, after the development of the Ko Displacement Theory (refs. 1–8), a new innovative structure shape prediction technology, called *Method for Real-Time Structure Shape-Sensing* (U.S. Patent Number 7,520,176) (ref. 3), was created. This new technology uses the Displacement Transfer Functions to transform rectilinearly distributed surface strains into out-of-plane deflections for mapping overall structure deformed shapes for visual displays. For applications, the surface strains can be obtained from conventional strain gauges, wireless strain sensors, or fiber optic strain sensors. However, for this technical publication, surface strains were analytically calculated from finite-element analysis to demonstrate and validate the proposed structural deformation prediction methodology.

By entering the surface strain data into the Displacement Transfer Functions, one can calculate slopes and deflections along each strain-sensing line on a given structure such as a wing. By using multiple strain-sensing lines, overall deformed shapes of a structure subjected to bending and torsion loadings can then be obtained. A total of seven sets of Displacement Transfer Functions were formulated in the past for

different structural geometries (refs. 1–9), and were found to be quite accurate in the shape predictions of actual flight vehicles (refs. 10 and 11).

By embodying the Displacement Transfer Functions, the rectilinearly distributed surface strains can also be input into the Stiffness and Load Transfer Functions to calculate structural stiffness (bending and torsion) and operational loads (bending moments, shear loads, and torques) for monitoring the operational loads of a flight-vehicle (ref. 12) in near real-time. The accuracy of this method for estimating operational loads on structures was analytically confirmed by using finite-element analysis of different aerospace structures such as tapered cantilever tubular beams, depth tapered un-swept wing boxes, depth tapered swept wing boxes, and the doubly-tapered Ikhana aircraft wing (ref. 13).

All the earlier Displacement Transfer Functions (refs. 1–9) were formulated based on the Shifted straight deflections perpendicular to the undeformed neutral axis. For the shape predictions of structures under large geometric nonlinear deformations, there was a need to reformulate a new set of Displacement Transfer Functions for structure shape predictions.

This technical publication is based on the actual curved displacement (curved distance traced by a material point from its undeformed position to its deformed position) and formulate the Curved Displacement Transfer Functions for shape predictions of structures under large geometric nonlinear deformations.

A long tapered cantilever tubular beam was chosen to assess the accuracy of the new Curved Displacement Transfer Functions. Linear and nonlinear finite-element analyses were performed on the tapered cantilever tubular beam to 1) analytically generate linear and nonlinear surface strains for use in the Curved Displacement Transfer Functions and 2) analytically generate beam deflections (benchmarks) for comparisons with theoretically predicted beam deflections. The Curved Displacement Transfer Functions were then programmed using the finite-element-generated surface strains as input data to calculate theoretical deflections. The shape prediction accuracies were then determined by comparing the theoretical deflections with the finite-element-generated deflections (benchmarks). The results show that the Curved Displacement Transfer Functions, just like the Shifted Displacement Transfer Functions (refs 1-9) are very accurate for shape predictions of structures under both linear and large geometric nonlinear deformations (beam-tip deflection reaching 58 percent of span).

REVIEW OF TECHNICAL BACKGROUND

To formulate the displacement theory (refs. 1–8), strain-sensing stations (strain measurement points) are to be discretely distributed along a strain-sensing line on the surface of the structure (for example, aircraft wing) (fig. 3). The depth-wise cross section of the structure along the strain-sensing line is called an imaginary “embedded beam” (not to be confused with the classical isolated Euler-Bernoulli beam). Each embedded beam was then discretized into multiple domains (strain-sensing station separation distances) with domain junctures matching the locations of the strain-sensing stations. By discretization, the variation of the embedded beam depth factor can be described with a piecewise linear function, and the surface strain variation can be described with either a piecewise linear or a piecewise nonlinear function. This approach enables the integration of the curvature equation of the deformed embedded beam to yield slope and deflection equations in recursive forms. The recursive slope and deflection equations are then combined into a single deflection equation in dual summation form. A set of three equations (recursive slope equation, recursive deflection equation, and dual-summation deflection equation) are called Displacement Transfer Functions, which are expressed in terms of the embedded beam geometrical parameters and surface strains, and contain no material properties. By entering surface strain data into the Displacement Transfer Functions, one can calculate slopes and deflections along the embedded beam. By using multiple strain-sensing lines, deflections at multiple strain-sensing stations can then be calculated for plotting the overall deformed shapes of the structure subjected to bending and torsion loads. The Displacement Transfer Functions are purely geometric in nature, and therefore, for a given density of strain-sensing stations, one can accurately compute the associated deflections, whether the input surface strains come from linear or nonlinear deformations.

BASIC EQUATIONS FOR THE DISPLACEMENT THEORY

The following first section is to geometrically establish the basic curvature-strain equation, from which different Displacement Transfer Functions can be formulated. The second section discusses different curvature-strain differential equations.

Curvature-Strain Relationship

Figure 4 shows the deformed state of an embedded beam with a changing depth factor, $c(s)$, where s is the curved coordinate along the elastic curve of the deformed embedded beam. The curvature-strain relationship can be established graphically from figure 4. The embedded beam elastic curve has a local radius of curvature, $R(s)$, within a small beam segment subtended by $d\theta$. The undeformed curve length, AB, lies on the beam neutral axis, and the deformed curve length, $A'B'$ $\{= AB\,[1+\varepsilon(s)]\}$, where $\varepsilon(s)$ is the surface strain, lies on the beam lower surface. From the two similar slender sectors, $O'AB$ and $O'A'B'$, one obtains the geometrical relationship described with equation (1):

$$\frac{O'A'}{O'A} = 1 + \frac{c(s)}{R(s)} = \frac{A'B'}{AB} = 1 + \varepsilon(s) \tag{1}$$

From equation (1), one obtains the curvature-strain equation (2):

$$\frac{1}{R(s)} = \frac{\varepsilon(s)}{c(s)} \tag{2}$$

Equation (2) geometrically relates the local curvature, $1/R(s)$, to the associated surface strain, $\varepsilon(s)$, and the depth factor, $c(s)$, of the embedded beam. Equation (2) is the basis for formulating Displacement Transfer Functions.

Traditional Curvature Equations for Vertical Deflections

Different forms of curvature-strain differential equations written in the x-y system have the following familiar forms as shown in equations (3) through (5) (for detailed discussions, see refs. 14 and 15). The mathematical differences between those equations are discussed.

1. Eularian Curvature Equation

$$\frac{1}{R(x)} = \frac{d^2y/dx^2}{[1+(dy/dx)^2]^{3/2}} = \frac{\varepsilon(x)}{c(x)} \tag{3}$$

It is important to mention that equation (3) is referenced to the deformed (movable) *x*-coordinate (that is, x-coordinate gives only the deformed location of a material point, but not the undeformed location).

2. Lagrangian Curvature Equation

$$\frac{1}{R(x)} = \frac{d^2y/dx^2}{\sqrt{1-(dy/dx)^2}} = \frac{\varepsilon(x)}{c(x)} \tag{4}$$

Equation (4) is in reference to the undeformed (fixed) *x*-coordinate (derivation in Appendix A, ref. 15).

Because of the nonlinear term, $(dy/dx)^2$, direct integrations of equations (3) and (4) can end up in extremely complex deflection equations, which have poor prediction accuracies at large deformations (details in ref. 15).

3. Shifted Curvature Equation

If the deformed material points are shifted back to their respective undeformed *x*-positions [that is, by setting axial displacement *u* to zero $(u \to 0)$] (fig. 5), the shifting condition $(u \to 0)$ will cause the nonlinear term, $(dy/dx)^2$, to become zero (Appendix A, ref. 15). Hence equation (4) becomes equation (5):

$$\frac{d^2y}{dx^2} = \frac{\varepsilon(x)}{c(x)} \tag{5}$$

Equation (5) is in reference to the undeformed *x*-coordinate, is called the shifted curvature-strain differential equation, and is not the traditional linearized form of the Eulerian curvature equation (3) which is in reference to the deformed *x*-coordinate.

Equation (5) is the basic curvature-strain differential equation used in the formulations of the Shifted Displacement Transfer Functions (ref. 15). Detailed discussions of equation (5) are provided in the subsequent Similarity of Shifted and Curved Formulations section.

FORMULATION OF THE SHIFTED DISPLACEMENT TRANSFER FUNCTIONS

The Shifted Displacement Transfer Functions were formulated earlier (refs. 1 and 4) by piecewise integrations of equation (5) for nonuniform embedded beams. The resulting equations are listed below as equations (6a), (6b), and (6c) and equations (7a), (7b), and (7c). As shown, equations (6a), (6b), and (6c) and equations (7a), (7b), and (7c) can degenerate into the limit cases of uniform embedded beams $(c_{i-1} = c_i = c)$. The limit cases were obtained by first expanding the logarithmic function, $\log_e(c_i/c_{i-1})$, in the neighborhood of $(c_i/c_{i-1}) \approx 1$, and then setting, $c_{i-1} = c_i = c$. Equations (6a), (6b), and (6c) and equations (7a), (7b), and (7c) listed below were used in the linear shape prediction analysis portion of the present technical publication.

Shifted Displacement Transfer Functions

The following Shifted Displacement Transfer Functions shown as equations (6a), (6b), and (6c) were formulated by using the piecewise-linear representation of the variation of the depth factor, $c(x)$, and using the piecewise-linear representation of the variation of the surface strain, $\varepsilon(x)$. The detailed mathematical derivations can be found in refs. 1 and 4.

Slope equation:

$$\tan\theta_i = \Delta l\left[\frac{\varepsilon_{i-1}-\varepsilon_i}{c_{i-1}-c_i}+\frac{\varepsilon_{i-1}c_i-\varepsilon_i c_{i-1}}{(c_{i-1}-c_i)^2}\log_e\frac{c_i}{c_{i-1}}\right]+\tan\theta_{i-1}$$
$$\xrightarrow[(c_{i-1}=c_i=c)]{\text{Uniform}}\frac{\Delta l}{2c}(\varepsilon_{i-1}+\varepsilon_i)+\tan\theta_{i-1} \qquad (6a)$$
$$(i=1,2,3,...,n)$$

Vertical deflection equation:

a. In recursive form:

$$y_i = (\Delta l)^2\left[\frac{\varepsilon_{i-1}-\varepsilon_i}{2(c_{i-1}-c_i)}-\frac{\varepsilon_{i-1}c_i-\varepsilon_i c_{i-1}}{(c_{i-1}-c_i)^3}\left(c_i\log_e\frac{c_i}{c_{i-1}}+(c_{i-1}-c_i)\right)\right]+y_{i-1}+\Delta l\tan\theta_{i-1}$$
$$\xrightarrow[(c_{i-1}=c_i=c)]{\text{Uniform}}\frac{(\Delta l)^2}{6c}(2\varepsilon_{i-1}+\varepsilon_i)+y_{i-1}+\Delta l\tan\theta_{i-1} \qquad (6b)$$
$$(i=1,2,3,...,n)$$

b. In summation form [equations (6a) and (6b) combined]:

$$y_i = \underbrace{(\Delta l)^2\sum_{j=1}^{i}\left\{\frac{\varepsilon_{j-1}-\varepsilon_j}{2(c_{j-1}-c_j)}-\frac{\varepsilon_{j-1}c_j-\varepsilon_j c_{j-1}}{(c_{j-1}-c_j)^3}\left[c_j\log_e\frac{c_j}{c_{j-1}}+(c_{j-1}-c_j)\right]\right\}}_{\text{Contributions from deflection terms}}$$
$$+\underbrace{(\Delta l)^2\sum_{j=1}^{i-1}\left\{(i-j)\left[\frac{\varepsilon_{j-1}-\varepsilon_j}{c_{j-1}-c_j}+\frac{\varepsilon_{j-1}c_j-\varepsilon_j c_{j-1}}{(c_{j-1}-c_j)^2}\log_e\frac{c_j}{c_{j-1}}\right]\right\}}_{\text{Contributions from slope terms}}+\underbrace{y_0+(i)\Delta l\tan\theta_0}_{=0\text{ for cantilever beams}} \qquad (6c)$$
$$\xrightarrow[(c_{i-1}=c_i=c)]{\text{Uniform}}\underbrace{\frac{(\Delta l)^2}{6c}\sum_{j=1}^{i}(2\varepsilon_{j-1}+\varepsilon_j)}_{\text{Contributions from deflection terms}}+\underbrace{\frac{(\Delta l)^2}{2c}\sum_{j=1}^{i-1}(i-j)(\varepsilon_{j-1}+\varepsilon_j)}_{\text{Contributions from slope terms}}+\underbrace{y_0+(i)\Delta l\tan\theta_0}_{=0\text{ for cantilever beams}}$$
$$(i=1,2,3,...,n)$$

Equations (6a), (6b), and (6c) are called the Shifted Displacement Transfer Functions for nonuniform embedded beams $(c_{i-1}\neq c_i)$, including the limit cases of uniform embedded beams $(c_{i-1}=c_i=c)$ (refs. 1 and 4).

Improved Shifted Displacement Transfer Functions

The following Improved Displacement Transfer Functions shown as equations (7a), (7b), and (7c) were formulated for nonuniform embedded beams by using piecewise-linear representation of the variation of the depth factor, $c(x)$, and using piecewise-nonlinear (quadratic) representation of the variation of the surface strain, $\varepsilon(x)$ (ref. 7).

Slope equation:

$$\tan\theta_i = \frac{\Delta l}{2(c_i - c_{i-1})^3}\left[(2c_i - c_{i-1})(c_i\varepsilon_{i-1} - 2c_{i-1}\varepsilon_i) + c_i c_{i-1}\varepsilon_{i+1}\right]\log_e\frac{c_i}{c_{i-1}}$$
$$-\frac{\Delta l}{4(c_i - c_{i-1})^2}\left[(5c_i - 3c_{i-1})\varepsilon_{i-1} - 2(3c_i - c_{i-1})\varepsilon_i + (c_i + c_{i-1})\varepsilon_{i+1}\right] + \tan\theta_{i-1} \qquad (7a)$$
$$\xrightarrow[(c_{i-1}=c_i=c)]{\text{Uniform}} \frac{\Delta l}{12c}(5\varepsilon_{i-1} + 8\varepsilon_i - \varepsilon_{i+1}) + \tan\theta_{i-1}$$
$$(i = 1,2,3,...,n)$$

Vertical Deflection Equations:

a. In recursive form:

$$y_i = \frac{(\Delta l)^2}{2(c_i - c_{i-1})^4}\left[(2c_i - c_{i-1})(c_i\varepsilon_{i-1} - 2c_{i-1}\varepsilon_i) + c_i c_{i-1}\varepsilon_{i+1}\right]\left[c_i\log_e\frac{c_i}{c_{i-1}} - (c_i - c_{i-1})\right]$$
$$-\frac{(\Delta l)^2}{12(c_i - c_{i-1})^2}\left[(8c_i - 5c_{i-1})\varepsilon_{i-1} - 2(5c_i - 2c_{i-1})\varepsilon_i + (2c_i + c_{i-1})\varepsilon_{i+1}\right] + y_{i-1} + \Delta l\tan\theta_{i-1} \qquad (7b)$$
$$\xrightarrow[(c_{i-1}=c_i=c)]{\text{Uniform}} \frac{(\Delta l)^2}{24c}(7\varepsilon_{i-1} + 6\varepsilon_i - \varepsilon_{i+1}) + y_{i-1} + \Delta l\tan\theta_{i-1}$$
$$(i = 1,2,3,...,n)$$

b. In summation form [equations (7a) and (7b) combined]:

$$y_i = \underbrace{(\Delta l)^2\sum_{j=1}^{i}\left\{\begin{array}{l}\frac{1}{2(c_j - c_{j-1})^4}\left[(2c_j - c_{j-1})(c_j\varepsilon_{j-1} - 2c_{j-1}\varepsilon_j) + c_j c_{j-1}\varepsilon_{j+1}\right]\left[c_j\log_e\frac{c_j}{c_{j-1}} - (c_j - c_{j-1})\right] \\ -\frac{1}{12(c_j - c_{j-1})^2}\left[(8c_j - 5c_{j-1})\varepsilon_{j-1} - 2(5c_j - 2c_{j-1})\varepsilon_j + (2c_j + c_{j-1})\varepsilon_{j+1}\right]\end{array}\right\}}_{\text{Contribution from deflection terms}}$$
$$+\underbrace{(\Delta l)^2\sum_{j=1}^{i-1}(i-j)\left\{\begin{array}{l}\frac{1}{2(c_j - c_{j-1})^3}\left[(2c_j - c_{j-1})(c_j\varepsilon_{j-1} - 2c_{j-1}\varepsilon_j) + c_j c_{j-1}\varepsilon_{j+1}\right]\log_e\frac{c_j}{c_{j-1}} \\ -\frac{1}{4(c_j - c_{j-1})^2}\left[(5c_j - 3c_{j-1})\varepsilon_{j-1} - 2(3c_j - c_{j-1})\varepsilon_j + (c_j + c_{j-1})\varepsilon_{j+1}\right]\end{array}\right\}}_{\text{Contributions from slope terms}} \qquad (7c)$$
$$+\underbrace{y_0 + i(\Delta l)\tan\theta_0}_{=0\text{ for cantilever beams}}$$
$$\xrightarrow[(c_{i-1}=c_i=c)]{\text{Uniform}} \underbrace{\frac{(\Delta l)^2}{24c}\sum_{j=1}^{i}(7\varepsilon_{j-1} + 6\varepsilon_j - \varepsilon_{j+1})}_{\text{Contributions from deflection terms}} + \underbrace{\frac{(\Delta l)^2}{12c}\sum_{j=1}^{i-1}(i-j)(5\varepsilon_{j-1} + 8\varepsilon_j - \varepsilon_{j+1})}_{\text{Contributions from slope terms}} + \underbrace{y_0 + (i)\Delta l\tan\theta_0}_{=0\text{ for cantilever beams}}$$
$$(i = 1,2,3,...,n)$$

Equations (7a), (7b), and (7c) are called the Improved Shifted Displacement Transfer Functions for nonuniform embedded beams $(c_{i-1} \neq c_i)$, including the limit cases of uniform embedded beams $(c_{i-1} = c_i = c)$ (ref. 7).

FORMULATION OF CURVED DISPLACEMENT TRANSFER FUNCTIONS

The following sections present mathematical processes needed for the formulation of the new Curved Displacement Transfer Functions. The formulation is based on curved deflections instead of traditional vertical deflections.

Curved Curvature Equations

For large bending deformations of beams (fig. 5), one must understand that the actual (true) deflection, $\hat{y}$, of a material point is a curved distance traced by the same material point from its initial undeformed position to its final deformed position. Thus, the conventional deflection, y, is merely the vertical component of the curved deflection, $\hat{y}$. Also see discussions about large deformations in refs. 16 and 17.

The basic curvature equation referenced to the curvilinear s - $\hat{y}$ system, instead of traditional Cartesian x - y system, can be expressed as equation (8):

$$\frac{1}{R(s)} = \frac{d\theta(s)}{ds} = \frac{d}{ds}\left(\frac{d\hat{y}}{ds}\right) = \frac{d^2\hat{y}}{ds^2} \quad ; \quad \theta(s) = \frac{d\hat{y}}{ds} \tag{8}$$

Equating equations (2) and (8) gives the curvature-strain differential equation (9) in the s - $\hat{y}$ system for large deformations:

$$\frac{d^2\hat{y}}{ds^2} = \frac{\varepsilon(s)}{c(s)} \tag{9}$$

Equation (9) is a purely geometrical relationship, containing no material properties. Assuming the length of neutral axis of the embedded beam remains the same (that is, $s = x$) after bending, equation (9) can be rewritten in reference to the undeformed *x*-system as equation (10):

$$\frac{d^2\hat{y}}{dx^2} = \frac{\varepsilon(x)}{c(x)} \tag{10}$$

The mathematical process for formulating the Curved Displacement Transfer Function is through the piecewise integration of equation (10) and is described as follows.

Piecewise Representations

To enable piecewise integrations of equation (10), the depth factor, $c(x)$, and the surface strain, $\varepsilon(x)$, can be expressed by either piecewise linear or piecewise nonlinear functions, described as follows (fig. 3) (refs. 1–8).

1. Depth factors

The variations of the embedded beam depth factor, $c(x)$, within each small domain, $x_{i-1} \le x \le x_i$ $(i = 1,2,3,...,n)$, can be expressed with the linear function given by equation (11):

$$c(x) = c_{i-1} + (c_i - c_{i-1})\frac{x - x_{i-1}}{\Delta l} \quad ; \quad (x_{i-1} \le x \le x_i) \tag{11}$$

2. Surface Strains

The variation of the surface bending strain, $\varepsilon(x)$, within each small domain, $x_{i-1} \le x \le x_i$, can be expressed by either a linear function given by equation (12) (ref. 4) or by a nonlinear function given by equations (13a) and (13b) (ref. 7):

a. Linear:

$$\varepsilon(x) = \varepsilon_{i-1} + (\varepsilon_i - \varepsilon_{i-1})\frac{x - x_{i-1}}{\Delta l} \quad ; \quad (x_{i-1} \le x \le x_i) \tag{12}$$

b. Nonlinear:

$$\varepsilon(x) = \varepsilon_{i-1} - \frac{3\varepsilon_{i-1} - 4\varepsilon_i + \varepsilon_{i+1}}{2\Delta l}(x - x_{i-1}) + \frac{\varepsilon_{i-1} - 2\varepsilon_i + \varepsilon_{i+1}}{2(\Delta l)^2}(x - x_{i-1})^2 \quad ; \quad (x_{i-1} \le x \le x_i) \tag{13a}$$

$$\varepsilon_{n+1} = \varepsilon_{n-2} - 3\varepsilon_{n-1} + 3\varepsilon_n \quad ; \quad (\text{at } i = n) \tag{13b}$$

Equation (13a) was generated by standard quadratic interpolation of strain values, $\{\varepsilon_{i-1}, \varepsilon_i, \varepsilon_{i+1}\}$, respectively at three equally spaced strain-sensing stations, $\{x_{i-1}, x_i, x_{i+1}\}$, and equation (13b) is the quadratic extrapolation equation to obtain extrapolated strain, ε_{i+1}, beyond the embedded beam tip (p. 33, ref. 7).

Piecewise Integrations

In view of equations (11), (13a), and (13b); the curvature-strain differential equation (10) can be piecewise integrated to yield the Curved Displacement Transfer Functions. The piecewise integration of equation (10) within the domain, $x_{i-1} \le x \le x_i$, between the two adjacent strain-sensing stations, $\{x_{i-1}, x_i\}$, yields the slope-angle equation (14):

$$\int_{x_{i-1}}^{x} \underbrace{\frac{d^2\hat{y}}{dx^2}}_{\text{Eq. (5)}} dx = \underbrace{\frac{d\hat{y}}{dx}}_{\theta(x)} - \underbrace{\left(\frac{d\hat{y}}{dx}\right)_{i-1}}_{\theta_{i-1}} = \int_{x_{i-1}}^{x} \frac{\underbrace{\varepsilon(x)}_{\text{Eq. (5)}}}{c(x)} dx \quad ; \quad (x_{i-1} \le x \le x_i) \tag{14}$$

which can be rewritten in the form of equation (15):

$$\theta(x) = \underbrace{\int_{x_{i-1}}^{x} \frac{\varepsilon(x)}{c(x)}\,dx}_{\text{Slope increment}} + \underbrace{\theta_{i-1}}_{\substack{\text{Slope}\\ \text{at } x_{i-1}}} \quad ; \quad (x_{i-1} \le x \le x_i) \tag{15}$$

Integration of the slope angle equation (14) yields the curved deflection equation (16):

$$\int_{x_{i-1}}^{x} \left[\underbrace{\frac{d\hat{y}}{dx}}_{\theta(x)} - \underbrace{\left(\frac{d\hat{y}}{dx}\right)_{i-1}}_{\theta_{i-1}} \right] dx = \hat{y}(x) - \underbrace{\hat{y}_{i-1}}_{\substack{\text{Deflection}\\ \text{at } x_{i-1}}} - \underbrace{\int_{x_{i-1}}^{x} \theta_{i-1}\,dx}_{\substack{\text{Deflection at } x\\ \text{due to } \theta_{i-1}}} = \underbrace{\int_{x_{i-1}}^{x} \int_{x_{i-1}}^{x} \frac{\varepsilon(x)}{c(x)}\,dx\,dx}_{\substack{\text{Right hand side}\\ \text{of equation (12)}}} \tag{16}$$

$$(x_{i-1} \le x \le x_i)$$

In view of equation (15), equation (16) can be rewritten in the form of equation (17):

$$\hat{y}(x) = \underbrace{\int_{x_{i-1}}^{x} \int_{x_{i-1}}^{x} \frac{\varepsilon(x)}{c(x)}\,dx\,dx}_{\text{Deflection increment above } \hat{y}_{i-1}} + \underbrace{(x - x_{i-1})\theta_{i-1}}_{\substack{\text{Deflection at } x\\ \text{due to } \theta_{i-1}}} + \underbrace{\hat{y}_{i-1}}_{\substack{\text{Deflection}\\ \text{at } x_{i-1}}} = \int_{x_{i-1}}^{x} \theta(x)\,dx + \hat{y}_{i-1} \tag{17}$$

$$(x_{i-1} \le x \le x_i)$$

Using piecewise representations of $\{c(x), \varepsilon(x)\}$ given by equations (11), (13a), and (13b); equations (15) and (17) can be integrated within the domain, $x_{i-1} \le x \le x_i$, to yield the slope and deflection equations in closed recursive and summation forms. A set of three equations (recursive slope equation, recursive deflection equation, and summation deflection equation) are called the Curved Displacement Transfer Functions. The mathematical processes are similar to those used in the piecewise integrations of the shifted curvature-strain differential equation (5) to formulate the Shifted Displacement Transfer Functions (refs. 1, 4, and 7). The detailed mathematical derivations of the Curved Displacement Transfer Functions are presented in Appendices A−H.

CURVED DISPLACEMENT TRANSFER FUNCTIONS

After piecewise integrations of equations (15) and (17), and going through a mathematical process similar to the one used in formulating the Shifted Displacement Transfer Functions (refs. 1, 4, and 7), one can obtain the Curved Displacement Transfer Functions shown as equations (18a), (18b), (18c), (19a), (19b), and (19c) for nonuniform embedded beams, including the limit cases of uniform embedded beams, $(c_{i-1} = c_i = c)$.

Curved Displacement Transfer Functions

The Curved Displacement Transfer Functions shown in equations (18a), (18b), and (18c) were formulated by carrying out piecewise integrations of equations (13) and (15) using the piecewise-linear representation of the depth factor $c(x)$ [eq. (11)] variation, and using the piecewise-linear representation of the surface strain $\varepsilon(x)$ [eq. (12)] variation. The detailed mathematical derivations are presented in Appendices A, B, C, and D.

Slope-angle equation (Appendices A and C):

$$\theta_i = \Delta l\left[\frac{\varepsilon_{i-1}-\varepsilon_i}{c_{i-1}-c_i}+\frac{\varepsilon_{i-1}c_i-\varepsilon_i c_{i-1}}{(c_{i-1}-c_i)^2}\log_e\frac{c_i}{c_{i-1}}\right]+\theta_{i-1}$$
$$\xrightarrow[(c_{i-1}=c_i=c)]{\text{Uniform}}\frac{\Delta l}{2c}(\varepsilon_{i-1}+\varepsilon_i)+\theta_{i-1} \qquad (18a)$$
$$(i=1,2,3,...,n)$$

Curved deflection equation:

a. In recursive form (Appendices A and C):

$$\hat{y}_i=(\Delta l)^2\left\{\frac{\varepsilon_{i-1}-\varepsilon_i}{2(c_{i-1}-c_i)}-\frac{\varepsilon_{i-1}c_i-\varepsilon_i c_{i-1}}{(c_{i-1}-c_i)^3}\left[c_i\log_e\frac{c_i}{c_{i-1}}+(c_{i-1}-c_i)\right]\right\}+\hat{y}_{i-1}+(\Delta l)\theta_{i-1}$$
$$\xrightarrow[(c_{i-1}=c_i=c)]{\text{Uniform}}\frac{(\Delta l)^2}{6c}(2\varepsilon_{i-1}+\varepsilon_i)+\hat{y}_{i-1}+(\Delta l)\theta_{i-1} \qquad (18b)$$
$$(i=1,2,3,...,n)$$

b. In summation form [equations (18a) and (18b) combined] (Appendices B and D):

$$\hat{y}_i=\underbrace{(\Delta l)^2\sum_{j=1}^{i}\left\{\frac{\varepsilon_{j-1}-\varepsilon_j}{2(c_{j-1}-c_j)}-\frac{\varepsilon_{j-1}c_j-\varepsilon_j c_{j-1}}{(c_{j-1}-c_j)^3}\left[c_j\log_e\frac{c_j}{c_{j-1}}+(c_{j-1}-c_j)\right]\right\}}_{\text{Contributions from deflection terms}}$$
$$+\underbrace{(\Delta l)^2\sum_{j=1}^{i-1}\left\{(i-j)\left[\frac{\varepsilon_{j-1}-\varepsilon_j}{c_{j-1}-c_j}+\frac{\varepsilon_{j-1}c_j-\varepsilon_j c_{j-1}}{(c_{j-1}-c_j)^2}\log_e\frac{c_j}{c_{j-1}}\right]\right\}}_{\text{Contribution from slope terms}}+\underbrace{\hat{y}_0+(i)(\Delta l)\theta_0}_{=0\text{ for cantilever beams}} \qquad (18c)$$
$$\xrightarrow[(c_{i-1}=c_i=c)]{\text{Uniform}}\underbrace{\frac{(\Delta l)^2}{6c}\sum_{j=1}^{i}(2\varepsilon_{j-1}+\varepsilon_j)}_{\text{Contributions from deflection terms}}+\underbrace{\frac{(\Delta l)^2}{2c}\sum_{j=1}^{i-1}(i-j)(\varepsilon_{j-1}+\varepsilon_j)}_{\text{Contributions from slope terms}}+\underbrace{\hat{y}_0+(i)(\Delta l)\theta_0}_{=0\text{ for cantilever beams}}$$
$$(i=1,2,3,...,n)$$

Equations (18a), (18b), and (18c) are called the Curved Displacement Transfer Functions for nonuniform embedded beams $(c_i \neq c_{i-1})$ (Appendices A and B) under large deformation with geometrical nonlinearity including the limit cases of uniform embedded beams $(c_{i-1}=c_i=c)$ (Appendices C and D).

Improved Curved Displacement Transfer Functions

The Improved Curved Improved Displacement Transfer Functions shown in equations (19a), (19b), and (19c) were formulated by carrying out piecewise integrations of equations (13) and (15) using a piecewise-linear representation of the depth factor $c(x)$ [eq. (9)] variation, and using a piecewise-nonlinear representation of the surface strain $\varepsilon(x)$ [eqs. (11a) and (11b)] variation. The detail mathematical derivations are presented in Appendices E, F, G, and H.

Slope-angle equation (Appendices E and G):

$$\theta_i = \frac{\Delta l}{2(c_i - c_{i-1})^3}\left[(2c_i - c_{i-1})(c_i\varepsilon_{i-1} - 2c_{i-1}\varepsilon_i) + c_i c_{i-1}\varepsilon_{i+1}\right]\log_e\frac{c_i}{c_{i-1}}$$
$$-\frac{\Delta l}{4(c_i - c_{i-1})^2}\left[(5c_i - 3c_{i-1})\varepsilon_{i-1} - 2(3c_i - c_{i-1})\varepsilon_i + (c_i + c_{i-1})\varepsilon_{i+1}\right] + \theta_{i-1} \qquad (19a)$$
$$\xrightarrow[(c_{i-1}=c_i=c)]{\text{Uniform}} \frac{\Delta l}{12c}(5\varepsilon_{i-1} + 8\varepsilon_i - \varepsilon_{i+1}) + \theta_{i-1}$$
$$(i = 1,2,3,...,n)$$

Curved-deflection equations:

a. In recursive form (Appendices E and G):

$$\hat{y}_i = \frac{(\Delta l)^2}{2(c_i - c_{i-1})^4}\left[(2c_i - c_{i-1})(c_i\varepsilon_{i-1} - 2c_{i-1}\varepsilon_i) + c_i c_{i-1}\varepsilon_{i+1}\right]\left[c_i\log_e\frac{c_i}{c_{i-1}} - (c_i - c_{i-1})\right]$$
$$-\frac{(\Delta l)^2}{12(c_i - c_{i-1})^2}\left[(8c_i - 5c_{i-1})\varepsilon_{i-1} - 2(5c_i - 2c_{i-1})\varepsilon_i + (2c_i + c_{i-1})\varepsilon_{i+1}\right] + \hat{y}_{i-1} + \Delta l\theta_{i-1} \qquad (19b)$$
$$\xrightarrow[(c_{i-1}=c_i=c)]{\text{Uniform}} \frac{(\Delta l)^2}{24c}(7\varepsilon_{i-1} + 6\varepsilon_i - \varepsilon_{i+1}) + \hat{y}_{i-1} + (\Delta l)\theta_{i-1}$$
$$(i = 1,2,3,...,n)$$

b. In summation form [equations (19a) and (19b) combined]: (Appendices F and H):

$$\hat{y}_i = \underbrace{(\Delta l)^2\sum_{j=1}^{i}\left\{\begin{array}{l}\frac{1}{2(c_j - c_{j-1})^4}\left[(2c_j - c_{j-1})(c_j\varepsilon_{j-1} - 2c_{j-1}\varepsilon_j) + c_j c_{j-1}\varepsilon_{j+1}\right]\left[c_j\log_e\frac{c_j}{c_{j-1}} - (c_j - c_{j-1})\right] \\ -\frac{1}{12(c_j - c_{j-1})^2}\left[(8c_j - 5c_{j-1})\varepsilon_{j-1} - 2(5c_j - 2c_{j-1})\varepsilon_j + (2c_j + c_{j-1})\varepsilon_{j+1}\right]\end{array}\right\}}_{\text{Contributions from deflection terms}}$$
$$+\underbrace{(\Delta l)^2\sum_{j=1}^{i-1}(i-j)\left\{\begin{array}{l}\frac{1}{2(c_j - c_{j-1})^3}\left[(2c_j - c_{j-1})(c_j\varepsilon_{j-1} - 2c_{j-1}\varepsilon_j) + c_j c_{j-1}\varepsilon_{j+1}\right]\log_e\frac{c_j}{c_{j-1}} \\ -\frac{1}{4(c_j - c_{j-1})^2}\left[(5c_j - 3c_{j-1})\varepsilon_{j-1} - 2(3c_j - c_{j-1})\varepsilon_j + (c_j + c_{j-1})\varepsilon_{j+1}\right]\end{array}\right\}}_{\text{Contributions from slope terms}}$$
$$+\underbrace{\hat{y}_0 + (i)(\Delta l)\theta_0}_{=0 \text{ for cantilever beams}} \qquad (19c)$$
$$\xrightarrow[(c_{i-1}=c_i=c)]{\text{Uniform}} \underbrace{\frac{(\Delta l)^2}{24c}\sum_{j=1}^{i}(7\varepsilon_{j-1} + 6\varepsilon_j - \varepsilon_{j+1})}_{\text{Contributions from deflection terms}} + \underbrace{\frac{(\Delta l)^2}{12c}\sum_{j=1}^{i-1}(i-j)(5\varepsilon_{j-1} + 8\varepsilon_j - \varepsilon_{j+1})}_{\text{Contributions from slope terms}} + \underbrace{\hat{y}_0 + (i)(\Delta l)\theta_0}_{=0 \text{ for cantilever beams}}$$
$$(i = 1,2,3,...,n)$$

Equations (19a), (19b), and (19c) are called the Improved Curved Displacement Transfer Functions for nonuniform embedded beams $(c_i \neq c_{i-1})$ (Appendices E and F), under large deformations with geometrical nonlinearity including the limit cases of uniform embedded beams $(c_{i-1} = c_i = c)$ (Appendices G and H). Equations (18a), (18b), (18c), (19a), (19b), and (19c) listed above were used in the nonlinear shape prediction analysis portion of the present technical publication.

It is important to mention that if $\{\hat{y}_i, \theta_i\}$ in equations (18a), (18b), (18c), (19a), (19b), and (19c) are replaced respectively with $\{y_i, \tan\theta_i\}$, then the Curved Displacement Transfer Functions shown in equations (18a), (18b), (18c), (19a), (19b), and (19c) will become the Shifted Displacement Transfer Functions shown in equations (16a), (16b), (16c), (17a), (17b), and (17c). As will be seen shortly, the vertical (straight) and curved deflections, $\{y_i, \hat{y}_i\}$, calculated respectively from the Shifted and Curved Displacement Transfer Functions turned out to be identical.

CHARACTERISTICS OF DISPLACEMENT TRANSFER FUNCTIONS

In the Shifted and Curved Displacement Transfer Functions, the vertical and curved deflections, $\{y_i, \hat{y}_i\}$, at the strain-sensing station, x_i, are expressed in terms of the inboard depth factors $(c_{0,}, c_1, c_2, ..., c_i)$ and the associated inboard surface strains $(\varepsilon_{0,}, \varepsilon_1, \varepsilon_2, ..., \varepsilon_i)$ [for eqs. (6a), (6b) (6,c); eqs. (18a), (18b) (18c)] or $(\varepsilon_0, \varepsilon_1, \varepsilon_2, ..., \varepsilon_{i+1})$ [for eqs. (7a), (7b), (7c); eqs. (19a), (19b), (19c)], including the values of $\{c_i, \varepsilon_i\}$ at the strain-sensing station, x_i, where deflections, $\{y_i, \hat{y}_i\}$, are calculated.

It is important to mention that equations (6a), (6b), (6c), (7a), (7b), (7c), (18a), (18b), (18c), (19a), (19b), and (19c) are purely geometrical relationships, containing no material properties. However, it must be understood that the surface strains, ε_i, implicitly contain the effect of material properties and internal structural configurations. Thus, in using equations (6a), (6b), (6c), (7a), (7b), (7c), (18a), (18b), (18c), (19a), (19b), and (19c) for shape predictions of complex structures such as aircraft wings, there is no need to know the material properties, nor the complex geometries of the internal structures.

STRUCTURE USED FOR SHAPE PREDICTION ANALYSES

The structure chosen for shape prediction analysis is a long tapered cantilever tubular beam with dimensions and material properties listed in table 1.

Table 1. Dimensions and material properties of a tapered cantilever tubular beam.

		Beam root dimensions		Beam tip dimensions		Material properties (for Nastran analysis)	
l, in	t, in	h_0, in	c_0, in	h_n, in	c_n, in	E, lb/in^2	ν
300	0.02296	8	4	2	1	10.5×10^6	0.3

Figure 3 shows a span-wise vertical cross-section (embedded beam) of the tapered cantilever tubular beam with strain-sensing lines located on both lower and upper surfaces. The embedded beam is discretized into n = 20 equal domains with domain length of $\Delta l = l/n =$ (300 in.)/20 = 15 in. Thus, there are n +1=21 equally spaced strain-sensing stations along each strain-sensing line. Different lateral loads P ={50, 100, 200, 300, 400, 500, 600}lb were applied at the beam tip to study the effect of geometric nonlinearity on the shape predictions under increasing loads (deformations). For the tubular beam, the

local depth factors, c_i $(i = 1,2,3,...,n)$, are the local outer radius of the tubular beam, and are known. As will be shown in the finite-element analyses, for the linear cases, the depth factors, c_i, remain unchanged because, the magnitudes of the pairs of lower and upper surface strains are identical regardless of the load level. Therefore, only the lower surface strains are needed for inputs to the Displacement Transfer Functions for shape calculations.

However, for large geometric nonlinear deformations (for example, the Helios flying wing shown in figure 1), the lower and the upper strain-sensing lines are needed because the magnitudes between the lower and upper surface strains will be slightly different due to the axial strain components induced by the curved-beam effect at large bending. Thus, both lower and upper surface strains are needed to calculate the deformation-dependent depth factors, c_i, which together with associated lower surface strains, ε_i, can then be input to the Displacement Transfer Functions for shape calculations.

FINITE-ELEMENT ANALYSES

The MSC/Nastran (MSC Software Corporation, Newport Beach, California) finite-element program (ref. 18) was used for both linear and nonlinear analyses of the tapered cantilever tubular beam subjected to different beam-tip loads. In this technical publication, the surface strains needed for input to the Displacement Transfer Functions for shape predictions were Nastran-generated and not experimentally measured. Also, the Nastran-generated deflections were used as reference benchmarks to study the shape prediction accuracies of the Displacement Transfer Functions.

Figures 6a and 6b show two types of finite-element models generated for the tapered cantilever tubular beam using shell elements (fig. 6a) and using beam elements (fig. 6b). When modeling the tubular beam with the shell elements, the nonlinear analysis could be carried out only up to certain low level nonlinear deformations, beyond which the nonlinear analysis would break down. Namely, the shell element stiffness would become ill conditioned (that is, mathematical singularity) due to a very large ratio between bending and membrane stiffness in a large displacement situation. When the beam elements were used, the nonlinear analysis could be carried out up to very large deformations without encountering the above-mentioned mathematical singularity.

Nastran Linear Analysis

The Nastran linear analysis (using a linear strain tensor) assumes a linear relationship between the load applied to a structure and the response of the structure. In using linear theory for large deformation analysis, the deflection of the structure is simply proportional to the apply load.

In the linear analysis, the Nastran displacement outputs provide vertical deflections, y, but zero axial x-displacements $(u = 0)$ (fig. 6a). The zero axial displacement implies the horizontal (x-direction) shifting of the vertical deflections to their respective undeformed x-positions. Therefore, the vertical deflections generated by the Nastran linear analysis can be compared with the vertical deflections calculated from the Shifted Displacement Transfer Functions using the Nastran-generated linear surface strains.

Nastran Nonlinear Analysis

In the geometric nonlinear large deflection problem (strain tensors contain second order terms) the stiffness of the structure depends on the displacement, and thus the deflection response is no longer a linear function of the load applied (refs. 18 and 19). For nonlinear analysis, both x- and y-displacements, $\{u, y\}$, are nonzero along the neutral axis (fig. 6b and fig.5). In the large deformations, the load is no longer vertical; it has followed the structure to its deformed state (fig. 6b). In the Nastran nonlinear analysis, the Follower Force Option command was used to force the applied load to be normal

to the deformed neutral axis without introducing an axial load component (fig.6b). For comparisons with the curved deflections, $\widehat{y}$, predicted from the Curved Displacement Transfer functions, the Nastran-displacement data of $\{u, y\}$ were used to generate the equivalent curved deflections, $\widehat{y}$, by using the deflection-conversion equations described in the following section.

STRAIGHT-TO-CURVED DEFLECTION CONVERSION

As previously mentioned, the Nastran linear analysis provided only vertical displacements, y, but zero axial displacements, $(u = 0)$, along the neutral axis (fig. 6a). However, in the Nastran nonlinear analysis, the Nastran outputs gave both vertical displacements, y, and axial displacements, $u(\neq 0)$, along the neutral axis (fig. 6b). To compare with the curved deflections, $\widehat{y}$, calculated from the Curved Displacement Transfer functions, the Nastran nonlinear displacement data of $\{u, y\}$ were used to generate Nastran versions of curved deflections, $\widehat{y}$.

Figure 7 shows the elastic curve of the deformed embedded beam. In figure 7, $\widehat{\theta}\{= \tan^{-1}[y_i/(x_i - u_i)]\}_i$ is the slope angle of a slanted straight line connecting the origin and deformed point, s_i, on the embedded beam elastic curve, and u_i is the magnitude of the axial displacement of deformed material point, s_i, along the undeformed x-axis. In figure 7, if the curved deflection, $\widehat{y}$, is considered as a circular arc, then $\widehat{\theta}_i$ will be an angle subtended by the arc length, $\widehat{y}$, which can then be related to the vertical deflection, y_i, through the following deflection-conversion equation (20) (fig. 7).

$$\widehat{y}_i \approx x_i \widehat{\theta}_i = x_i \underbrace{\left[\tan^{-1}\left(\frac{y_i}{x_i - u_i} \right) \right]}_{\widehat{\theta}_i} \tag{20}$$

Equation (20) was used to convert Nastran displacement data of $\{u_i, y_i\}$ into Nastran versions of curved deflections, $\widehat{y}_i$, for comparison with theoretically predicted curved deflections, $\widehat{y}_i$, from the Curved Displacement Transfer functions.

CURVED-BEAM EFFECT IN NONLINEAR DEFORMATIONS

In the Nastran linear finite-element analysis of the tapered cantilever tubular beam, the Nastran strain outputs showed that the magnitudes of the lower and upper bending strains at the same cross section are always identical regardless of loading levels. The equal magnitudes of the lower and upper bending strains implies that the neutral axis is always located at the half depth of the embedded beam, and no axial strains are induced under linear bending.

However, in the Nastran nonlinear analysis, the Nastran strain outputs show that the magnitudes of the lower and upper surface strains at the same cross section are not exactly the same under large bending. The magnitudes of the lower surface strains are slightly larger than the magnitudes of the associated upper surface strains especially in the outboard flexible region. The magnitude difference of the lower and upper surface strains could be attributed to a slight shifting of the neutral axis toward the bent concave side of the embedded beam due to curved-beam effect.

Before using the Displacement Transfer Functions, the correct depth factor and surface strains must be used. The following two methods: 1) Neutral-axis shifting method or 2) Axial-strain elimination method can be used to calculate the correct depth factor or correct surface bending strains for use in the Displacement Transfer Functions.

Neutral-Axis-Shifting Method

As shown in figure 8, if the difference between the lower and upper surface strains magnitudes is due to neutral axis shifting, then one can use pairs of the lower and upper strains, $\{\varepsilon_i, \overline{\varepsilon}_i\}$, to calculate the unknown lower depth factors, c_i (or upper depth factor $\overline{c}_i$) $(i = 1,2,3,...,n)$, from the depth-factor equation (21):

$$c_i = \frac{-\overline{\varepsilon}_i}{\varepsilon_i - \overline{\varepsilon}_i} h_i \quad ; \quad \overline{c}_i = h_i - c_i \quad ; \quad (i = 1,2,3,...,n) \tag{21}$$

in which h_i $(i = 1,2,3,...,n)$ is the depth of the embedded beam at $x = x_i$. For the current linearly tapered embedded beam (fig. 3), the depth, h_i, can be calculated from the following depth equation (22):

$$h_i = h_0 - \frac{x_i}{l}(h_0 - h_n) \quad ; \quad (i = 1,2,3,...,n) \tag{22}$$

in which $\{h_0, h_n\}$ are respectively the depths of the embedded beam at the embedded beam root $(x = x_0 = 0)$ and at the embedded beam tip $(x = x_n = l)$.

When the shifted lower depth factor, c_i (eq. 21), is used, the associated lower surface strain, ε_i, must also be used for input to the Displacement Transfer Functions. As will be seen shortly, the neutral axis shifting method can automatically nullify the axial strain effect.

Axial-Strain Elimination Method

If the known depth factor $c_i = h_i/2$ of the embedded beam (fig. 3) is to be used, one can consider the unequal magnitudes of the lower and upper surface strains contain both bending and axial strain components. In view of figure 9, by averaging the magnitudes of the lower and upper surface strains $(\varepsilon_i > 0, \overline{\varepsilon}_i < 0)$, axial strain components can be eliminated to yield the true bending strains given by equation (23) (fig. 9):

$$\text{True bending strain} = \frac{\varepsilon_i - \overline{\varepsilon}_i}{2} \quad ; \quad (i = 1,2,3,...,n) \tag{23}$$

For entering the true bending strains, $(\varepsilon_i - \overline{\varepsilon}_i)/2$, into the Displacement Transfer Functions, the known depth factor, $c_i (= h_i/2)$, must be used.

Strain-to-Depth Factor Ratios

For exploration purpose, the strain-to-depth factor ratios for the above two methods [eqs. (21) and (23)] can be written in the following forms as equations (24) and (25):

For neutral-axis-shifting case [rewriting eq. (21)]:

$$\frac{-\overline{\varepsilon}_i}{c_i} = \frac{\varepsilon_i - \overline{\varepsilon}_i}{h_i} \tag{24}$$

For axial-strain elimination case [from eq. (23)]:

$$\frac{1}{c_i}\left(\frac{\varepsilon_i-\bar{\varepsilon}_i}{2}\right)=\frac{2}{h_i}\left(\frac{\varepsilon_i-\bar{\varepsilon}_i}{2}\right)=\frac{\varepsilon_i-\bar{\varepsilon}_i}{h_i} \tag{25}$$

Note from equations (24) and (25) that the strain-to-depth factor ratios for the two methods are identical. Since all the Displacement Transfer Functions from equations (6a), (6b), (6c), (7a), (7b), (7c), (18a), (18b), (18c), (19a), (19b), and (19c) are expressed in terms of strain-to-depth factor ratios, the slopes and deflections calculated using the two input methods turned out to be extremely close as will be seen in the Numerical Results section.

PREDICTION ERROR EQUATIONS

The Nastran-generated deflections were used as benchmark data to study the theoretical deflection prediction errors. Let $\{y_i, \widehat{y}_i\}$, respectively denote the vertical and curved deflections predicted, respectively from the Shifted and the Curved Displacement Transfer Functions, and let $\{(y_i)_{NL}, (\widehat{y}_i)_{NN}\}$, respectively denote the corresponding Nastran-calculated linear and nonlinear deflections. Then, the prediction error is defined by the following prediction error equations (26) and (27), respectively for vertical and curved deflection cases:

Vertical deflection case (linear analysis):

$$\text{Prediction error} \equiv \left[\frac{y_i}{(y_i)_{NL}}-1\right]\times 100\% \tag{26}$$

Curved deflection case (nonlinear analysis):

$$\text{Prediction error} \equiv \left[\frac{\widehat{y}_i}{(\widehat{y}_i)_{NN}}-1\right]\times 100\% \tag{27}$$

Equations (26) and (27) were used to determine the prediction errors of the Shifted and Curved Displacement Transfer Functions.

NUMERICAL RESULTS

The complete set of strain and deflection data generated by Nastran linear and nonlinear analyses of the tapered cantilever tubular beam are tabulated in Appendix I for different beam-tip load *P*.

Nastran Linear Cases

All the data generated for the Nastran linear cases are listed in tables I1−I7 of Appendix I. Note from tables I1−I7 that for the Nastran linear cases, the lower and the upper surface strains at the same strain-sensing cross sections have the same magnitudes. The Nastran outputs gave only vertical deflections, y_i, and zero axial displacements (that is, $u_i = 0$) (fig. 6a). Thus, Nastran linear case is equivalent to the Shifted formulation. In the last columns of tables I1−I7, the corresponding theoretical vertical deflections, y_i, were calculated from the Shifted Displacement Transfer Functions in equation (6b) using the known

depth factors, $c_i(=h_i/2)$, and Nastran lower surface strains, ε_i, listed in tables I1−I7. The theoretical deflections, y_i, calculated from equation (7b) are not listed because both equations (6b) and (7b) gave practically identical vertical deflections with maximum difference of only 0.08 percent at the beam-tip for the present low-tapered cantilever tubular beam. The data listed in tables I1−I7 of Appendix I were used in plotting the following linear strain curves and vertical deflection curves for visual display.

1. Nastran Linear Strain Curves

Figure 10 shows surface strain curves associated at different load levels generated from Nastran linear analysis of the tapered cantilever tubular beam based on data listed in tables I1− I7 of Appendix I. Note that for linear cases, the magnitudes of the lower and upper surface strains at the same axial location are identical, and increase linearly with increasing load, *P*. Note from figure 10 that for the present tapered tubular beam, with tip-to-root depth ratio, $(c_n/c_0) = 1/4$, the linear strains increase almost linearly in the span-wise direction in the inboard regions, reaching the peaks in the outboard regions, and then decrease rapidly down to zero at the beam tip.

2. Vertical Deflection Curves

Figure 11 shows vertical deflection curves for the tapered cantilever tubular beam at different loading levels calculated from the Shifted Displacement Transfer Functions [eq. (6b)] and from Nastran linear analysis based on the data listed in tables I1−I7 of Appendix I.

As shown in figure 11, the theoretical deflection curves [eq. (6b)] practically fell on top of the corresponding Nastran-generated deflection curves, even up to very large bending under *P* = 600 lb, with beam-tip deflection reaching 94 percent of the beam span (see table I7 of Appendix I), and beam-tip slope angle reaching 66 deg. (ref. 15). The good agreement between the vertical (straight) deflections calculated from the Shifted Displacement Transfer Functions and from Nastran linear analysis, gives confidence in the mathematical formulations of the Shifted Displacement Transfer Functions.

Nastran Nonlinear Cases

All the data generated for the Nastran nonlinear cases are listed in tables I8–I14 of Appendix I. The Nastran outputs gave both axial and vertical displacement, $\{u_i, y_i\}$ (fig. 6b). Thus, Nastran nonlinear analysis is equivalent to the Curved formulation. Note from tables I8–I14 that the magnitudes of the lower surface strains are slightly larger than the magnitudes of the associated upper surface strains. Such lower and upper strain magnitude differentials could be attributed to the curved-beam effect, which induces slight axial tensile strain components under nonlinear bending.

In the last columns of, the theoretical curved deflection, $\hat{y}_i$ were calculated from the Curved Displacement Transfer Functions [eq. (18b)] using the known depth factors, $c_i(=h_i/2)$, and the true bending strains $(\varepsilon_i - \bar{\varepsilon}_i)/2$ [eq. (23)] using the Nastran-nonlinear strain data, $\{\varepsilon_i, \bar{\varepsilon}_i\}$, listed in tables I8–I14 of Appendix I. The theoretical deflections, $\hat{y}_i$, calculated from equation (19b) are not listed because both equations (18b) and (19b) gave practically identical curved deflections for the present low-tapered cantilever tubular beam case. For highly tapered flexible beam cases, equations (18b) and (19b) can give slightly different curved deflections, $\hat{y}_i$ (ref. 7). The data listed in tables I8−I14 of Appendix I were then used in plotting the following nonlinear strain curves and curved deflection curves for visual display.

1. Nastran Nonlinear Strain Curves

Figure 12 shows surface strain curves associated with different load levels generated from Nastran nonlinear analysis of the tapered cantilever tubular beam using data listed in tables I7−I14 of Appendix I. In the plots of the upper surface strains, which are negative, only the magnitudes were used (dashed curves).

For the nonlinear cases, the magnitudes of lower and upper surface strains at each load level are no longer identical. Note from figure 12, that for the load less than P=100 lb, the lower and upper strain curves are equal. However, when the load level exceeds P=100 lb, the magnitudes of upper strains in the outboard region become slightly less than the corresponding lower strains, and the difference between each set of lower and upper strain curves increases with increasing load. The difference between the lower and upper strain magnitude for the present tubular beam case can be attributed to the curvature effect induced by nonlinear bending, causing slight neutral axis shifting toward the compression boundary (fig. 8).

2. Curved Deflection Curves

Figure 13 shows the curved deflection curves for the tapered cantilever tubular beam at different loading levels calculated from the Curved Displacement Transfer Functions [eq. (18b)] and from Nastran nonlinear analysis. For convenience, the horizontal displacements are neglected, and the deformed material points were plotted on their respective undeformed x-locations.

As shown in figure 13, the theoretical deflection curves [eq. (18b)] practically fell on top of the corresponding Nastran-generated deflection curves, even up to very large nonlinear bending under P = 600 lb, with beam-tip deflection reaching 58 percent of the beam span, and beam-tip slope angle reaching 69 deg. (see table 2 and table I14 of Appendix I).

Lastly, by using Nastran nonlinear strains as inputs, the theoretical curved deflection curves [calculated from eq. (18b)] and the corresponding Nastran-generated curved deflection curves [calculated from eq. (20)] are graphically coincidental (fig. 13). The excellent agreement between the curved deflections calculated from the Curved Displacement Transfer Functions and from Nastran nonlinear analysis, gives confidence in the mathematical formulations of the Curved Displacement Transfer Functions.

Comparisons of Neutral-Axis Shifting Method and Axial-Strain Elimination Method

Based on Nastran-generated nonlinear surface strains for a typical case of P=600 lb listed in table I14 of Appendix I, both the neutral-axis-shifting method and the axial-strain-elimination method were used to obtain correct data for input to the Curved Displacement Transfer Functions [eq. (18b)] for calculations of the slope angle, θ_i, and curved deflections, $\hat{y}_i$, for nonlinear deformations. The resulting data are compared in table 2.

Table 2. Comparisons of slopes and curved deflections, $\{\theta_i, \hat{y}_i\}$, calculated from Curved Displacement Transfer Functions [eq. (18a) and (18b) for the *P*=600 lb nonlinear case using two input methods: 1) Neutral-axis-shifting method and 2) Axial-strain-elimination method based on the Nastran nonlinear strain data of table I14 of Appendix I.

	Neutral-axis-shifting method Using calculated c_i [eq.(21)] and Nastran nonlinear lower surface strains ε_i (table I14)			Axial-strain-elimination method Using known $c_i(=h_i/2)$ and true bending strains $(\varepsilon_i - \overline{\varepsilon}_i)/2$ [eq. (23)]		
i	c_i, in Calculated eq. (21)	θ_i, deg Eq. (18a)	$\hat{y}_i$, in Eq. (18b)	c_i, in Known $(=h_i/2)$	θ_i, deg Eq. (18a)	$\hat{y}_i$, in Eq. (18b)
0	4.002	0.000	0.000	4.000	0.000	0.000
1	3.852	2.541	0.330	3.850	2.541	0.330
2	3.703	5.208	1.342	3.700	5.208	1.342
3	3.554	8.006	3.069	3.550	8.006	3.069
4	3.406	10.940	5.546	3.400	10.940	5.545
5	3.258	14.018	8.809	3.250	14.018	8.809
6	3.109	17.243	12.898	3.100	17.243	12.898
7	2.961	20.619	17.851	2.950	20.619	17.851
8	2.814	24.149	23.708	2.800	24.149	23.708
9	2.666	27.836	30.509	2.650	27.835	30.509
10	2.519	31.675	38.296	2.500	31.675	38.296
11	2.371	35.662	47.107	2.350	35.662	47.107
12	2.224	39.786	56.981	2.200	39.785	56.980
13	2.077	44.027	67.949	2.050	44.027	67.949
14	1.931	48.355	80.041	1.900	48.355	80.040
15	1.785	52.724	93.271	1.750	52.724	93.271
16	1.641	57.058	107.644	1.600	57.057	107.643
17	1.501	61.227	123.133	1.450	61.227	123.132
18	1.367	65.013	139.669	1.300	65.015	139.668
19	1.264	67.992	157.103	1.150	68.001	157.104
20	No data (0/0)	69.439^	175.138*	1.000	69.416^	175.138*

^Negligible differences (0.0331%) *Identical at beam tip,

Notice from table 2 that the slope angles, θ_i, and curved deflections, $\hat{y}_i$, calculated respectively from equations (18a) and (18b) based on the Neutral-axis-shifting method and the Axial-strain-elimination method are extremely close. These results show that either method could be used for the present tubular beam case, for which the neutral axis is located at the half depth of the embedded beam. Remember that the Axial-strain-elimination method is used to eliminate axial strains only when the neutral axis is located at the half depth of the undeformed embedded beam. For a complex structure (for example, aircraft wings) with unknown neutral axis location, the Neutral-axis-shifting method can be used to calculate the unknown depth factors, c_i.

Figure 14 shows the plots of both calculated and known depth factors, c_i, using the c_i-data listed in table 2. Note that the calculated depth-factor curve lies slightly above the known depth-factor curve, $c_i(=h_i/2)$, implying slight shifting of the neutral axis toward the concave (compression) side of the deformed embedded beam, especially in the outboard region. The reason for the neutral axis shift is that under large deformations, the difference between the magnitudes of the lower and upper surface strains at

the same cross section increases in the highly bent outboard region (fig.12). Note that at the beam tip, no data point is shown (table 2) because the beam-tip surface strains are zero, causing equation (21) to give indefinite 0/0 value.

Linear-Nonlinear Transition

Figure 15 shows the plots of Nastran-generated beam-tip deflections, $\{y_n, \hat{y}_n\}$, as functions of applied load, *P*. The corresponding theoretical deflection curves calculated from the Shifted deflection equation (6a) and Curved deflection equation (18a), respectively using Nastran linear and nonlinear strain data, graphically fell on top of the corresponding Nastran deflection curves. Using Nastran linear strains, the vertical deflection, y_n, is a linear function of applied load, *P*. Therefore, the linear large deformation is simply the scaled up version of the small deformation. However, using Nastran nonlinear strains, the curved deflection, $\hat{y}_n$, increases convex upwardly with the applied load, *P*. Note from figure 15 that the linear and nonlinear beam-tip deflection curves are practically the same up to *P*=100 lb, at which the beam-tip deflection to span ratio is $(y_n/l) = (\hat{y}_n/l) \approx 0.156$, Beyond *P*=100 lb, the linear and nonlinear beam-tip deflection curves diverge. Therefore, for the present tapered cantilever tubular beam, the normalized deflection of $(y_n/l) = 0.156$ can be considered as the borderline between linear and nonlinear deformation regimes.

For the current long tapered cantilever tubular beam under the tip load of *P*=600 lb., the beam-tip-deflection-to-span ratio is $(y_n/l) = (\hat{y}_n/l) =$ (175.138 in.)/(300 in.) = 0.58, which is larger than the Helios case of (beam-tip-deflection)/(half-span) = (40 ft)/(123.5 ft) = 0.32.

Similarity of Shifted and Curved Formulations

Note that the curvature-strain differential equations (5) and (8) have identical right-hand sides, $\varepsilon(x)/c(x)$. For exploratory purposes, the vertical deflection, y, calculated from equation (6b) (Shifted formulation) and the curved deflection, $\hat{y}$, calculated from equation (18b) (Curved formulation) are compared for the *P*=600 lb nonlinear case. In the calculations of deflections, $\{y, \hat{y}\}$, the calculated depth factors, c_i [eq. (21)], and the nonlinear lower surface strains, ε_i (table I14 of Appendix I), were used as inputs. Table 3 lists the calculated results for the *P*=600 lb nonlinear case.

Table 3. Comparisons of slope angles, θ_i, and deflections, $\{y_i, \hat{y}_i\}$, calculated from Shifted and Curved Displacement Transfer Functions for the *P*=600 lb nonlinear case; calculated depth factors, c_i (second column of table 2), and nonlinear lower surface strains, ε_i, of table I14 of Appendix I were used as inputs.

			Shifted Displacement Transfer Functions			Curved Displacement Transfer Functions		
i	c_i, in Calculated Eq. (21)	ε_i, in/in Nastran nonlinear lower surface strain (table I14)	$\tan\theta_i$ Eq. (6a)	θ_i, deg Eq. (6a)	y_i, in Eq. (6b)	θ_i, rad Eq. (18a)	θ_i, deg Eq. (18a)	$\hat{y}_i$, in Eq. (18b)
0	4.002	0.01155	0.000	0.000	0.000	0.000	0.000	0.000
1	3.852	0.01167	0.044	2.540	0.330	0.044	2.541	0.330
2	3.703	0.01177	0.091	5.194	1.342	0.091	5.208	1.342
3	3.554	0.01185	0.140	7.954	3.069	0.140	8.006	3.069
4	3.406	0.01191	0.191	10.810	5.545	0.191	10.940	5.545
5	3.258	0.01195	0.245	13.748	8.809	0.245	14.018	8.809
6	3.109	0.01194	0.301	16.749	12.898	0.301	17.243	12.898
7	2.961	0.01190	0.360	19.792	17.851	0.360	20.619	17.851
8	2.814	0.01182	0.421	22.855	23.708	0.421	24.149	23.708
9	2.666	0.01168	0.486	25.911	30.509	0.486	27.835	30.509
10	2.519	0.01148	0.553	28.935	38.296	0.553	31.675	38.296
11	2.371	0.01120	0.622	31.899	47.107	0.622	35.662	47.107
12	2.224	0.01084	0.694	34.776	56.980	0.694	39.785	56.980
13	2.077	0.01038	0.768	37.539	67.949	0.768	44.027	67.949
14	1.931	0.00980	0.844	40.163	80.040	0.844	48.355	80.040
15	1.785	0.00909	0.920	42.620	93.271	0.920	52.724	93.271
16	1.641	0.00819	0.996	44.881	107.643	0.996	57.057	107.643
17	1.501	0.00706	1.069	46.900	123.132	1.069	61.227	123.132
18	1.367	0.00559	1.135	48.611	139.668	1.135	65.015	139.668
19	1.264	0.00355	1.187	49.883	157.104	1.187	68.001	157.104
20	1.000	0.00037	1.212^	50.464	175.138*	1.212^	69.416	175.138*

*Identical ^Identical

Note also from table 3 that the deflections, $\{y_i, \hat{y}_i\}$, calculated respectively from the Shifted deflection equation (6b) and Curved deflection equation (18b) using Nastran nonlinear surface strains, turned out to be identical. Note also that the Curved slope angle, $(\theta_i)_{Curved}$, which is the true slope angle of the deformed embedded beam, reaching up to $(\theta_i)_{Curved} \approx 69$ deg at the beam tip. On the other hand, the Shifted slope angle $(\theta_i)_{Shifted}$ is slightly smaller because the Shifting process reduces the slope angle, causing the Shifted slope angle to reach up to only $(\theta_n)_{Shifted} \approx 50$ deg at the Shifted beam-tip (fig 5). However, as shown in table 3, the slope $(\tan\theta_i)_{Shifted}$ calculated from the Shifted slope equation (6a) has exactly the same value as the corresponding slope angle $(\theta_i)_{Curved}$ calculated from the Curved slope equation (18a) [that is, $(\tan\theta_i)_{Shifted} = (\theta_i)_{Curved}$].

Figure 16 shows the span-wise plots of slope angles $\{(\theta_i)_{Shifted}, (\theta_i)_{Curved}\}$ and deflections $\{y_i, \widehat{y}_i\}$ based on the data listed in table 3 for *P*=600 lb Nastran nonlinear case. Note from figure 16 that the deflection curves of $\{y_i, \widehat{y}_i\}$ form a single curve because $(y_i = \widehat{y}_i)$. The $(\theta_i)_{Shifted}$-curve practically falls on top of the $(\theta_i)_{Curved}$-curve in the inboard region up to strain-sensing station i = 4, and then gradually diverge downward from the $(\theta_i)_{Curved}$-curve toward the beam tip $(i = n)$.

Deflection Identity $(y_i = \widehat{y}_i)$

The unexpected discovery of the deflection identity, $y_i = \widehat{y}_i$ (table 3, fig. 16), indicates that the Shifted vertical deflection, y_i, is actually the straightened version of the Curved deflection, $\widehat{y}_i$. This deflection identity, $y_i = \widehat{y}_i$, can be explained as follows: The Shifting of the deformed material points (lying along the neutral axis) to their respective original undeformed *x*-positions [that is, $u \to 0$] causes $(dy/dx)^2 \to 0$ (details in Appendix A, ref. 9), thus the Lagrangian curvature equation (4) is reduced to the mathematical form similar to the Curved curvature equation (10) as shown below in equation (28):

$$\frac{1}{R(x)} = \frac{d^2y/dx^2}{\sqrt{1-(dy/dx)^2}} \xrightarrow[\text{Shifting} = (u \to 0) \\ = [(dy/dx)^2 = 0]]{} \frac{\overbrace{d^2y/dx^2}^{\text{Increased to maintain same } \varepsilon(s)/c(s)}}{\underbrace{\sqrt{1-0}}_{\text{Increased}}} = \frac{d^2y}{\underbrace{dx^2}_{\text{Shifted}}} = \frac{d^2\widehat{y}}{\underbrace{dx^2}_{\text{Curved}}} = \frac{\varepsilon(s)}{c(s)} \tag{28}$$

Equation (28) shows that, based on the same undeformed *x*-system, the correct Shifting process will cause the value of y to match the value of $\widehat{y}$ to maintain the same value of $\varepsilon(x)/c(x)$, resulting in the deflection identity $y_i = \widehat{y}_i$ (table 3).

Correct Shifting

The original horizontal shifting of point A' to point A'' shown in figure 5 was found not to be an accurate process of obtaining the true Shifted deflection, y, and, therefore, the shifting process need to be modified.

Figure 17 is the amended figure 5 and graphically shows that the correct Shifting is not the horizontal Shifting (fig. 5), but is to move point A' to point A'' in such a way as to bend the curved deflection, $\widehat{y}$, into the equivalent Shifted vertical deflection, y. Thus, the Shifted Displacement Transfer Functions, just like the Curved Displacement Transfer Functions, are also applicable to shape predictions of structures under large geometric nonlinear deformations provided the value of the Shifted slope $(\tan\theta_i)_{Shifted}[=(\theta_i)_{Curved}]$ is treated as the true slope angle because the shifting process will reduce the true slope angle, $\angle B'A'C$, to a smaller shifted angle, $\angle B''A''C'$ (see fig. 3 and table 3).

Prediction Errors

Table 4 lists the beam-tip deflections $\{y_n, \widehat{y}_n\}$ of the tapered cantilever tubular beam under all loading cases calculated respectively from the Shifted [eq. (6b)] and Curved [eq. (18b)] Displacement Transfer Functions, and from Nastran linear and nonlinear analyses. The percent prediction errors listed in table 4 were calculated from the error equations (26) and (27) respectively for vertical and curved deflection cases.

Table 4. Comparisons of beam-tip deflections, $\{y_n, \widehat{y}_n\}$, of the tapered cantilever tubular beam, calculated from Shifted and Curved Displacement Transfer Functions and from Nastran linear and nonlinear analyses.

	Straight deflection y_n, in			Curved deflection $\widehat{y}_n$, in		
P, lb	Nastran linear (Reference)	Shifted Displacement Transfer Functions Eq. (6b)	Error, % Eq. (26)	Nastran nonlinear (Reference)	Curved Displacement Transfer Functions Eq. (18b)	Error, % Eq. (27)
50	23.406	23.424	0.0769*	23.210	23.220	0.0431
100	46.811	46.828	0.0363	45.337	45.374	0.0816
200	93.623	93.669	0.0491	83.903	84.082	0.2133
300	140.434	140.502	0.0484	114.508	114.820	0.2725
400	187.245	187.314	0.0369	138.776	139.187	0.2962*
500	234.057	234.161	0.0444	158.439	158.866	0.2695
600	280.868	280.970	0.0363	174.763	175.138	0.2146

*Peak errors

Note from table 4 that at *P*=600 lb, the beam-tip curved deflections, $\widehat{y}_n$, (predicted or Nastran-generated) is only about 62 percent of the corresponding beam-tip vertical deflections, y_n (predicted or Nastran-generated). Note also that for vertical deflection cases, the prediction errors are extremely small, in the range of 0.0363 percent to 0.0769 percent, with a peak prediction error of 0.0769 percent that occurred at *P*=50 lb. For the curved deflection cases, the prediction errors are slightly larger than the vertical deflection cases, but still in the small range of 0.0431 percent to 0.2962 percent, with the peak prediction error of 0.2962 percent (3.85 times the peak prediction error of 0.0769 percent for the vertical deflection case) occurring at *P*=400 lb.

Figure 18 shows the prediction errors listed in table 4 plotted as functions of applied beam-tip load *P* for vertical and curved deflection cases. For the vertical deflection cases, the prediction error curve is almost horizontal, indicating that the prediction error is practically insensitive to the applied load, *P*. For the curved deflection cases, the prediction error increases convex upwardly with applied load, reaching the peak of 0.2962 percent at *P*=400 lb, and then slightly tapering down to 0.2146 percent at *P*=600 lb. Keep in mind that the Nastran curved deflection $(\widehat{y})_{NN}$ appearing in the prediction error equation (27) (fig. 5) is calculated from the straight-to curve-deflection conversion equation (20), which gives circular arc deflection for $(\widehat{y})_{NN}$. However, the theoretical curved deflection $\widehat{y}$ is not a true circular arc. The slight decrease in the prediction errors beyond *P*=400 lb (fig. 18) could be attributed to the slight decrease in the difference between $\widehat{y}$ (non-circular curve) and $(\widehat{y})_{NN}$ (circular curve) at increasing bending with outboard region bend more than the inboard region because of the tapered beam (table 4).

DISCUSSIONS

To use the Shifted and Curved Displacement Transfer Functions to calculate out-of-plane deflections for structure deformed shape predictions, the following input parameters are required.

1. Lower and upper surface strains, $\{\varepsilon_i, \overline{\varepsilon}_i\}$ $(i = 1,2,3,...,n)$—measured at strain-sensing stations evenly distributed along the lower and upper strain-sensing lines on the embedded beam surfaces (assuming the location of neutral axis of the embedded beam is unknown). For the calculations of overall deformed shape of the structure (For example, aircraft wing) under bending and torsion loading, an additional embedded beam is needed to form four-line sensing system.

2. Domain lengths, $\Delta l (\equiv l/n)$—once the distribution of strain-sensing stations is defined, the domain length, Δl, (strain-sensing station separation distance) is specified.

3. Embedded beam depth, h_i, at strain-sensing stations *i* (known for a given structure).

4. Depth factors, c_i $(i = 1,2,3,...,n)$—usually unknown for complex structures, and must be calculated from equation (21) for each embedded beam using pairs of lower and upper surface strains, $\{\varepsilon_i, \overline{\varepsilon}_i\}$, and the embedded beam depth, h_i.

If the depth factors, c_i, are known, only the lower surface strain-sensing line is needed (fig. 3). For very large geometric nonlinear deformations, the neutral axis can shift with the load level and, therefore, the depth factors must be constantly updated using equation (21) at each loading level.

CONCLUDING REMARKS

Using the true curved deflection, $\hat{y}$, the embedded beam curvature-strain differential equation was piecewise integrated to formulate the Curved Displacement Transfer Functions for geometrical nonlinear large deformation structure shape predictions. Nastran linear and nonlinear analyses were performed on a tapered tubular cantilever beam to analytically obtain surface strains needed for inputs to the Shifted and Curved Displacement Transfer Functions for shape predictions. The Nastran-generated deflections were then used as a validation reference to study the shape prediction accuracies of the Shifted and Curved Displacement Transfer Functions. Some highlights of the results are listed below.

1. For large deformations, one must use the true curved deflection, the curvilinear distance traced by a material point from its undeformed position to its deformed position. The traditional vertical deflection is merely a vertical component of the true curved deflection.

2. The vertical deflections calculated from the Shifted Displacement Transfer Functions and the corresponding curved deflections calculated from the Curved Displacement Transfer Functions were found to be exactly the same, implying that the vertical deflections based on the Shifted formulation are actually the straightened version of the curved deflections based on the Curved formulation.

3. By replacing $\{\hat{y}_i, (\theta_i)_{Curved}\}$ with $\{y_i, (\tan\theta_i)_{Shifted}\}$, the Curved Displacement Transfer Functions can become the Shifted Displacement Transfer Functions.

4. Both the Shifted and Curved Displacement Transfer Functions are very accurate, and are applicable to the shape predictions of the cantilever tubular beam under geometrical nonlinear large deformations with beam-tip deflection reaching as high as 58 percent of the span, for which the beam-tip slope angle reaches 69 deg.

5. The Shifted and Curved Displacement Transfer Functions are purely geometric in nature, and therefore, one can compute the correct deflections whether the input surface strains come from linear or nonlinear deformations.

6. For vertical deflection cases, the prediction error of using the Shifted Displacement Transfer Functions is in the negligible range of (0.0363−0.0769) percent, and is practically insensitive to the change of applied load.

7. For the curved deflection cases, the prediction errors of using the Curved Displacement Transfer Functions are in the small range of (0.0431−0.2962) percent, slightly larger than the vertical deflection cases; because Nastran curved deflection is a circular arc, but the theoretical curved deflection is not a circular arc.

8. For nonlinear deformations, the magnitudes of the lower and upper surface strains at the same strain-sensing station can be slightly different because of the curved-beam effect, which induces neutral axis shifting and small axial strain components.

9. For nonlinear deformations, either the Neutral-Axis-Shifting Method or the Axial-Strain-Elimination Method can be used to obtain correct data (depth factors, bending strains) for input to the Displacement Transfer Functions for shape calculations.

FIGURES

ED03-0180-02

Figure 1. A super-long flying wing Helios prototype (wing span 247 ft) under very high wing dihedral deformation just before breaking up.

ED03-0180-03

Figure 2. Helios Prototype broke-up in mid-air on June 26, 2003 at 2800 ft altitude under very large wing dihedral deformation (wing tip deflection reaching 40 ft), and fell into the Pacific Ocean.

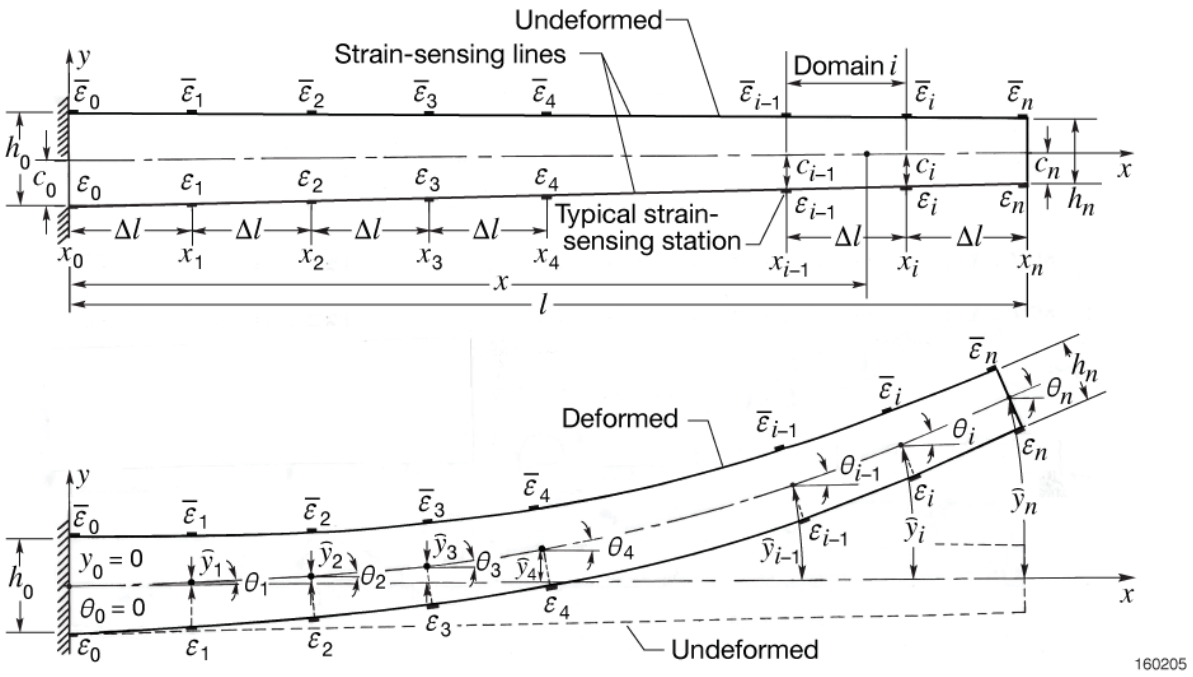

Figure 3. Embedded beam (depth-wise cross section) of the tapered cantilever tubular beam with strain-sensing stations evenly distributed along lower and upper surface strain-sensing lines.

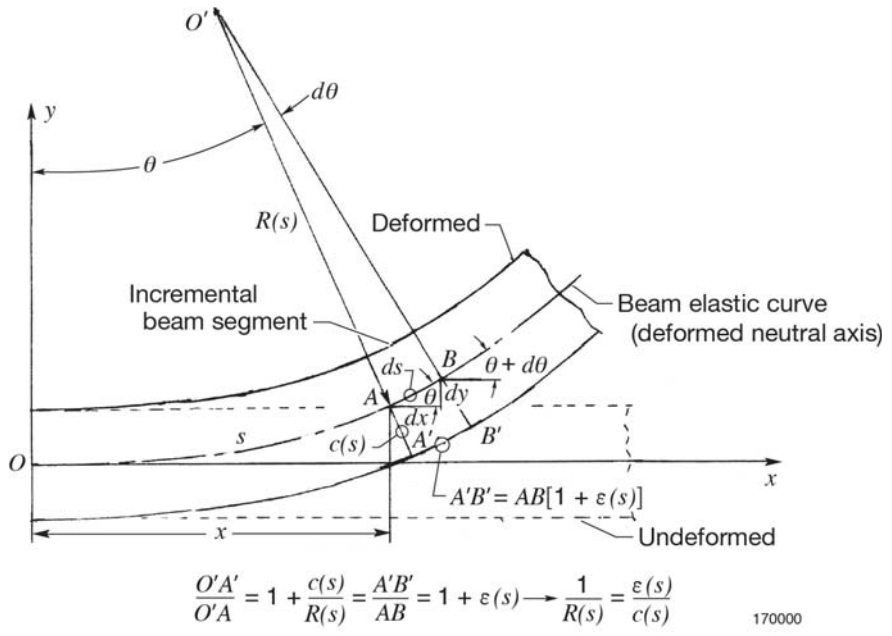

Figure 4. Small segment of a deformed nonuniform embedded beam for geometrically relating local radius of curvature, $R(s)$, to associated surface bending strain, $\varepsilon(s)$, and depth factor, $c(s)$.

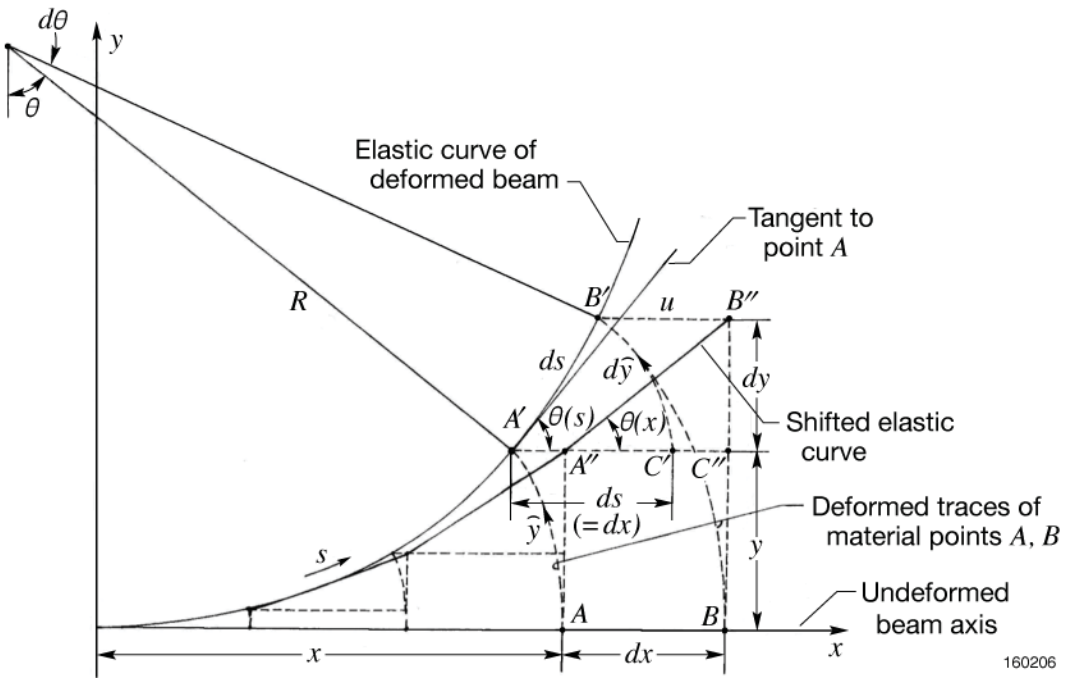

Figure 5. Actual elastic curve of a deformed embedded beam, showing true curved deflections, $\hat{y}$; the curvilinear distances traced by the material points from their undeformed positions to respective deformed positions. Horizontal Shifting converts curved deflection, $\hat{y}$, into vertical deflection, y, with reduced slope angle (ref. 15).

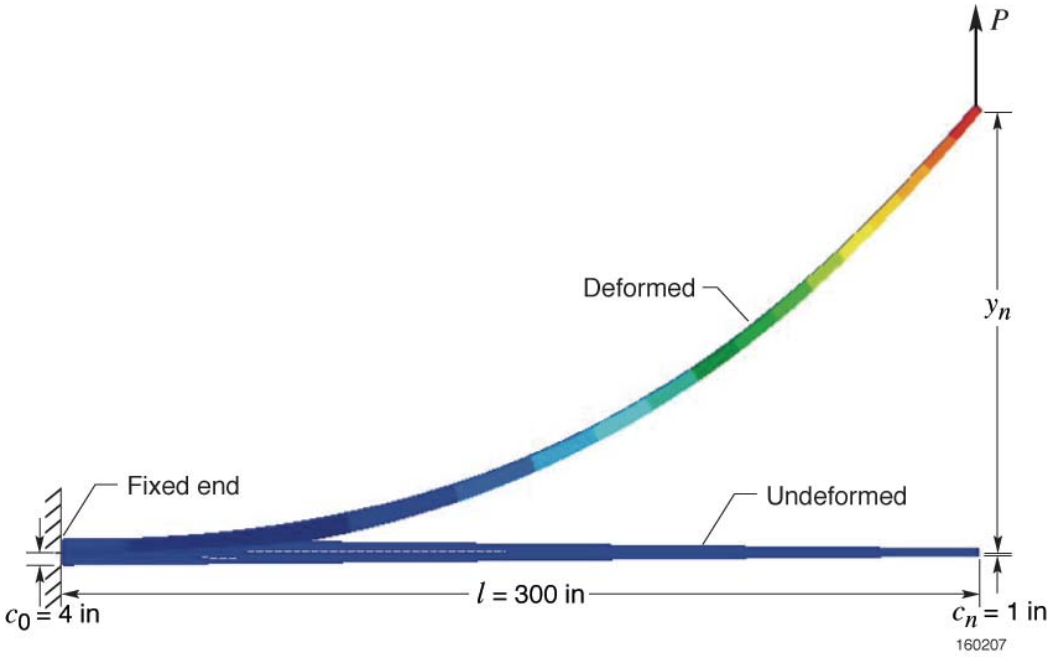

Figure 6a. Shell-element model for linear analysis.

Figure 6. Undeformed and deformed shapes of Nastran models of the tapered cantilever tubular beam subjected to beam tip load, *P*, for linear and nonlinear analyses.

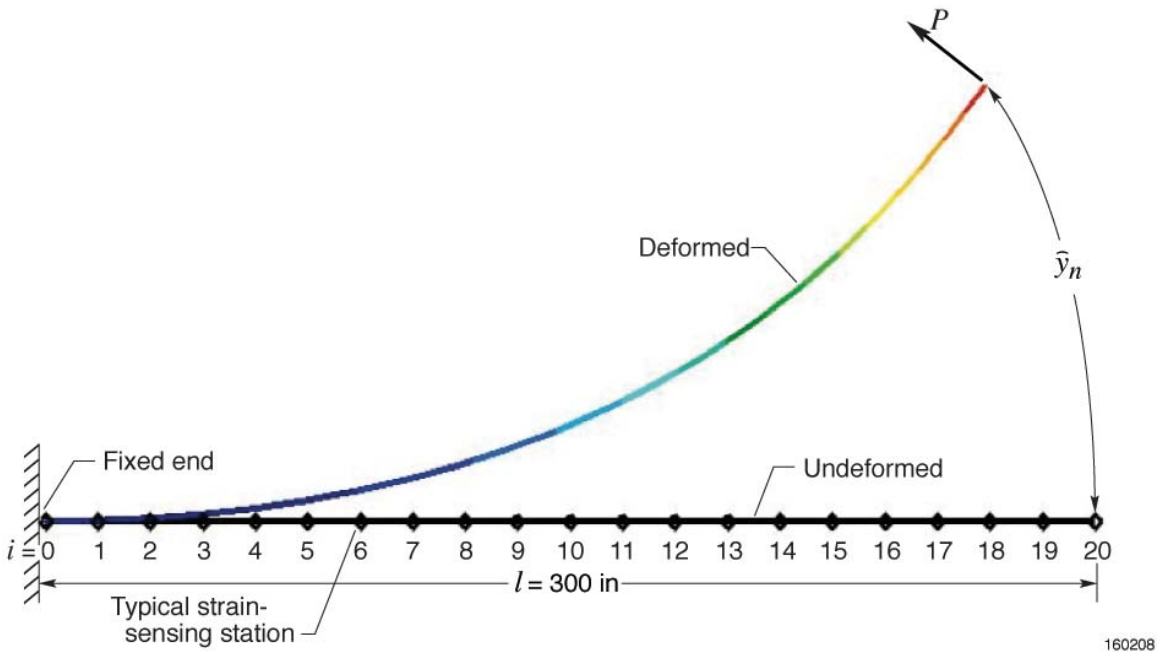

Figure 6b. Beam-element model for nonlinear analysis.

Figure 6. Concluded.

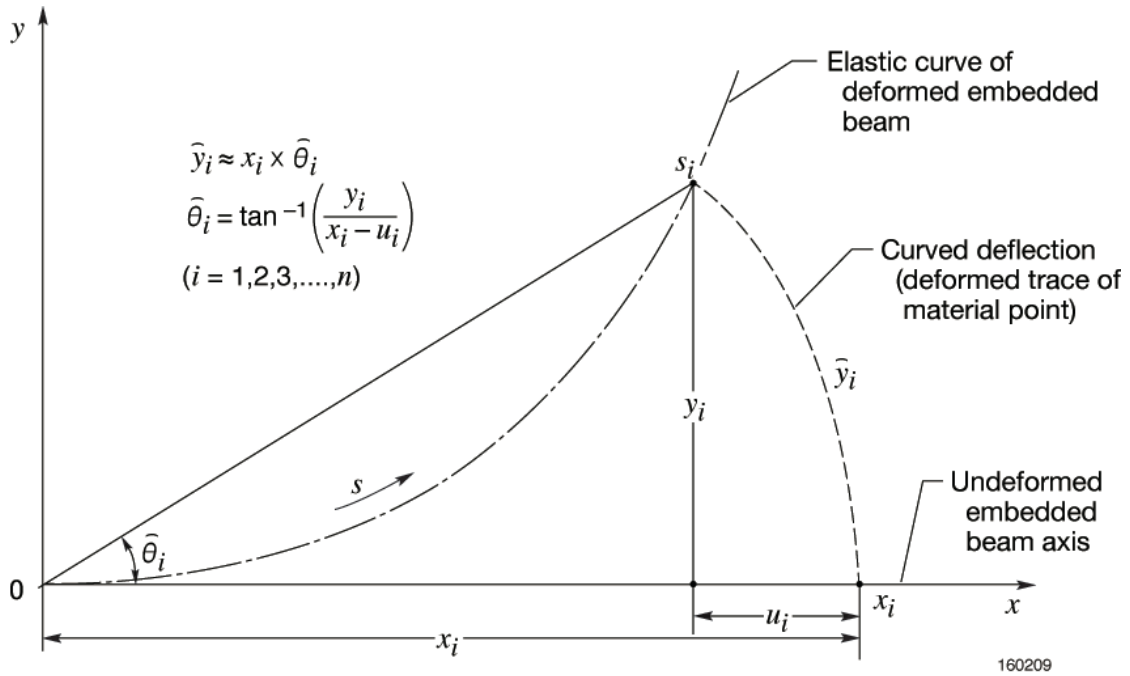

Figure 7. Graphically converting Nastran nonlinear deflection outputs, $\{u_i, y_i\}$, into a circular arc length, $\widehat{y}_i$, for comparison with the theoretical curved deflection, $\widehat{y}_i$.

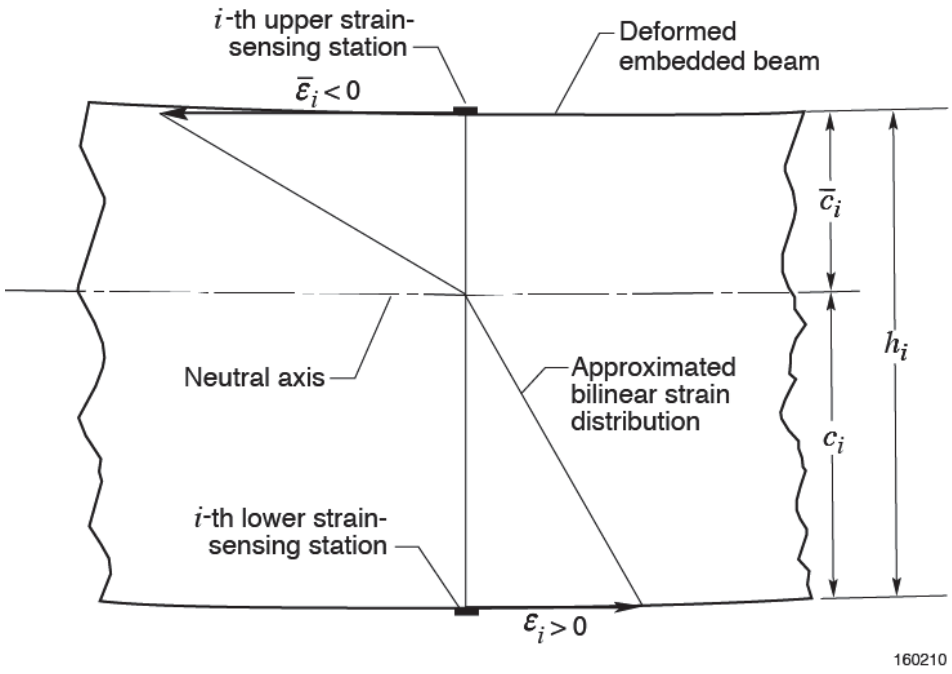

$$c_i = \frac{-\bar{\varepsilon}_i}{\varepsilon_i - \bar{\varepsilon}_i} h_i \quad ; \quad \bar{c}_i = h_i - c_i \quad ; \quad (i = 1,2,3,...,n)$$

Figure 8. Using lower and upper surface strains, $\{\varepsilon_i, \bar{\varepsilon}_i\}$, to obtain lower and upper depth factors, $\{c_i, \bar{c}_i\}$, based on neutral axis shifting in nonlinear bending.

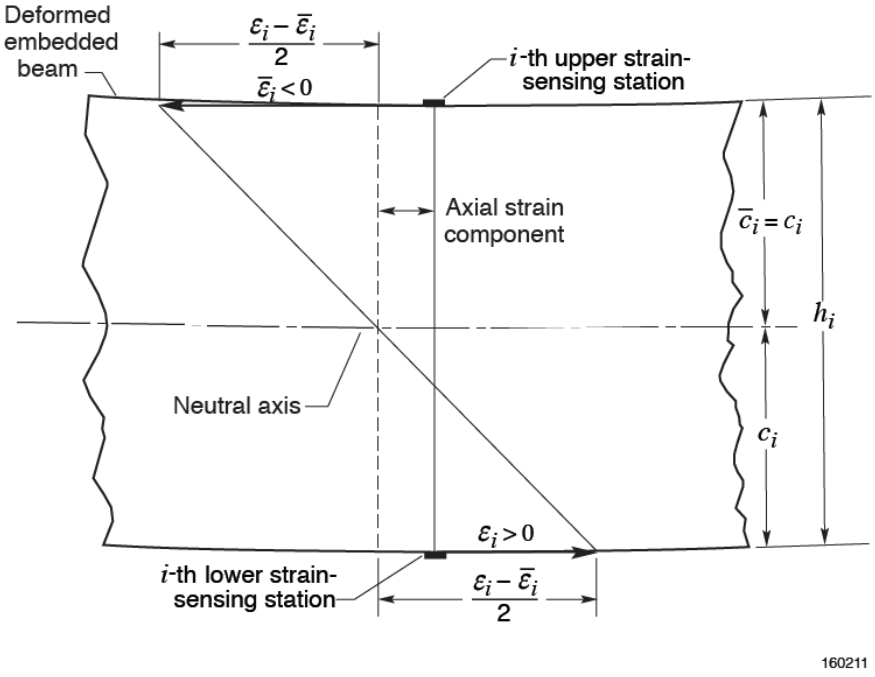

Figure 9. Using lower and upper surface strains, $\{\varepsilon_i, \bar{\varepsilon}_i\}$, to obtain true bending strains, $(\varepsilon_i - \bar{\varepsilon}_i)/2$, eliminating axial strain components induced in nonlinear bending; known depth factor, $c_i = h_i/2$.

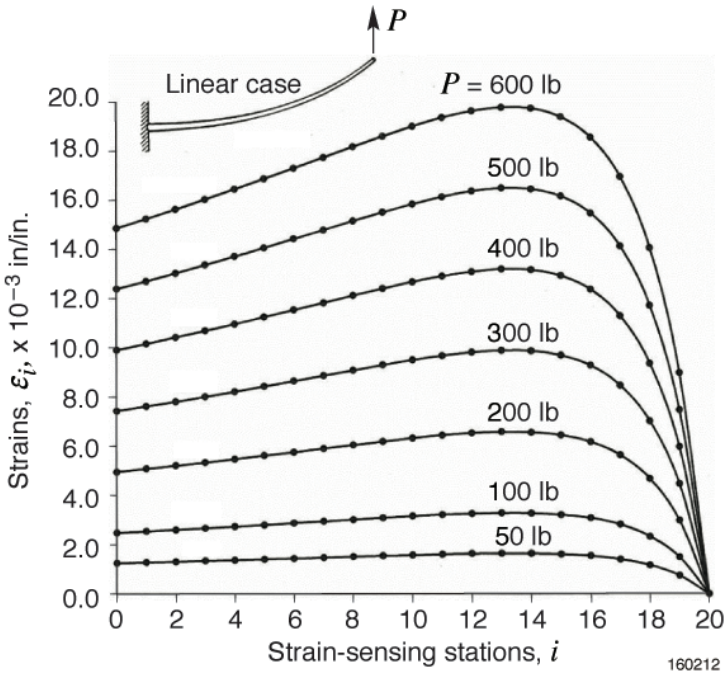

Figure 10. Span-wise distributions of lower surface strains, $\varepsilon_i(=-\overline{\varepsilon}_i)$, generated from Nastran linear analysis of the tapered cantilever tubular beam subjected to different beam-tip load, *P*.

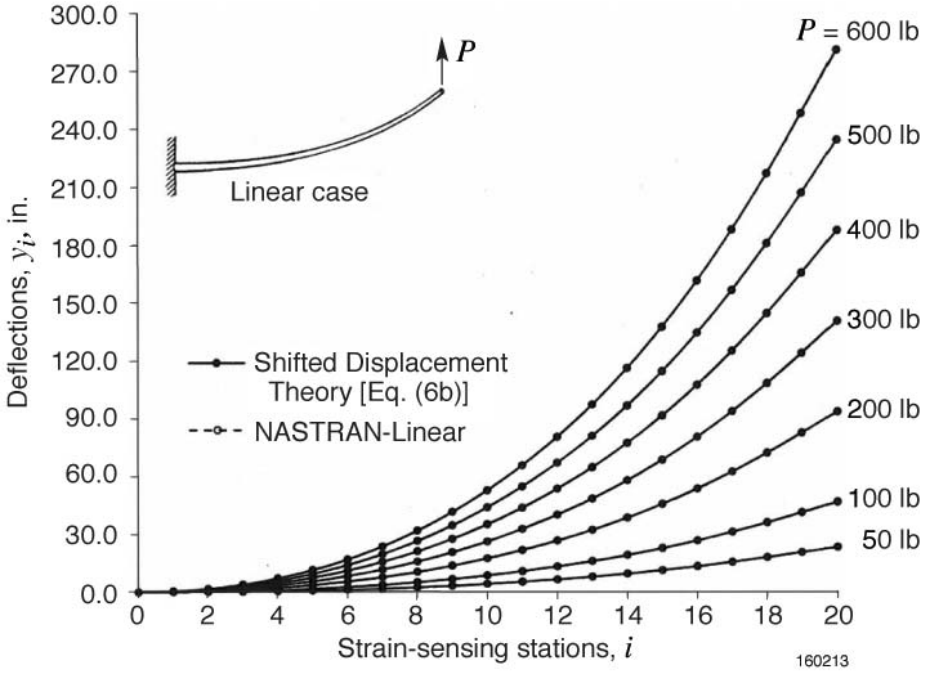

Figure 11. Comparisons of vertical deflection curves for the tapered cantilever tubular beam under a different beam-tip load, *P*, calculated from the Shifted Displacement Transfer Functions [eq. (6b)] and calculated from Nastran linear analysis.

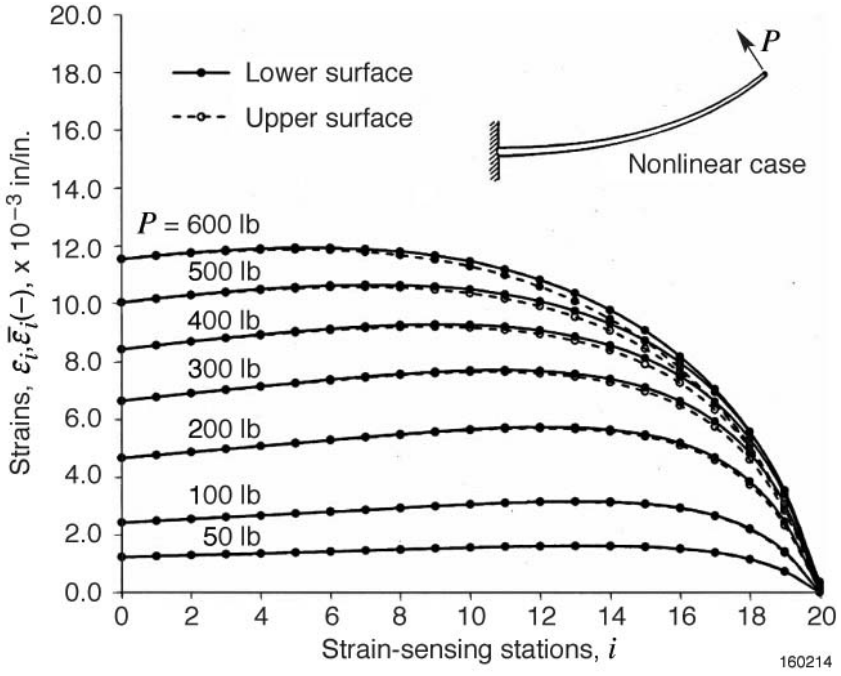

Figure 12. Span-wise distributions of lower and upper surface strains, $\varepsilon_i (\geq -\bar{\varepsilon}_i)$, generated from Nastran nonlinear analysis of the tapered cantilever tubular beam subjected to a different beam-tip load, *P*.

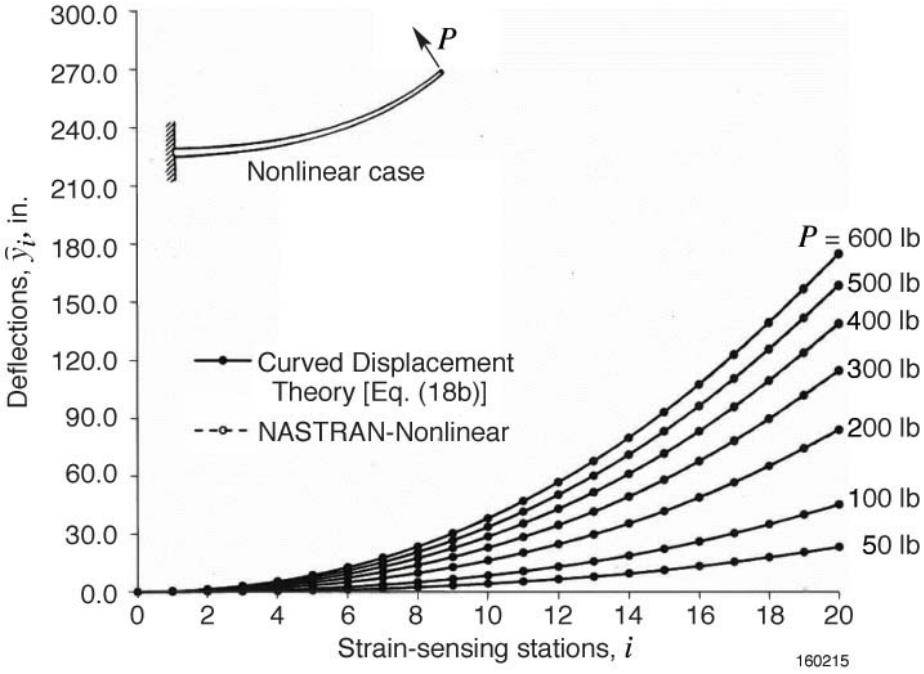

Figure 13. Comparisons of curved deflection curves for the tapered cantilever beam at a different beam-tip load, *P*, calculated from the Curved Displacement Transfer Functions [eq. (18b)] and calculated from Nastran nonlinear analysis.

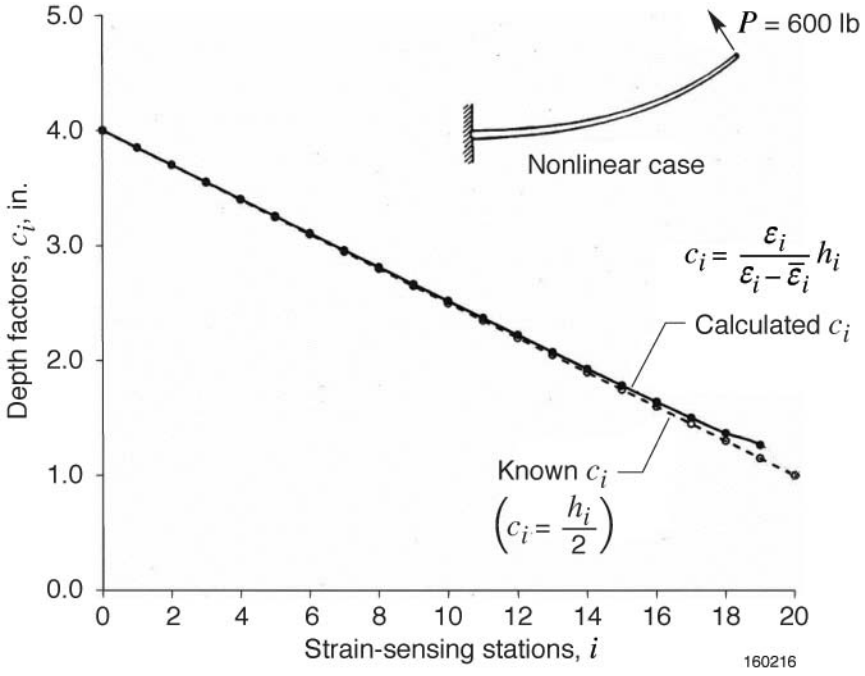

Figure 14. Plots of known and calculated depth factors, c_i, for the tapered cantilever tubular beam showing slight neutral axis shifting due geometric nonlinear deformations, especially in the outboard region; *P*=600 lb nonlinear strain case.

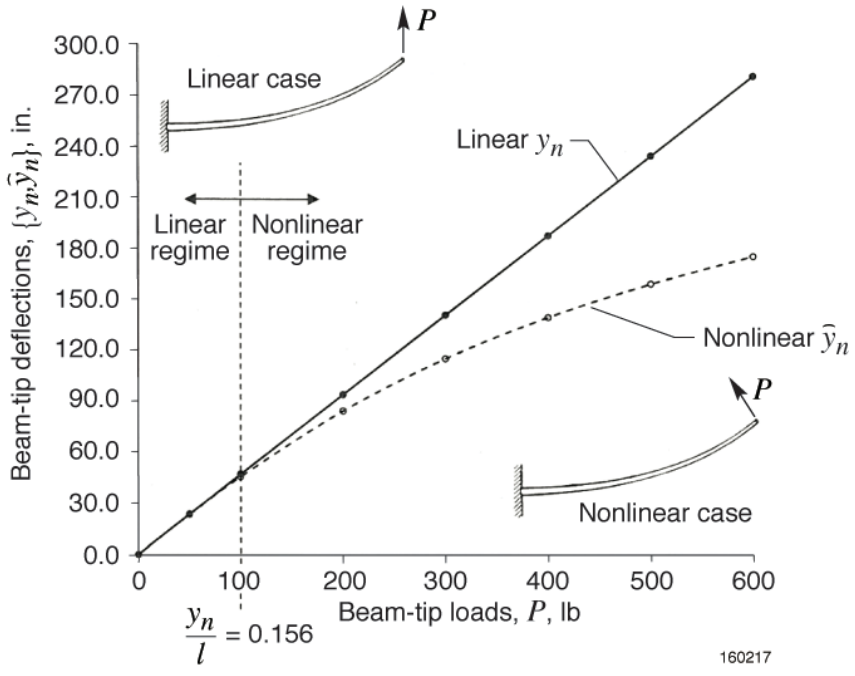

Figure 15. Linear (vertical) and nonlinear (curved) beam-tip deflections, $\{y_n, \hat{y}_n\}$, of the tapered cantilever tubular beam plotted as functions of the applied beam-tip load, *P*. The theoretical deflection curves [eqs. (6b) and (18b)] and the corresponding Nastran-generated linear and nonlinear deflection curves are graphically indistinguishable.

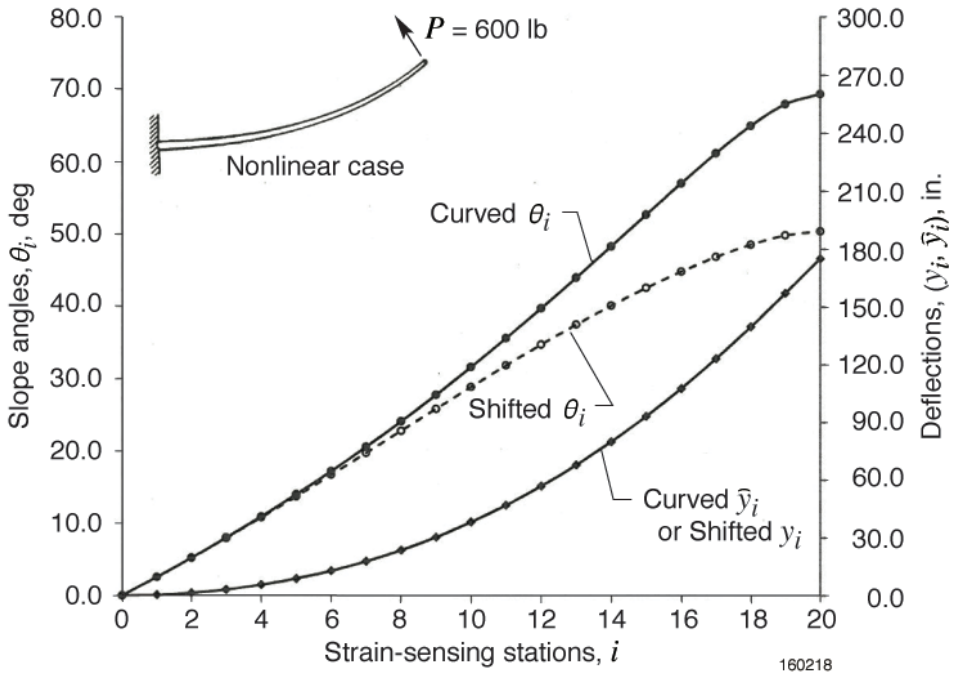

Figure 16. Span-wise plots of slope angle, θ_i, and deflections, $\{y_n, \hat{y}_n\}$, of the tapered cantilever tubular beam calculated from the Shifted and Curved Displacement Transfer Functions [eqs. (6a), (6b), (18a) and, (18b)] using the same Nastran-nonlinear strain data for *P*=600 lb listed in table 3.

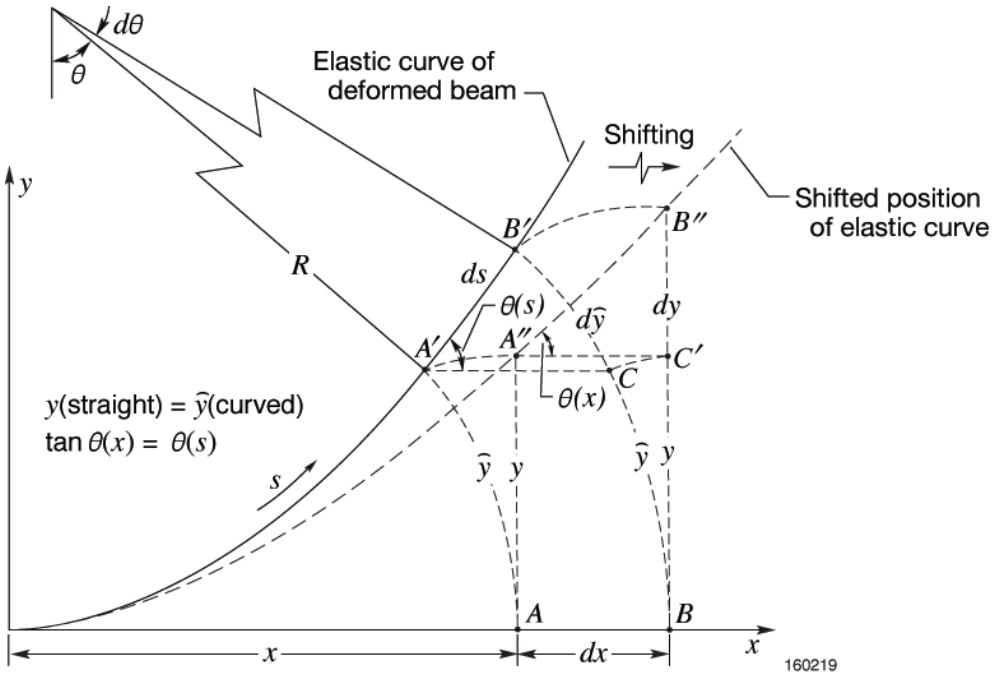

Figure 17. Correct Shifting of deformed material points to their respective undeformed *x*-locations to bend curved deflection, $\hat{y}$, into an equivalent straight (vertical) deflection, $y\ (=\hat{y})$; actual slope angle, $\theta(s)$, turns into slope, $\tan\theta(x)[=\theta(s)]$, for the Shifted case.

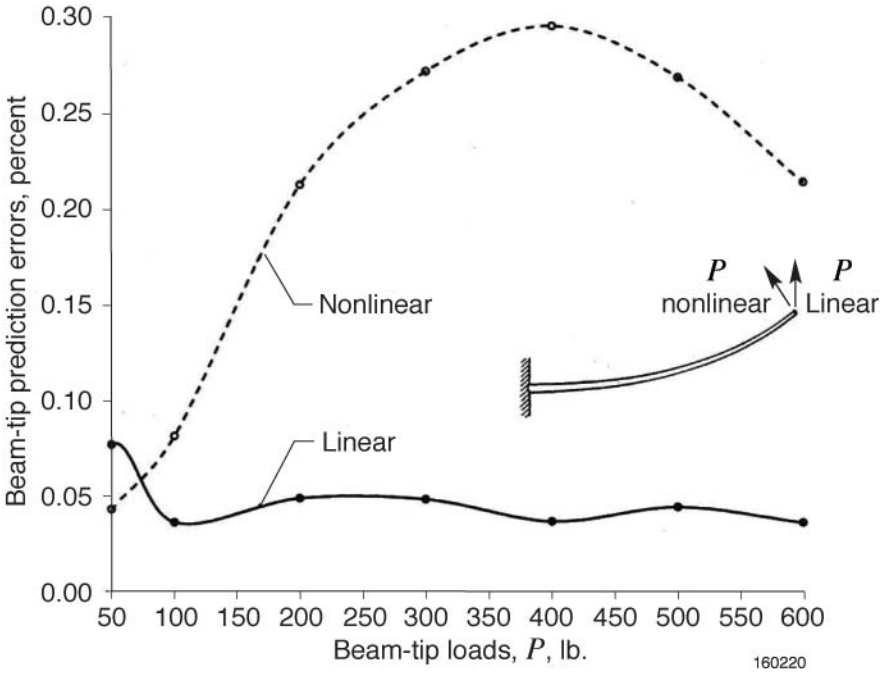

Figure 18. Plots of linear (vertical) and nonlinear (curved) beam-tip deflection prediction errors as functions of beam-tip load, *P*.

APPENDIX A
DERIVATIONS OF SLOPE ANGLE AND CURVED DEFLECTION EQUATIONS IN RECURSIVE FORMS FOR NONUNIFORM EMBEDDED BEAMS

Appendix A shows the mathematical details of stepwise integrations of the slope equation (15) and the deflection equation (17) for the nonuniform embedded beams to obtain the final mathematical forms given respectively by nonuniform parts of equations (18a) and (18b).

Piecewise Linear Strain Representations

For the piecewise integrations of the slope equation (15) and deflection equation (17), both the depth factors and surface strains, $\{c(x),\varepsilon(x)\}$, in the domain $x_{i-1} \le x \le x_i$ between the two adjacent strain-sensing stations, $\{x_{i-1},x_i\}$, can be expressed with linear functions given respectively by equations (A1) and (A2) [duplications of equations (11) and (12) respectively]:

$$c(x) = c_{i-1} - (c_{i-1} - c_i)\frac{x - x_{i-1}}{\Delta l} \quad ; \quad (x_{i-1} \le x \le x_i) \tag{A1}$$

$$\varepsilon(x) = \varepsilon_{i-1} - (\varepsilon_{i-1} - \varepsilon_i)\frac{x - x_{i-1}}{\Delta l} \quad ; \quad (x_{i-1} \le x \le x_i) \tag{A2}$$

Slope Angle Equation

The slope angle, $\theta(x)$, of the nonuniform embedded beam in the domain $x_{i-1} \le x \le x_i$ between the two adjacent strain-sensing stations $\{x_{i-1},x_i\}$ is given by equation (A3) [duplication of equation (15)]:

$$\theta(x) = \underbrace{\int_{x_{i-1}}^{x} \frac{\varepsilon(x)}{c(x)}dx}_{\text{Slope increment}} + \underbrace{\theta_{i-1}}_{\substack{\text{Slope} \\ \text{at } x_{i-1}}} \quad ; \quad (x_{i-1} \le x \le x_i) \tag{A3}$$

Substitute equations (A1) and (A2) into equation (A3), and carrying out the integration as follows in equation (A4) (ref. 21):

$$\theta(x) = \int_{x_{i-1}}^{x} \left[\frac{\varepsilon_{i-1} - (\varepsilon_{i-1} - \varepsilon_i)\dfrac{x - x_{i-1}}{\Delta l}}{c_{i-1} - (c_{i-1} - c_i)\dfrac{x - x_{i-1}}{\Delta l}} \right] dx + \theta_{i-1} =$$

$$= \frac{\varepsilon_{i-1} - \varepsilon_i}{(c_{i-1} - c_i)}(x - x_{i-1}) + \frac{\dfrac{c_{i-1}(\varepsilon_{i-1} - \varepsilon_i)}{\Delta l} - \dfrac{\varepsilon_{i-1}(c_{i-1} - c_i)}{\Delta l}}{\dfrac{(c_{i-1} - c_i)^2}{(\Delta l)^2}} \left\{ \log_e \left[-\frac{(c_{i-1} - c_i)}{\Delta l}(x - x_{i-1}) + c_{i-1} \right] - \log_e c_{i-1} \right\} + \theta_{i-1}$$

$$= \frac{\varepsilon_{i-1}-\varepsilon_i}{(c_{i-1}-c_i)}(x-x_{i-1}) + \Delta l \frac{\varepsilon_{i-1}c_i - \varepsilon_i c_{i-1}}{(c_{i-1}-c_i)^2}\left\{\log_e\left[-\frac{(c_{i-1}-c_i)}{\Delta l}(x-x_{i-1})+c_{i-1}\right]-\log_e c_{i-1}\right\}+\theta_{i-1} \qquad \text{(A4)}$$

At the strain-sensing station, x_i, one can write $x_i - x_{i-1} \equiv \Delta l$, and equation (A4) yields the slope angle $\theta_i[\equiv \theta(x_i)]$ at the strain-sensing station, x_i, as equation (A5):

$$\theta_i = \frac{\varepsilon_{i-1}-\varepsilon_i}{(c_{i-1}-c_i)}\Delta l + \Delta l \frac{\varepsilon_{i-1}c_i - \varepsilon_i c_{i-1}}{(c_{i-1}-c_i)^2}\left(\log_e c_i - \log_e c_{i-1}\right)+\theta_{i-1} \qquad ; \quad (i=1,2,3,...,n) \qquad \text{(A5)}$$

After grouping terms, equation (A5) becomes the final form of the slope-angle equation (A6) for the nonuniform embedded beams:

$$\theta_i = \Delta l\left[\frac{\varepsilon_{i-1}-\varepsilon_i}{(c_{i-1}-c_i)} - \frac{\varepsilon_{i-1}c_i - \varepsilon_i c_{i-1}}{(c_{i-1}-c_i)^2}\log_e\frac{c_i}{c_{i-1}}\right]+\theta_{i-1} \quad ; \quad (i=1,2,3,...,n) \qquad \text{(A6)}$$

Equation (A6) is the nonuniform part of equation (18a) in the text.

Curved Deflection Equations

The curved deflection, $\hat{y}(x)$, of the nonuniform embedded beam in the domain $x_{i-1} \le x \le x_i$ between the two adjacent strain-sensing stations, $\{x_{i-1}, x_i\}$, is given by equation (A7) [see equation (17)]:

$$\hat{y}(x) = \int_{x_{i-1}}^{x}\underbrace{\left[\int_{x_{i-1}}^{x}\frac{\varepsilon(x)}{c(x)}dx+\theta_{i-1}\right]}_{\theta(x)}dx+\hat{y}_{i-1} = \int_{x_{i-1}}^{x}\theta(x)dx+\hat{y}_{i-1} \quad ; \quad (x_{i-1}\le x\le x_i) \qquad \text{(A7)}$$

Substitute equations (A1) and (A2) into equation (A7), and carrying out the integration as follows in equation (A8) (ref. 4):

$$\hat{y}(x) = \int_{x_{i-1}}^{x}\underbrace{\left[\int_{x_{i-1}}^{x}\frac{\varepsilon_{i-1}-(\varepsilon_{i-1}-\varepsilon_i)\dfrac{x-x_{i-1}}{\Delta l}}{c_{i-1}-(c_{i-1}-c_i)\dfrac{x-x_{i-1}}{\Delta l}}+\theta_{i-1}\right]}_{\theta(x)}dx+\hat{y}_{i-1} =$$

$$= \int_{x_{i-1}}^{x_i}\left\{\frac{\varepsilon_{i-1}-\varepsilon_i}{(c_{i-1}-c_i)}(x-x_{i-1}) + \Delta l\frac{\varepsilon_{i-1}c_i-\varepsilon_i c_{i-1}}{(c_{i-1}-c_i)^2}\left[\log_e\left(-\frac{(c_{i-1}-c_i)}{\Delta l}(x-x_{i-1})+c_{i-1}\right)-\log_e c_{i-1}\right]\right\}dx$$
$$+\hat{y}_{i-1}+(x-x_{i-1})\theta_{i-1}$$

$$= \frac{\varepsilon_{i-1}-\varepsilon_i}{2(c_{i-1}-c_i)}(x-x_{i-1})^2 + \Delta l \frac{\frac{\varepsilon_{i-1}c_i-\varepsilon_i c_{i-1}}{(c_{i-1}-c_i)^2}}{-\frac{(c_{i-1}-c_i)}{\Delta l}}\left[\frac{-(c_{i-1}-c_i)}{\Delta l}(x-x_{i-1})+c_{i-1}\right]\times$$

$$\times\left\{\left[\log_e\left(\frac{-(c_{i-1}-c_i)}{\Delta l}(x-x_{i-1})+c_{i-1}\right)-\log_e c_{i-1}\right]-\left(-\frac{(c_{i-1}-c_i)}{\Delta l}\right)(x-x_{i-1})\right\}+\hat{y}_{i-1}+(x-x_{i-1})\theta_{i-1} \quad \text{(A8)}$$

At the strain-sensing station, x_i, one can write $x_i - x_{i-1} \equiv \Delta l$, and equation (A8) yields the curved deflection, $\hat{y}_i[\equiv \hat{y}(x_i)]$, at the strain-sensing station, x_i, as equation (A9):

$$\hat{y}_i = \frac{\varepsilon_{i-1}-\varepsilon_i}{2(c_{i-1}-c_i)}(\Delta l)^2 - (\Delta l)^2\frac{\varepsilon_{i-1}c_i-\varepsilon_i c_{i-1}}{(c_{i-1}-c_i)^3}\times$$

$$\times\left\{\left[\frac{-(c_{i-1}-c_i)}{\Delta l}\Delta l + c_{i-1}\right]\left[\log_e\left(\frac{-(c_{i-1}-c_i)}{\Delta l}\Delta l + c_{i-1}\right)-\log_e c_{i-1}\right]+\frac{(c_{i-1}-c_i)}{\Delta l}\Delta l\right\}+\hat{y}_{i-1}+(\Delta l)\theta_{i-1}$$

$$= (\Delta l)^2\left\{\frac{\varepsilon_{i-1}-\varepsilon_i}{2(c_{i-1}-c_i)}-\frac{\varepsilon_{i-1}c_i-\varepsilon_i c_{i-1}}{(c_{i-1}-c_i)^3}\left[c_i\left(\log_e c_i-\log_e c_{i-1}\right)+(c_{i-1}-c_i)\right]\right\}+\hat{y}_{i-1}+(\Delta l)\theta_{i-1} \quad \text{(A9)}$$

$$(i=1,2,3,...,n)$$

Equation (A9) can be written in the final form of the deflection equation for the nonuniform embedded beams as equation (A10):

$$\hat{y}_i = (\Delta l)^2\left\{\frac{\varepsilon_{i-1}-\varepsilon_i}{2(c_{i-1}-c_i)}-\frac{\varepsilon_{i-1}c_i-\varepsilon_i c_{i-1}}{(c_{i-1}-c_i)^3}\left[c_i\log_e\frac{c_i}{c_{i-1}}+(c_{i-1}-c_i)\right]\right\}+\hat{y}_{i-1}+(\Delta l)\theta_{i-1} \quad \text{(A10)}$$

$$(i=1,2,3,...,n)$$

Equation (A10) is the nonuniform part of equation (18b) in the text.

APPENDIX B
DERIVATIONS OF CURVED DEFLECTION EQUATIONS IN SUMMATION FORMS FOR NONUNIFORM EMBEDDED BEAMS

Appendix B presents mathematical steps to obtain the final dual summation forms given by the nonuniform part of equation (18c). The slope-angle equation (A6) and the deflection equation (A10) in recursive forms for nonuniform embedded beams are duplicated below as equations (B1) and (B2).

Slope angle equation:

$$\theta_i = \Delta l \left[\frac{\varepsilon_{i-1} - \varepsilon_i}{(c_{i-1} - c_i)} - \frac{\varepsilon_{i-1} c_i - \varepsilon_i c_{i-1}}{(c_{i-1} - c_i)^2} \log_e \frac{c_i}{c_{i-1}} \right] + \theta_{i-1} \quad ; \quad (i = 1,2,3,...,n) \tag{B1}$$

Curved deflection equation:

$$\hat{y}_i = (\Delta l)^2 \left\{ \frac{\varepsilon_{i-1} - \varepsilon_i}{2(c_{i-1} - c_i)} - \frac{\varepsilon_{i-1} c_i - \varepsilon_i c_{i-1}}{(c_{i-1} - c_i)^3} \left[c_i \log_e \frac{c_i}{c_{i-1}} + (c_{i-1} - c_i) \right] \right\} + \hat{y}_{i-1} + (\Delta l)\theta_{i-1} \tag{B2}$$
$$(i = 1,2,3,...,n)$$

Equations (B1) and (B2) can be combined into a single deflection equation in dual summation form as follows. Writing out equation (B2) for different indices, *i*, and making use of the indicial relationships expressed in equations (B1) and (B2), one obtains equations (B3) through (B6):

For $i = 1$:

$$\hat{y}_1 = (\Delta l)^2 \left\{ \frac{\varepsilon_0 - \varepsilon_1}{2(c_0 - c_1)} - \frac{\varepsilon_0 c_1 - \varepsilon_1 c_0}{(c_0 - c_1)^3} \left[c_1 \log_e \frac{c_1}{c_0} + (c_0 - c_1) \right] \right\} + \hat{y}_0 + (\Delta l)\theta_0 \tag{B3}$$

For $i = 2$:

$$\hat{y}_2 = (\Delta l)^2 \left\{ \frac{\varepsilon_1 - \varepsilon_2}{2(c_1 - c_2)} - \frac{\varepsilon_1 c_2 - \varepsilon_2 c_1}{(c_1 - c_2)^3} \left[c_2 \log_e \frac{c_2}{c_1} + (c_1 - c_2) \right] \right\} + \hat{y}_1 + (\Delta l)\theta_1$$

$$= (\Delta l)^2 \left\{ \frac{\varepsilon_1 - \varepsilon_2}{2(c_1 - c_2)} - \frac{\varepsilon_1 c_2 - \varepsilon_2 c_1}{(c_1 - c_2)^3} \left[c_2 \log_e \frac{c_2}{c_1} + (c_1 - c_2) \right] \right\}$$

$$+ \overbrace{(\Delta l)^2 \left\{ \frac{\varepsilon_0 - \varepsilon_1}{2(c_0 - c_1)} - \frac{\varepsilon_0 c_1 - \varepsilon_1 c_0}{(c_0 - c_1)^3} \left[c_1 \log_e \frac{c_1}{c_0} + (c_0 - c_1) \right] \right\} + \hat{y}_0}^{\hat{y}_1} + (\Delta l)\theta_0$$

$$+ \overbrace{(\Delta l)^2 \left[\frac{\varepsilon_0 - \varepsilon_1}{c_0 - c_1} + \frac{\varepsilon_0 c_1 - \varepsilon_1 c_0}{(c_0 - c_1)^2} \log_e \frac{c_1}{c_0} \right]}^{(\Delta l)\theta_1} + (\Delta l)\theta_0$$

$$= (\Delta l)^2 \left\{ \frac{\varepsilon_1 - \varepsilon_2}{2(c_1 - c_2)} - \frac{\varepsilon_1 c_2 - \varepsilon_2 c_1}{(c_1 - c_2)^3} \left[c_2 \log_e \frac{c_2}{c_1} + (c_1 - c_2) \right] + \frac{\varepsilon_0 - \varepsilon_1}{2(c_0 - c_1)} - \frac{\varepsilon_0 c_1 - \varepsilon_1 c_0}{(c_0 - c_1)^3} \left[c_1 \log_e \frac{c_1}{c_0} + (c_0 - c_1) \right] \right\}$$
$$+ (\Delta l)^2 \left[\frac{\varepsilon_0 - \varepsilon_1}{c_0 - c_1} + \frac{\varepsilon_0 c_1 - \varepsilon_1 c_0}{(c_0 - c_1)^2} \log_e \frac{c_1}{c_0} \right] + \hat{y}_0 + 2(\Delta l)\theta_0$$

(B4)

For $i = 3$:

$$\hat{y}_3 = (\Delta l)^2 \left\{ \frac{\varepsilon_2 - \varepsilon_3}{2(c_2 - c_3)} - \frac{\varepsilon_2 c_3 - \varepsilon_3 c_2}{(c_2 - c_3)^3} \left[c_3 \log_e \frac{c_3}{c_2} + (c_2 - c_3) \right] \right\} + \hat{y}_2 + (\Delta l)\theta_2$$
$$= (\Delta l)^2 \left\{ \frac{\varepsilon_2 - \varepsilon_3}{2(c_2 - c_3)} - \frac{\varepsilon_2 c_3 - \varepsilon_3 c_2}{(c_2 - c_3)^3} \left[c_3 \log_e \frac{c_3}{c_2} + (c_2 - c_3) \right] \right\}$$
$$+ \overbrace{\left\{ \begin{array}{l} (\Delta l)^2 \left\{ \frac{\varepsilon_1 - \varepsilon_2}{2(c_1 - c_2)} - \frac{\varepsilon_1 c_2 - \varepsilon_2 c_1}{(c_1 - c_2)^3} \left[c_2 \log_e \frac{c_2}{c_1} + (c_1 - c_2) \right] + \frac{\varepsilon_0 - \varepsilon_1}{2(c_0 - c_1)} - \frac{\varepsilon_0 c_1 - \varepsilon_1 c_0}{(c_0 - c_1)^3} \left[c_1 \log_e \frac{c_1}{c_0} + (c_0 - c_1) \right] \right\} \\ + (\Delta l)^2 \left[\frac{\varepsilon_0 - \varepsilon_1}{c_0 - c_1} + \frac{\varepsilon_0 c_1 - \varepsilon_1 c_0}{(c_0 - c_1)^2} \log_e \frac{c_1}{c_0} \right] + \hat{y}_0 + 2(\Delta l)\theta_0 \end{array} \right\}}^{\hat{y}_2}$$
$$+ \overbrace{(\Delta l)^2 \left[\frac{\varepsilon_1 - \varepsilon_2}{c_1 - c_2} + \frac{\varepsilon_1 c_2 - \varepsilon_2 c_1}{(c_1 - c_2)^2} \log_e \frac{c_2}{c_1} + \frac{\varepsilon_0 - \varepsilon_1}{c_0 - c_1} + \frac{\varepsilon_0 c_1 - \varepsilon_1 c_0}{(c_0 - c_1)^2} \log_e \frac{c_1}{c_0} \right] + (\Delta l)\theta_0}^{(\Delta l)\theta_2}$$
$$= (\Delta l)^2 \left\{ \frac{\varepsilon_2 - \varepsilon_3}{2(c_2 - c_3)} - \frac{\varepsilon_2 c_3 - \varepsilon_3 c_2}{(c_2 - c_3)^3} \left[c_3 \log_e \frac{c_3}{c_2} + (c_2 - c_3) \right] + \frac{\varepsilon_1 - \varepsilon_2}{2(c_1 - c_2)} - \frac{\varepsilon_1 c_2 - \varepsilon_2 c_1}{(c_1 - c_2)^3} \left[c_2 \log_e \frac{c_2}{c_1} + (c_1 - c_2) \right] \right.$$
$$\left. + \frac{\varepsilon_0 - \varepsilon_1}{2(c_0 - c_1)} - \frac{\varepsilon_0 c_1 - \varepsilon_1 c_0}{(c_0 - c_1)^3} \left[c_1 \log_e \frac{c_1}{c_0} + (c_0 - c_1) \right] \right\}$$
$$+ (\Delta l)^2 \left[\frac{\varepsilon_1 - \varepsilon_2}{c_1 - c_2} + \frac{\varepsilon_1 c_2 - \varepsilon_2 c_1}{(c_1 - c_2)^2} \log_e \frac{c_2}{c_1} + 2\frac{\varepsilon_0 - \varepsilon_1}{c_0 - c_1} + 2\frac{\varepsilon_0 c_1 - \varepsilon_1 c_0}{(c_0 - c_1)^2} \log_e \frac{c_1}{c_0} \right] + \hat{y}_0 + 3(\Delta l)\theta_0$$

(B5)

For $i = 4$:

$$\hat{y}_4 = (\Delta l)^2 \left\{ \frac{\varepsilon_3 - \varepsilon_4}{2(c_3 - c_4)} - \frac{\varepsilon_3 c_4 - \varepsilon_4 c_3}{(c_3 - c_4)^3} \left[c_4 \log_e \frac{c_4}{c_3} + (c_3 - c_4) \right] \right\} + \hat{y}_3 + (\Delta l)\theta_3$$

$$= (\Delta l)^2 \left\{ \frac{\varepsilon_3 - \varepsilon_4}{2(c_3 - c_4)} - \frac{\varepsilon_3 c_4 - \varepsilon_4 c_3}{(c_3 - c_4)^3} \left[c_4 \log_e \frac{c_4}{c_3} + (c_3 - c_4) \right] \right\}$$

$$+ \overbrace{\left\{ \begin{array}{l} (\Delta l)^2 \left\{ \frac{\varepsilon_2 - \varepsilon_3}{2(c_2 - c_3)} - \frac{\varepsilon_2 c_3 - \varepsilon_3 c_2}{(c_2 - c_3)^3} \left[c_3 \log_e \frac{c_3}{c_2} + (c_2 - c_3) \right] + \frac{\varepsilon_1 - \varepsilon_2}{2(c_1 - c_2)} - \frac{\varepsilon_1 c_2 - \varepsilon_2 c_1}{(c_1 - c_2)^3} \left[c_2 \log_e \frac{c_2}{c_1} + (c_1 - c_2) \right] \right. \\ \left. \quad + \frac{\varepsilon_0 - \varepsilon_1}{2(c_0 - c_1)} - \frac{\varepsilon_0 c_1 - \varepsilon_1 c_0}{(c_0 - c_1)^3} \left[c_1 \log_e \frac{c_1}{c_0} + (c_0 - c_1) \right] \right\} \\ + (\Delta l)^2 \left[\frac{\varepsilon_1 - \varepsilon_2}{c_1 - c_2} + \frac{\varepsilon_1 c_2 - \varepsilon_2 c_1}{(c_1 - c_2)^2} \log_e \frac{c_2}{c_1} + 2\frac{\varepsilon_0 - \varepsilon_1}{c_0 - c_1} + 2\frac{\varepsilon_0 c_1 - \varepsilon_1 c_0}{(c_0 - c_1)^2} \log_e \frac{c_1}{c_0} \right] + \hat{y}_0 + 3(\Delta l)\theta_0 \end{array} \right\}}^{\hat{y}_3}$$

$$+ \overbrace{\left\{ \begin{array}{l} (\Delta l)^2 \left[\frac{\varepsilon_2 - \varepsilon_3}{c_2 - c_3} + \frac{\varepsilon_2 c_3 - \varepsilon_3 c_2}{(c_2 - c_3)^2} \log_e \frac{c_3}{c_2} + \frac{\varepsilon_1 - \varepsilon_2}{c_1 - c_2} + \frac{\varepsilon_1 c_2 - \varepsilon_2 c_1}{(c_1 - c_2)^2} \log_e \frac{c_2}{c_1} \right. \\ \left. \quad + \frac{\varepsilon_0 - \varepsilon_1}{c_0 - c_1} + \frac{\varepsilon_0 c_1 - \varepsilon_1 c_0}{(c_0 - c_1)^2} \log_e \frac{c_1}{c_0} \right] + (\Delta l)\theta_0 \end{array} \right\}}^{(\Delta l)\theta_3}$$

$$= (\Delta l)^2 \left\{ \frac{\varepsilon_3 - \varepsilon_4}{2(c_3 - c_4)} - \frac{\varepsilon_3 c_4 - \varepsilon_4 c_3}{(c_3 - c_4)^3} \left[c_4 \log_e \frac{c_4}{c_3} + (c_3 - c_4) \right] + \frac{\varepsilon_2 - \varepsilon_3}{2(c_2 - c_3)} - \frac{\varepsilon_2 c_3 - \varepsilon_3 c_2}{(c_2 - c_3)^3} \left[c_3 \log_e \frac{c_3}{c_2} + (c_2 - c_3) \right] \right.$$
$$\left. + \frac{\varepsilon_1 - \varepsilon_2}{2(c_1 - c_2)} - \frac{\varepsilon_1 c_2 - \varepsilon_2 c_1}{(c_1 - c_2)^3} \left[c_2 \log_e \frac{c_2}{c_1} + (c_1 - c_2) \right] + \frac{\varepsilon_0 - \varepsilon_1}{2(c_0 - c_1)} - \frac{\varepsilon_0 c_1 - \varepsilon_1 c_0}{(c_0 - c_1)^3} \left[c_1 \log_e \frac{c_1}{c_0} + (c_0 - c_1) \right] \right\}$$
$$+ (\Delta l)^2 \left[\frac{\varepsilon_2 - \varepsilon_3}{c_2 - c_3} + \frac{\varepsilon_2 c_3 - \varepsilon_3 c_2}{(c_2 - c_3)^2} \log_e \frac{c_3}{c_2} + 2\frac{\varepsilon_1 - \varepsilon_2}{c_1 - c_2} + 2\frac{\varepsilon_1 c_2 - \varepsilon_2 c_1}{(c_1 - c_2)^2} \log_e \frac{c_2}{c_1} + 3\frac{\varepsilon_0 - \varepsilon_1}{c_0 - c_1} + 3\frac{\varepsilon_0 c_1 - \varepsilon_1 c_0}{(c_0 - c_1)^2} \log_e \frac{c_1}{c_0} \right]$$
$$+ \hat{y}_0 + 4(\Delta l)\theta_0 \qquad \text{(B6)}$$

Based on the indicial progression patterns in equations (B3) through (B6), one can write the curved deflection, $\hat{y}_i$, in a generalized form with two summations (with different summation limits) as equation (B7):

$$\hat{y}_i = (\Delta l)^2 \sum_{j=1}^{i} \left\{ \frac{\varepsilon_{j-1} - \varepsilon_j}{2(c_{j-1} - c_j)} - \frac{\varepsilon_{j-1} c_j - \varepsilon_j c_{j-1}}{(c_{j-1} - c_j)^3} \left[c_j \log_e \frac{c_j}{c_{j-1}} + (c_{j-1} - c_j) \right] \right\}$$
$$+ (\Delta l)^2 \sum_{j=1}^{i-1} (i - j) \left[\frac{\varepsilon_{j-1} - \varepsilon_j}{c_{j-1} - c_j} + \frac{\varepsilon_{j-1} c_j - \varepsilon_j c_{j-1}}{(c_{j-1} - c_j)^2} \log_e \frac{c_j}{c_{j-1}} \right] + \hat{y}_0 + (i)(\Delta l)\theta_0 \qquad \text{(B7)}$$
$$(i = 1, 2, 3, ..., n)$$

Equation (B7) is the nonlinear part of equation (18c) in the text. A set of three equations (B1), (B2), and (B7) are called Curved Displacement Transfer Functions for the nonuniform embedded beams.

It must be mentioned that equations (B1), (B2), and (B7)} or eqs. (18a)−(18c) in the text cannot be applied directly to the uniform embedded beam because, in the limit of $(c_{i-1} = c_i)$, the logarithmic terms and the denominators with $(c_{i-1} - c_i)$ factors will go to zero [that is, $\log_e(c_i / c_{i-1}) = 0$, $(c_{i-1} - c_i) = 0$], causing mathematical indeterminacy. Therefore, for the uniform embedded beams, slope and deflection equations can be derived separately using a constant depth factor, $c(x) = c$, in the piecewise integrations of equation (13) as shown in Appendix C.

APPENDIX C
DERIVATIONS OF SLOPE ANGLE AND CURVED DEFLECTION EQUATIONS IN RECURSIVE FORMS FOR UNIFORM EMBEDDED BEAMS

Appendix C presents the details of integrations of the slope angle equation (15) and the curved deflection equation (17) for the uniform beams based on piecewise linear strain representations to obtain the uniform parts of equations (18a) and (18b) for the uniform embedded beams.

Slope Angle Equation

For the uniform embedded beam with constant depth factor, $c(x) = c$, the slope angle equation (15) [or equation (A3) of Appendix A] for the domain $x_{i-1} \le x \le x_i$ between the two adjacent strain-sensing stations, $\{x_{i-1}, x_i\}$, becomes equation (C1):

$$\theta(x) = \underbrace{\int_{x_{i-1}}^{x} \frac{\varepsilon(x)}{c} dx}_{\text{Slope increment}} + \underbrace{\theta_{i-1}}_{\substack{\text{Slope} \\ \text{at } x_{i-1}}} \quad ; \quad (x_{i-1} \le x \le x_i) \tag{C1}$$

Based on the linear representation of surface strains, $\varepsilon(x)$, in the domain $x_{i-1} \le x \le x_i$ shown in equation (C2):

$$\varepsilon(x) = \varepsilon_{i-1} - (\varepsilon_{i-1} - \varepsilon_i)\frac{x - x_{i-1}}{\Delta l} \quad ; \quad (x_{i-1} \le x \le x_i) \tag{C2}$$

equation (C1) can be integrated to yield equation (C3) (ref. 21):

$$\begin{aligned} \theta(x) &= \frac{1}{c}\int_{x_{i-1}}^{x} \left[\varepsilon_{i-1} - (\varepsilon_{i-1} - \varepsilon_i)\frac{x - x_{i-1}}{\Delta l} \right] dx + \theta_{i-1} \\ &= \frac{1}{c}\left[\varepsilon_{i-1}(x - x_{i-1}) - (\varepsilon_{i-1} - \varepsilon_i)\frac{(x - x_{i-1})^2}{2\Delta l} \right] + \theta_{i-1} \end{aligned} \tag{C3}$$

At the strain-sensing station, x_i, one can write $x_i - x_{i-1} \equiv \Delta l$, and equation (C3) yields the slope angle, $\theta_i [\equiv \theta(x_i)]$, at the strain-sensing station, x_i, as equation (C4):

$$\theta_i = \frac{1}{c}\left[\varepsilon_{i-1}(\Delta l) - (\varepsilon_{i-1} - \varepsilon_i)\frac{(\Delta l)^2}{2\Delta l} \right] + \theta_{i-1} \quad ; \quad (i = 1,2,3,...,n) \tag{C4}$$

After grouping terms, equation (C4) takes on the final form of the slope angle equation for the uniform embedded beam as equation (C5):

$$\theta_i = \frac{\Delta l}{2c}\left(\varepsilon_{i-1} + \varepsilon_i\right) + \theta_{i-1} \quad ; \quad (i = 1,2,3,...,n) \tag{C5}$$

Equation (C5) is the uniform part of equation (18a) in the text.

Curved Deflection Equations

For the uniform embedded beam with constant depth factor, $c(x) = c$, the curved deflection equation (17) for the uniform embedded beam in the domain $x_{i-1} \le x \le x_i$ between the two adjacent strain-sensing stations, $\{x_{i-1}, x_i\}$, becomes equation (C6):

$$\hat{y}(x) = \int_{x_{i-1}}^{x} \underbrace{\left[\int_{x_{i-1}}^{x} \frac{\varepsilon(x)}{c} dx + \theta_{i-1} \right]}_{\theta(x)} dx + \hat{y}_{i-1} = \int_{x_{i-1}}^{x} \theta(x)\, dx + \hat{y}_{i-1} \quad ; \quad (x_{i-1} \le x \le x_i) \tag{C6}$$

Substitute equation (C2) into equation (C6), and carrying out the integrations as follows in equation (C7) (ref. 19):

$$\begin{aligned} \hat{y}(x) &= \frac{1}{c} \int_{x_{i-1}}^{x} \int_{x_{i-1}}^{x} \left[\varepsilon_{i-1} - (\varepsilon_{i-1} - \varepsilon_i) \frac{x - x_{i-1}}{\Delta l} \right] dx\, dx + \hat{y}_{i-1} + \int_{x_{i-1}}^{x} \theta_{i-1}\, dx \\ &= \frac{1}{c} \int_{x_{i-1}}^{x} \left[\varepsilon_{i-1}(x - x_{i-1}) - (\varepsilon_{i-1} - \varepsilon_i) \frac{(x - x_{i-1})^2}{2\Delta l} \right] dx + \hat{y}_{i-1} + (x - x_{i-1})\theta_{i-1} \\ &= \frac{1}{c} \left[\varepsilon_{i-1} \frac{(x - x_{i-1})^2}{2} - (\varepsilon_{i-1} - \varepsilon_i) \frac{(x - x_{i-1})^3}{6\Delta l} \right] + \hat{y}_{i-1} + (x - x_{i-1})\theta_{i-1} \end{aligned} \tag{C7}$$

At the strain-sensing station, x_i, one can write $x_i - x_{i-1} \equiv \Delta l$, and equation (C7) yields the curved deflection, $\hat{y}_i [\equiv \hat{y}(x_i)]$ at the strain-sensing station, x_i, as equation (C8):

$$\hat{y}_i = \frac{1}{c} \left[\varepsilon_{i-1} \frac{(\Delta l)^2}{2} - (\varepsilon_{i-1} - \varepsilon_i) \frac{(\Delta l)^3}{6\Delta l} \right] + \hat{y}_{i-1} + (\Delta l)\theta_{i-1} \quad ; \quad (i = 1,2,3,...,n) \tag{C8}$$

After grouping terms, equation (C8) takes on the final form of curved deflection equation for the uniform embedded beam as equation (C9):

$$\hat{y}_i = \frac{(\Delta l)^2}{6c} \left(2\varepsilon_{i-1} + \varepsilon_i \right) + \hat{y}_{i-1} + (\Delta l)\theta_{i-1} \quad ; \quad (i = 1,2,3,...,n) \tag{C9}$$

Equation (C9) is the uniform part of equation (18b) in the text.

APPENDIX D
DERIVATIONS OF CURVED DEFLECTION EQUATIONS IN SUMMATION FORMS FOR UNIFORM EMBEDDED BEAMS

Appendix D presents mathematical steps to obtain the final summation forms of the curved deflection equation given by the uniform part of equations (18c) using the slope angle equation (C5) and the curved deflection equation (C9) in recursive forms for uniform embedded beams. Equations (C5) and (C6) are duplicated below respectively as equations (D1) and (D2):

$$\theta_i = \frac{\Delta l}{2c}\left(\varepsilon_{i-1} + \varepsilon_i\right) + \theta_{i-1} \qquad ; \qquad (i = 1,2,3,...,n) \tag{D1}$$

$$\hat{y}_i = \frac{(\Delta l)^2}{6c}\left(2\varepsilon_{i-1} + \varepsilon_i\right) + \hat{y}_{i-1} + (\Delta l)\theta_{i-1} \qquad ; \qquad (i = 1,2,3,...,n) \tag{D2}$$

By combining equations (D1) and (D2), one can obtain a single curved deflection equation for $\hat{y}_i$, which can be written out for different indices, *i*, in the forms of equations (D3) through (D6):

For *i* = 1:

$$\hat{y}_1 = \frac{(\Delta l)^2}{6c}\left(2\varepsilon_0 + \varepsilon_1\right) + (\Delta l)\theta_0 + \hat{y}_0 \tag{D3}$$

For *i* = 2:

$$\begin{aligned}
\hat{y}_2 &= \frac{(\Delta l)^2}{6c}\left(2\varepsilon_1 + \varepsilon_2\right) + \hat{y}_1 + (\Delta l)\theta_1 \\
&= \frac{(\Delta l)^2}{6c}\left(2\varepsilon_1 + \varepsilon_2\right) + \underbrace{\frac{(\Delta l)^2}{6c}\left(2\varepsilon_0 + \varepsilon_1\right) + (\Delta l)\theta_0 + \hat{y}_0}_{\hat{y}_1} + \underbrace{\frac{(\Delta l)^2}{2c}\left(\varepsilon_0 + \varepsilon_i\right) + (\Delta l)\theta_0}_{(\Delta l)\theta_1} \\
&= \frac{(\Delta l)^2}{6c}\left(2\varepsilon_1 + \varepsilon_2\right) + \frac{(\Delta l)^2}{6c}\left(2\varepsilon_0 + \varepsilon_1\right) + \frac{(\Delta l)^2}{2c}\left(\varepsilon_0 + \varepsilon_i\right) + \hat{y}_0 + 2(\Delta l)\theta_0
\end{aligned} \tag{D4}$$

For *i* = 3:

$$\begin{aligned}
\hat{y}_3 &= \frac{(\Delta l)^2}{6c}\left(2\varepsilon_2 + \varepsilon_3\right) + \hat{y}_2 + (\Delta l)\theta_2 \\
&= \frac{(\Delta l)^2}{6c}\left(2\varepsilon_2 + \varepsilon_3\right) + \underbrace{\frac{(\Delta l)^2}{6c}\left(2\varepsilon_1 + \varepsilon_2\right) + \frac{(\Delta l)^2}{6c}\left(2\varepsilon_0 + \varepsilon_1\right) + \frac{(\Delta l)^2}{2c}\left(\varepsilon_0 + \varepsilon_i\right) + \hat{y}_0 + 2(\Delta l)\theta_0}_{\hat{y}_2} \\
&\quad + \underbrace{\frac{(\Delta l)^2}{2c}\left(\varepsilon_1 + \varepsilon_2\right) + \frac{(\Delta l)^2}{2c}\left(\varepsilon_0 + \varepsilon_1\right) + (\Delta l)\theta_0}_{(\Delta l)\theta_2}
\end{aligned} \tag{D5}$$

$$= \frac{(\Delta l)^2}{6c}(2\varepsilon_2 + \varepsilon_3) + \frac{(\Delta l)^2}{6c}(2\varepsilon_1 + \varepsilon_2) + \frac{(\Delta l)^2}{6c}(2\varepsilon_0 + \varepsilon_1) + \frac{(\Delta l)^2}{2c}(\varepsilon_1 + \varepsilon_2) + 2\frac{(\Delta l)^2}{2c}(\varepsilon_0 + \varepsilon_1)$$
$$+ \hat{y}_0 + 3(\Delta l)\theta_0$$

For $i = 4$:

$$\hat{y}_4 = \frac{(\Delta l)^2}{6c}(2\varepsilon_3 + \varepsilon_4) + \hat{y}_3 + (\Delta l)\theta_3$$
$$= \frac{(\Delta l)^2}{6c}(2\varepsilon_3 + \varepsilon_4) + \underbrace{\left\{\begin{array}{l} \frac{(\Delta l)^2}{6c}(2\varepsilon_2 + \varepsilon_3) + \frac{(\Delta l)^2}{6c}(2\varepsilon_1 + \varepsilon_2) + \frac{(\Delta l)^2}{6c}(2\varepsilon_0 + \varepsilon_1) \\ + \frac{(\Delta l)^2}{2c}(\varepsilon_1 + \varepsilon_2) + 2\frac{(\Delta l)^2}{2c}(\varepsilon_0 + \varepsilon_1) + \hat{y}_0 + 3(\Delta l)\theta_0 \end{array}\right\}}_{\hat{y}_3} \qquad \text{(D6)}$$
$$+ \underbrace{\frac{(\Delta l)^2}{2c}(\varepsilon_2 + \varepsilon_3) + \frac{(\Delta l)^2}{2c}(\varepsilon_1 + \varepsilon_2) + \frac{(\Delta l)^2}{2c}(\varepsilon_0 + \varepsilon_1) + (\Delta l)\theta_0}_{(\Delta l)\theta_3}$$
$$= \frac{(\Delta l)^2}{6c}(2\varepsilon_3 + \varepsilon_4) = \frac{(\Delta l)^2}{6c}(2\varepsilon_2 + \varepsilon_3) + \frac{(\Delta l)^2}{6c}(2\varepsilon_1 + \varepsilon_2) + \frac{(\Delta l)^2}{6c}(2\varepsilon_0 + \varepsilon_1)$$
$$+ \frac{(\Delta l)^2}{2c}(\varepsilon_2 + \varepsilon_3) + 2\frac{(\Delta l)^2}{2c}(\varepsilon_1 + \varepsilon_2) + 3\frac{(\Delta l)^2}{2c}(\varepsilon_0 + \varepsilon_1) + \hat{y}_0 + 4(\Delta l)\theta_0$$

Based on the indicial progression patterns in equations (D3) through (D6), one can write the deflection, $\hat{y}_i$, in a generalized form with two summations (with different summation limits) as equation (D7):

$$\hat{y}_i = \underbrace{\frac{(\Delta l)^2}{6c}\sum_{j=1}^{i}(2\varepsilon_{j-1} + \varepsilon_j)}_{\text{Contributions from deflection terms}} + \underbrace{\frac{(\Delta l)^2}{2c}\sum_{j=1}^{i-1}(i-j)(\varepsilon_{j-1} + \varepsilon_j)}_{\text{Contributions from slope terms}} + \underbrace{\hat{y}_0 + (i)(\Delta l)\theta_0}_{=0 \text{ for cantilever beams}} \qquad \text{(D7)}$$
$$(i = 1,2,3,...,n)$$

Equation (D7) is the uniform part of equation (18c) in the text. A set of three equations {(D1), (D2), and (D7)} are called the Curved Displacement Transfer Functions for the uniform embedded beams.

APPENDIX E
DERIVATIONS OF IMPROVED SLOPE ANGLE AND CURVED DEFLECTION EQUATIONS IN RECURSIVE FORMS FOR NONUNIFORM EMBEDDED BEAMS

Appendix E presents the details of integrations of the slope angle equation (15) and the curved deflection equation (17) for the nonuniform embedded beams to obtain the final mathematical forms given respectively by the nonuniform parts of equations (19a) and (19b).

Piecewise Nonlinear Strain Representations

For the piecewise integrations of the slope angle equation (15) and the curved deflection equation (17), the depth factors and surface strains, $\{c(x),\varepsilon(x)\}$, in the domain $x_{i-1} \le x \le x_i$ between the two adjacent strain-sensing stations, $\{x_{i-1},x_i\}$, are described respectively with the following linear and nonlinear functions [eqs. (E1) and (E2)] [duplications of equations (11) and (13a)} respectively]:

$$c(x) = c_{i-1} + (c_i - c_{i-1})\frac{x - x_{i-1}}{\Delta l} \quad ; \quad (x_{i-1} \le x \le x_i) \tag{E1}$$

$$\varepsilon(x) = \varepsilon_{i-1} - \frac{3\varepsilon_{i-1} - 4\varepsilon_i + \varepsilon_{i+1}}{2\Delta l}(x - x_{i-1}) + \frac{\varepsilon_{i-1} - 2\varepsilon_i + \varepsilon_{i+1}}{2(\Delta l)^2}(x - x_{i-1})^2 \quad ; \quad (x_{i-1} \le x \le x_i) \tag{E2}$$

Improved Slope Angle Equations

The slope angle, $\theta(x)$ of the nonuniform embedded beam in the domain $x_{i-1} \le x \le x_i$ between the two adjacent strain-sensing stations, $\{x_{i-1},x_i\}$, is given by equation (E3) [duplication of equation (15)]:

$$\theta(x) = \underbrace{\int_{x_{i-1}}^{x} \frac{\varepsilon(x)}{c(x)}dx}_{\text{Slope increment}} + \underbrace{\theta_{i-1}}_{\substack{\text{Slope} \\ \text{at } x_{i-1}}} \quad ; \quad (x_{i-1} \le x \le x_i) \tag{E3}$$

Substitution of equations (E1) and (E2) into equation (E3) yields equations (E4) through (E8):

$$\theta(x) = \int_{x_{i-1}}^{x} \left[\frac{\varepsilon_{i-1} - \frac{3\varepsilon_{i-1} - 4\varepsilon_i + \varepsilon_{i+1}}{2\Delta l}(x - x_{i-1}) + \frac{\varepsilon_{i-1} - 2\varepsilon_i + \varepsilon_{i+1}}{2(\Delta l)^2}(x - x_{i-1})^2}{c_{i-1} + \frac{c_i - c_{i-1}}{2\Delta l}(x - x_{i-1})} \right] dx + \theta_{i-1} \tag{E4}$$

Let

$$A \equiv -\frac{3\varepsilon_{i-1} - 4\varepsilon_i + \varepsilon_{i+1}}{2\Delta l} \tag{E5}$$

$$B \equiv \frac{\varepsilon_{i-1} - 2\varepsilon_i + \varepsilon_{i+1}}{2(\Delta l)^2} \tag{E6}$$

$$C \equiv \frac{c_i - c_{i-1}}{\Delta l} \tag{E7}$$

$$\xi \equiv (x - x_{i-1}) \tag{E8}$$

then equation (E4) takes on the following simplified form shown in equation (E9):

$$\theta(x) = \int_0^{\xi} \frac{\varepsilon_{i-1} + A\xi + B\xi^2}{c_{i-1} + C\xi} d\xi + \theta_{i-1} \tag{E9}$$

After carrying out integration of equation (E9), one obtains equation (E10) (ref. 19):

$$\theta(\xi) = \left[\underbrace{\frac{\varepsilon_{i-1}}{C} \log_e (c_{i-1} + C\xi)}_{\text{Integration of 1st term in eq. (E-4)}} + \underbrace{A\frac{\xi}{C} - A\frac{c_{i-1}}{C^2} \log_e (c_{i-1} + C\xi)}_{\text{Integration of 2nd term in eq. (E-4)}} + \underbrace{\frac{B}{C^3}\left[\frac{1}{2}(c_{i-1} + C\xi)^2 - 2c_{i-1}(c_{i-1} + C\xi) + c_{i-1}^2 \log_e (c_{i-1} + C\xi) \right]}_{\text{Integration of 3rd term in eq (E-4)}} \right]_0^{\xi} + \theta_{i-1}$$

$$\begin{aligned}
&= \left(\frac{\varepsilon_{i-1}}{C} - A\frac{c_{i-1}}{C^2} + B\frac{c_{i-1}^2}{C^3} \right) \log_e (c_{i-1} + C\xi) + \frac{A}{C}\xi + \frac{1}{2}\frac{B}{C^3}(c_{i-1} + C\xi)^2 - 2\frac{B}{C^3}c_{i-1}(c_{i-1} + C\xi) \\
&- \left(\frac{\varepsilon_{i-1}}{C} - A\frac{c_{i-1}}{C^2} + B\frac{c_{i-1}^2}{C^3} \right) \log_e c_{i-1} - \frac{1}{2}\frac{B}{C^3}c_{i-1}^2 + 2\frac{B}{C^3}c_{i-1}^2 + \theta_{i-1} \\
&= \frac{1}{C^3}\left[C^2\varepsilon_{i-1} - ACc_{i-1} + Bc_{i-1}^2 \right] \left[\log_e (c_{i-1} + C\xi) - \log_e c_{i-1} \right] + \frac{A}{C}\xi \\
&+ \frac{1}{2}\frac{B}{C^3}\left[(c_{i-1} + C\xi)^2 - c_{i-1}^2 \right] - 2\frac{B}{C^3}c_{i-1}\left[(c_{i-1} + C\xi) - c_{i-1} \right] + \theta_{i-1}
\end{aligned} \tag{E10}$$

$$\begin{aligned}
&= \frac{1}{C^3}\left[C^2\varepsilon_{i-1} - ACc_{i-1} + Bc_{i-1}^2 \right] \left[\log_e (c_{i-1} + C\xi) - \log_e c_{i-1} \right] + \frac{A}{C}\xi \\
&+ \frac{1}{2}\frac{B}{C^2}(2c_{i-1}\xi + C\xi^2) - 2\frac{B}{C^2}c_{i-1}\xi + \theta_{i-1}
\end{aligned}$$

$$\begin{aligned}
&= \frac{1}{C^3}\left[C^2\varepsilon_{i-1} - ACc_{i-1} + Bc_{i-1}^2 \right] \left[\log_e (c_{i-1} + C\xi) - \log_e c_{i-1} \right] + \frac{A}{C}\xi \\
&+ \frac{1}{2}\frac{B}{C^2}\left[-2c_{i-1}\xi + C\xi^2 \right] + \theta_{i-1}
\end{aligned}$$

In view of the definitions in equations (E5), (E6), (E7), and (E8), equation (E10) takes on the following form shown in equation (E11):

$$\theta(x)=\frac{(\Delta l)^3}{(c_i-c_{i-1})^3}\left[\varepsilon_{i-1}\frac{(c_i-c_{i-1})^2}{(\Delta l)^2}+\frac{(3\varepsilon_{i-1}-4\varepsilon_i+\varepsilon_{i+1})}{2\Delta l}\frac{(c_i-c_{i-1})}{\Delta l}c_{i-1}+\frac{(\varepsilon_{i-1}-2\varepsilon_i+\varepsilon_{i+1})}{2(\Delta l)^2}c_{i-1}^2\right]\times$$
$$\times\left[\log_e\left(c_{i-1}+\frac{c_i-c_{i-1}}{\Delta l}(x-x_{i-1})\right)-\log_e c_{i-1}\right]-\frac{(3\varepsilon_{i-1}-4\varepsilon_i+\varepsilon_{i+1})}{2\Delta l}\frac{\Delta l}{c_i-c_{i-1}}(x-x_{i-1})$$
$$+\frac{1}{2}\frac{(\varepsilon_{i-1}-2\varepsilon_i+\varepsilon_{i+1})}{2(\Delta l)^2}\frac{(\Delta l)^2}{(c_i-c_{i-1})^2}\left[-2c_{i-1}(x-x_{i-1})+\frac{c_i-c_{i-1}}{\Delta l}(x-x_{i-1})^2\right]+\theta_{i-1}$$

$$=\frac{\Delta l}{(c_i-c_{i-1})^3}\underbrace{\left[\varepsilon_{i-1}(c_i-c_{i-1})^2+\frac{1}{2}(3\varepsilon_{i-1}-4\varepsilon_i+\varepsilon_{i+1})(c_i-c_{i-1})c_{i-1}+\frac{1}{2}(\varepsilon_{i-1}-2\varepsilon_i+\varepsilon_{i+1})c_{i-1}^2\right]}_{I_1}\times \tag{E11}$$
$$\times\left[\log_e\left(c_{i-1}+\frac{c_i-c_{i-1}}{\Delta l}(x-x_{i-1})\right)-\log_e c_{i-1}\right]$$
$$\underbrace{-\frac{3\varepsilon_{i-1}-4\varepsilon_i+\varepsilon_{i+1}}{2(c_i-c_{i-1})}(x-x_{i-1})+\frac{\varepsilon_{i-1}-2\varepsilon_i+\varepsilon_{i+1}}{4(c_i-c_{i-1})^2}\left[-2c_{i-1}(x-x_{i-1})+\frac{c_i-c_{i-1}}{\Delta l}(x-x_{i-1})^2\right]}_{I_2}+\theta_{i-1}$$
$$(x_{i-1}\le x\le x_i)$$

In equation (E11), the two terms $\{I_1,I_2\}$ can be simplified through grouping terms as follows in equation (E12) and (E13):

$$I_1\equiv\varepsilon_{i-1}(c_i-c_{i-1})^2+\frac{1}{2}(3\varepsilon_{i-1}-4\varepsilon_i+\varepsilon_{i+1})(c_i-c_{i-1})c_{i-1}+\frac{1}{2}(\varepsilon_{i-1}-2\varepsilon_i+\varepsilon_{i+1})c_{i-1}^2$$
$$=\left[(c_i-c_{i-1})^2+\frac{3}{2}(c_i-c_{i-1})c_{i-1}+\frac{1}{2}c_{i-1}^2\right]\varepsilon_{i-1}-\left[2(c_i-c_{i-1})c_{i-1}+c_{i-1}^2\right]\varepsilon_i+\frac{1}{2}\left[(c_i-c_{i-1})c_{i-1}+c_{i-1}^2\right]\varepsilon_{i+1}$$
$$=\left(c_i^2-2c_ic_{i-1}+c_{i-1}^2+\frac{3}{2}c_ic_{i-1}-\frac{3}{2}c_{i-1}^2+\frac{1}{2}c_{i-1}^2\right)\varepsilon_{i-1}-(2c_i-c_{i-1})c_{i-1}\varepsilon_i+\frac{1}{2}c_ic_{i-1}\varepsilon_{i+1} \tag{E12}$$
$$=\frac{1}{2}\left[(2c_i-c_{i-1})c_i\varepsilon_{i-1}-2(2c_i-c_{i-1})c_{i-1}\varepsilon_i+c_ic_{i-1}\varepsilon_{i+1}\right]$$

$$I_2 \equiv -\frac{(3\varepsilon_{i-1}-4\varepsilon_i+\varepsilon_{i+1})}{2(c_i-c_{i-1})}(x-x_{i-1})+\frac{\varepsilon_{i-1}-2\varepsilon_i+\varepsilon_{i+1}}{4(c_i-c_{i-1})^2}\left[-2c_{i-1}(x-x_{i-1})+\frac{(c_i-c_{i-1})}{\Delta l}(x-x_{i-1})^2\right]$$

$$=\frac{1}{2(c_i-c_{i-1})^2}\left[(-3\varepsilon_{i-1}+4\varepsilon_i-\varepsilon_{i+1})(c_i-c_{i-1})-(\varepsilon_{i-1}-2\varepsilon_i+\varepsilon_{i+1})c_{i-1}\right](x-x_{i-1})$$

$$+\frac{\varepsilon_{i-1}-2\varepsilon_i+\varepsilon_{i+1}}{4(c_i-c_{i-1})}\frac{(x-x_{i-1})^2}{\Delta l}$$

$$=\frac{1}{2(c_i-c_{i-1})^2}\left\{\left[-3(c_i-c_{i-1})-c_{i-1}\right]\varepsilon_{i-1}+\left[4(c_i-c_{i-1})+2c_{i-1}\right]\varepsilon_i+\left[-(c_i-c_{i-1})-c_{i-1}\right]\varepsilon_{i+1}\right\}(x-x_{i-1})$$

$$+\frac{\varepsilon_{i-1}-2\varepsilon_i+\varepsilon_{i+1}}{4(c_i-c_{i-1})}\frac{(x-x_{i-1})^2}{\Delta l}$$

$$=\frac{1}{2(c_i-c_{i-1})^2}\left[(2c_{i-1}-3c_i)\varepsilon_{i-1}+2(2c_i-c_{i-1})\varepsilon_i-c_i\varepsilon_{i+1}\right](x-x_{i-1})+\frac{\varepsilon_{i-1}-2\varepsilon_i+\varepsilon_{i+1}}{4(c_i-c_{i-1})}\frac{(x-x_{i-1})^2}{\Delta l} \qquad \text{(E13)}$$

Substitutions of equations (E12) and (E13) into equation (E11) yields equation (E14):

$$\theta(x)=\frac{\Delta l}{2(c_i-c_{i-1})^3}\left[(2c_i-c_{i-1})(c_i\varepsilon_{i-1}-2c_{i-1}\varepsilon_i)+c_ic_{i-1}\varepsilon_{i+1}\right]\left[\log_e\left(c_{i-1}+\frac{c_i-c_{i-1}}{\Delta l}(x-x_{i-1})\right)-\log_e c_{i-1}\right]$$

$$+\frac{1}{2(c_i-c_{i-1})^2}\left[(2c_{i-1}-3c_i)\varepsilon_{i-1}+2(2c_i-c_{i-1})\varepsilon_i-c_i\varepsilon_{i+1}\right](x-x_{i-1})$$

$$+\frac{\varepsilon_{i-1}-2\varepsilon_i+\varepsilon_{i+1}}{4(c_i-c_{i-1})}\frac{(x-x_{i-1})^2}{\Delta l}+\theta_{i-1}$$

$$(x_{i-1}\le x\le x_i) \qquad \text{(E14)}$$

At the strain-sensing station x_i, one can write $x_i-x_{i-1}\equiv\Delta l$, and equation (E14) gives the slope, $\theta_i[\equiv\theta(x_i)]$, at the strain-sensing station, x_i, as equation (E15):

$$\theta_i=\frac{\Delta l}{2(c_i-c_{i-1})^3}\left[(2c_i-c_{i-1})(c_i\varepsilon_{i-1}-2c_{i-1}\varepsilon_i)+c_ic_{i-1}\varepsilon_{i+1}\right]\log_e\frac{c_i}{c_{i-1}}$$

$$+\underbrace{\frac{\Delta l}{2(c_i-c_{i-1})^2}\left[(2c_{i-1}-3c_i)\varepsilon_{i-1}+2(2c_i-c_{i-1})\varepsilon_i-c_i\varepsilon_{i+1}\right]+\frac{\varepsilon_{i-1}-2\varepsilon_i+\varepsilon_{i+1}}{4(c_i-c_{i-1})}}_{I_3}+\theta_{i-1} \qquad \text{(E15)}$$

$$(i=1,2,3,...,n)$$

The term I_3 in equation (E15) can be simplified as follows in equation (E16):

$$
\begin{aligned}
I_3 &\equiv \frac{\Delta l}{2(c_i - c_{i-1})^2}\left[(2c_{i-1} - 3c_i)\varepsilon_{i-1} + 2(2c_i - c_{i-1})\varepsilon_i - c_i\varepsilon_{i+1}\right] + \frac{\varepsilon_{i-1} - 2\varepsilon_i + \varepsilon_{i+1}}{4(c_i - c_{i-1})}\Delta l \\
&= \frac{\Delta l}{2(c_i - c_{i-1})^2}\left\{\left[2c_{i-1} - 3c_i + \frac{1}{2}(c_i - c_{i-1})\right]\varepsilon_{i-1} + \left[2(2c_i - c_{i-1}) - (c_i - c_{i-1})\right]\varepsilon_i \right. \\
&\qquad \left. - \left[c_i - \frac{1}{2}(c_i - c_{i-1})\right]\varepsilon_{i+1}\right\} \\
&= -\frac{\Delta l}{4(c_i - c_{i-1})^2}\left[(5c_i - 3c_{i-1})\varepsilon_{i-1} - 2(3c_i - c_{i-1})\varepsilon_i + (c_i + c_{i-1})\varepsilon_{i+1}\right]
\end{aligned}
\tag{E16}
$$

In view of equation (E16), equation (E15) takes on the final form as equation (E17):

$$
\begin{aligned}
\theta_i &= \frac{\Delta l}{2(c_i - c_{i-1})^3}\left[(2c_i - c_{i-1})(c_i\varepsilon_{i-1} - 2c_{i-1}\varepsilon_i) + c_i c_{i-1}\varepsilon_{i+1}\right]\log_e\frac{c_i}{c_{i-1}} \\
&\quad - \frac{\Delta l}{4(c_i - c_{i-1})^2}\left[(5c_i - 3c_{i-1})\varepsilon_{i-1} - 2(3c_i - c_{i-1})\varepsilon_i + (c_i + c_{i-1})\varepsilon_{i+1}\right] + \theta_{i-1} \\
&\qquad\qquad (i = 1,2,3,...,n)
\end{aligned}
\tag{E17}
$$

Equation (E17) is the nonlinear part of equation (19a) in the text.

Improved Curved Deflection Equations

The curved deflection, $\hat{y}(x)$, of the nonuniform embedded beam in the domain $x_{i-1} \le x \le x_i$ between the two adjacent strain-sensing stations, $\{x_{i-1}, x_i\}$, can be expressed as equation (E18) [see eq. (17)]:

$$
\hat{y}(x) = \int_{x_{i-1}}^{x} \underbrace{\left[\int_{x_{i-1}}^{x} \frac{\varepsilon(x)}{c(x)}dx + \theta_{i-1}\right]}_{\theta(x)} dx + \hat{y}_{i-1} = \int_{x_{i-1}}^{x} \theta(x)\,dx + \hat{y}_{i-1} \quad ; \quad (x_{i-1} \le x \le x_i)
\tag{E18}
$$

Substitution of equation (E14) into equation (E18) yields equation (E19):

$$
\begin{aligned}
\hat{y}(x) &= \frac{\Delta l}{2(c_i - c_{i-1})^3}\left[(2c_i - c_{i-1})(c_i\varepsilon_{i-1} - 2c_{i-1}\varepsilon_i) + c_i c_{i-1}\varepsilon_{i+1}\right] \times \\
&\qquad \times \int_{x_{i-1}}^{x}\left[\log_e\left(c_{i-1} + \frac{c_i - c_{i-1}}{\Delta l}(x - x_{i-1})\right) - \log_e c_{i-1}\right]dx \\
&\quad + \frac{1}{2(c_i - c_{i-1})^2}\left[(2c_{i-1} - 3c_i)\varepsilon_{i-1} + 2(2c_i - c_{i-1})\varepsilon_i - c_i\varepsilon_{i+1}\right]\int_{x_{i-1}}^{x}(x - x_{i-1})dx \\
&\quad + \frac{\varepsilon_{i-1} - 2\varepsilon_i + \varepsilon_{i+1}}{4(c_i - c_{i-1})}\int_{x_{i-1}}^{x}\frac{(x - x_{i-1})^2}{\Delta l}dx + \int_{x_{i-1}}^{x}\theta_{i-1}\,dx + \hat{y}_{i-1}
\end{aligned}
\tag{E19}
$$

Carrying out the integration of equation (E19), one obtains equation (E20) (ref. 21):

$$\hat{y}(x)=\frac{\Delta l}{2(c_i-c_{i-1})^3}\Big\{\Big[(2c_i-c_{i-1})(c_i\varepsilon_{i-1}-2c_{i-1}\varepsilon_i)+c_ic_{i-1}\varepsilon_{i+1}\Big]\times$$
$$\times\Bigg[\frac{\Delta l}{c_i-c_{i-1}}\Bigg\langle\Bigg(c_{i-1}+\frac{c_i-c_{i-1}}{\Delta l}(x-x_i)\Bigg)\log_e\Bigg(c_{i-1}+\frac{c_i-c_{i-1}}{\Delta l}(x-x_i)\Bigg)$$
$$-\frac{c_i-c_{i-1}}{\Delta l}(x-x_i)-c_{i-1}\log c_{i-1}\Bigg\rangle-(x-x_{i-1})\log_e c_{i-1}\Bigg]\Big\}$$
$$+\frac{1}{4(c_i-c_{i-1})^2}\Big[(2c_{i-1}-3c_i)\varepsilon_{i-1}+2(2c_i-c_{i-1})\varepsilon_i-c_i\varepsilon_{i+1}\Big](x-x_i)^2$$
$$+\frac{\varepsilon_{i-1}-2\varepsilon_i+\varepsilon_{i+1}}{12(c_i-c_{i-1})}\frac{(x-x_i)^3}{\Delta l}+(x-x_i)\theta_{i-1}+\hat{y}_{i-1}$$
$$(x_{i-1}\le x\le x_i) \qquad \text{(E20)}$$

At the strain-sensing station, x_i , one can write $x_i-x_{i-1}\equiv\Delta l$, and equation (E20) gives the curved deflection, $\hat{y}_i[\equiv\hat{y}(x_i)]$, at the strain-sensing station, x_i , as follows in equation (E21):

$$\hat{y}_i=\frac{(\Delta l)^2}{2(c_i-c_{i-1})^4}\Big\{\Big[(2c_i-c_{i-1})(c_i\varepsilon_{i-1}-2c_{i-1}\varepsilon_i)+c_ic_{i-1}\varepsilon_{i+1}\Big]\times$$
$$\times\Big[c_i\log_e c_i-(c_i-c_{i-1})-c_{i-1}\log_e c_{i-1}-(c_i-c_{i-1})\log_e c_{i-1}\Big]\Big\}$$
$$+\frac{(\Delta l)^2}{4(c_i-c_{i-1})^2}\Bigg[(2c_{i-1}-3c_i)\varepsilon_{i-1}+2(2c_i-c_{i-1})\varepsilon_i-c_i\varepsilon_{i+1}+\frac{1}{3}(\varepsilon_{i-1}-2\varepsilon_i+\varepsilon_{i+1})(c_i-c_{i-1})\Bigg]$$
$$+\hat{y}_{i-1}+(\Delta l)\theta_{i-1}$$
$$=\frac{(\Delta l)^2}{2(c_i-c_{i-1})^4}\Big[(2c_i-c_{i-1})(c_i\varepsilon_{i-1}-2c_{i-1}\varepsilon_i)+c_ic_{i-1}\varepsilon_{i+1}\Big]\Big[c_i(\log_e c_i-\log_e c_{i-1})-(c_i-c_{i-1})\Big]$$
$$+\frac{(\Delta l)^2}{4(c_i-c_{i-1})^2}\Bigg[\Bigg(2c_{i-1}-3c_i+\frac{c_i}{3}-\frac{c_{i-1}}{3}\Bigg)\varepsilon_{i-1}+\Bigg(4c_i-2c_{i-1}-\frac{2}{3}c_i+\frac{2}{3}c_{i-1}\Bigg)\varepsilon_i+\Bigg(-c_i+\frac{c_i}{3}-\frac{c_{i-1}}{3}\Bigg)\varepsilon_{i+1}\Bigg]$$
$$+\hat{y}_{i-1}+(\Delta l)\theta_{i-1}$$
$$(i=1,2,3,...,n) \qquad \text{(E21)}$$

After grouping terms, equation (E21) becomes equation (E22):

$$\hat{y}_i=\frac{(\Delta l)^2}{2(c_i-c_{i-1})^4}\Big[(2c_i-c_{i-1})(c_i\varepsilon_{i-1}-2c_{i-1}\varepsilon_i)+c_ic_{i-1}\varepsilon_{i+1}\Big]\Bigg[c_i\log_e\frac{c_i}{c_{i-1}}-(c_i-c_{i-1})\Bigg]$$
$$-\frac{(\Delta l)^2}{12(c_i-c_{i-1})^2}\Big[(8c_i-5c_{i-1})\varepsilon_{i-1}-2(5c_i-2c_{i-1})\varepsilon_i+(2c_i+c_{i-1})\varepsilon_{i+1}\Big]+\hat{y}_{i-1}+(\Delta l)\theta_{i-1} \qquad \text{(E22)}$$
$$(i=1,2,3,...,n)$$

Equation (E22) is the nonuniform part of equation (19b) in the text.

APPENDIX F
DERIVATIONS OF IMPROVED CURVED DEFLECTION EQUATIONS IN SUMMATION FORMS FOR NONUNIFORM EMBEDDED BEAMS

Appendix F presents the mathematical derivations of the nonuniform parts of the summation curved deflection equation (19c). The Improved slope angle equation (E17) and Improved curved deflection equation (E22) are duplicated below as equations (F1) and (F2) respectively:

$$\theta_i = \frac{\Delta l}{2(c_i - c_{i-1})^3}\left[(2c_i - c_{i-1})(c_i\varepsilon_{i-1} - 2c_{i-1}\varepsilon_i) + c_i c_{i-1}\varepsilon_{i+1}\right]\log_e \frac{c_i}{c_{i-1}}$$
$$- \frac{\Delta l}{4(c_i - c_{i-1})^2}\left[(5c_i - 3c_{i-1})\varepsilon_{i-1} - 2(3c_i - c_{i-1})\varepsilon_i + (c_i + c_{i-1})\varepsilon_{i+1}\right] + \theta_{i-1} \qquad (F1)$$
$$(i = 1,2,3,...,n)$$

$$\hat{y}_i = \frac{(\Delta l)^2}{2(c_i - c_{i-1})^4}\left[(2c_i - c_{i-1})(c_i\varepsilon_{i-1} - 2c_{i-1}\varepsilon_i) + c_i c_{i-1}\varepsilon_{i+1}\right]\left[c_i \log_e \frac{c_i}{c_{i-1}} - (c_i - c_{i-1})\right]$$
$$- \frac{(\Delta l)^2}{12(c_i - c_{i-1})^2}\left[(8c_i - 5c_{i-1})\varepsilon_{i-1} - 2(5c_i - 2c_{i-1})\varepsilon_i + (2c_i + c_{i-1})\varepsilon_{i+1}\right] + \hat{y}_{i-1} + (\Delta l)\theta_{i-1} \qquad (F2)$$
$$(i = 1,2,3,...,n)$$

Equations (F1) and (F2) can be combined into a single deflection equation in dual summation form as follows. Writing out equation (F2) for different indices, *i*, and making use of the indicial relationships expressed in equations (F1) and (F2), one obtains equations (F3) and (F4):

For *i* =1:

$$\hat{y}_1 = \frac{(\Delta l)^2}{2(c_1 - c_0)^4}\left[(2c_1 - c_0)c_1\varepsilon_0 - 2(2c_1 - c_0)c_0\varepsilon_1 + c_1 c_0\varepsilon_2\right]\left[c_1 \log_e \frac{c_1}{c_0} - (c_1 - c_0)\right] \qquad (F3)$$
$$- \frac{(\Delta l)^2}{12(c_1 - c_0)^2}\left[(8c_1 - 5c_0)\varepsilon_0 - 2(5c_1 - 2c_0)\varepsilon_1 + (2c_1 + c_0)\varepsilon_2\right] + \hat{y}_0 + (\Delta l)\theta_0$$

For *i* = 2:

$$\hat{y}_2 = \frac{(\Delta l)^2}{2(c_2 - c_1)^4}\left[(2c_2 - c_1)c_2\varepsilon_1 - 2(2c_2 - c_1)c_1\varepsilon_2 + c_2 c_1\varepsilon_3\right]\left[c_2 \log_e \frac{c_2}{c_1} - (c_2 - c_1)\right]$$
$$- \frac{(\Delta l)^2}{12(c_2 - c_1)^2}\left[(8c_2 - 5c_1)\varepsilon_1 - 2(5c_2 - 2c_1)\varepsilon_2 + (2c_2 + c_1)\varepsilon_3\right] + \hat{y}_1 + (\Delta l)\theta_1$$
$$= \frac{(\Delta l)^2}{2(c_2 - c_1)^4}\left[(2c_2 - c_1)c_2\varepsilon_1 - 2(2c_2 - c_1)c_1\varepsilon_2 + c_2 c_1\varepsilon_3\right]\left[c_2 \log_e \frac{c_2}{c_1} - (c_2 - c_1)\right]$$
$$- \frac{(\Delta l)^2}{12(c_2 - c_1)^2}\left[(8c_2 - 5c_1)\varepsilon_1 - 2(5c_2 - 2c_1)\varepsilon_2 + (2c_2 + c_1)\varepsilon_3\right]$$

$$+\underbrace{\begin{Bmatrix}\dfrac{(\Delta l)^2}{2(c_1-c_0)^4}\left[(2c_1-c_0)c_1\varepsilon_0-2(2c_1-c_0)c_0\varepsilon_1+c_1c_0\varepsilon_2\right]\left[c_1\log_e\dfrac{c_1}{c_0}-(c_1-c_0)\right]\\ -\dfrac{(\Delta l)^2}{12(c_1-c_0)^2}\left[(8c_1-5c_0)\varepsilon_0-2(5c_1-2c_0)\varepsilon_1+(2c_1+c_0)\varepsilon_2\right]+\hat{y}_0+(\Delta l)\theta_0\end{Bmatrix}}_{\hat{y}_1}$$

$$+\underbrace{\begin{Bmatrix}\dfrac{(\Delta l)^2}{2(c_1-c_0)^3}\left[(2c_1-c_0)c_1\varepsilon_0-2(2c_1-c_0)c_0\varepsilon_1+c_1c_0\varepsilon_2\right]\log_e\dfrac{c_1}{c_0}\\ -\dfrac{(\Delta l)^2}{4(c_1-c_0)^2}\left[(5c_1-3c_0)\varepsilon_0-2(3c_1-c_0)\varepsilon_1+(c_1+c_0)\varepsilon_2\right]+(\Delta l)\theta_0\end{Bmatrix}}_{(\Delta l)\theta_1} \tag{F4}$$

After grouping terms, equation (F4) becomes equations (F5) and (F6):

$$\hat{y}_2=\begin{Bmatrix}\dfrac{(\Delta l)^2}{2(c_2-c_1)^4}\left[(2c_2-c_1)c_2\varepsilon_1-2(2c_2-c_1)c_1\varepsilon_2+c_2c_1\varepsilon_3\right]\left[c_2\log_e\dfrac{c_2}{c_1}-(c_2-c_1)\right]\\ -\dfrac{(\Delta l)^2}{12(c_2-c_1)^2}\left[(8c_2-5c_1)\varepsilon_1-2(5c_2-2c_1)\varepsilon_2+(2c_2+c_1)\varepsilon_3\right]\end{Bmatrix}$$

$$+\begin{Bmatrix}\dfrac{(\Delta l)^2}{2(c_1-c_0)^4}\left[(2c_1-c_0)c_1\varepsilon_0-2(2c_1-c_0)c_0\varepsilon_1+c_1c_0\varepsilon_2\right]\left[c_1\log_e\dfrac{c_1}{c_0}-(c_1-c_0)\right]\\ -\dfrac{(\Delta l)^2}{12(c_1-c_0)^2}\left[(8c_1-5c_0)\varepsilon_0-2(5c_1-2c_0)\varepsilon_1+(2c_1+c_0)\varepsilon_2\right]+\hat{y}_0\end{Bmatrix} \tag{F5}$$

$$+(2-1)\begin{Bmatrix}\dfrac{(\Delta l)^2}{2(c_1-c_0)^3}\left[(2c_1-c_0)c_1\varepsilon_0-2(2c_1-c_0)c_0\varepsilon_1+c_1c_0\varepsilon_2\right]\log_e\dfrac{c_1}{c_0}\\ -\dfrac{(\Delta l)^2}{4(c_1-c_0)^2}\left[(5c_1-3c_0)\varepsilon_0-2(3c_1-c_0)\varepsilon_1+(c_1+c_0)\varepsilon_2\right]\end{Bmatrix}+2(\Delta l)\theta_0$$

For $i=3$:

$$
\begin{aligned}
\hat{y}_3 &= \frac{(\Delta l)^2}{2(c_3-c_2)^4}\left[(2c_3-c_2)c_3\varepsilon_2-2(2c_3-c_2)c_2\varepsilon_3+c_3c_2\varepsilon_4\right]\left[c_3\log_e\frac{c_3}{c_2}-(c_3-c_2)\right] \\
&\quad -\frac{(\Delta l)^2}{12(c_3-c_2)^2}\left[(8c_3-5c_2)\varepsilon_2-2(5c_3-2c_2)\varepsilon_3+(2c_3+c_2)\varepsilon_4\right]+\hat{y}_2+(\Delta l)\theta_2 \\
&= \left\{\begin{array}{l}
\dfrac{(\Delta l)^2}{2(c_3-c_2)^4}\left[(2c_3-c_2)c_3\varepsilon_2-2(2c_3-c_2)c_2\varepsilon_3+c_3c_2\varepsilon_4\right]\left[c_3\log_e\dfrac{c_3}{c_2}-(c_3-c_2)\right] \\
-\dfrac{(\Delta l)^2}{12(c_3-c_2)^2}\left[(8c_3-5c_2)\varepsilon_2-2(5c_3-2c_2)\varepsilon_3+(2c_3+c_2)\varepsilon_4\right]
\end{array}\right\} \\
&\quad + \underbrace{\left\{\begin{array}{l}
\dfrac{(\Delta l)^2}{2(c_2-c_1)^4}\left[(2c_2-c_1)c_2\varepsilon_1-2(2c_2-c_1)c_1\varepsilon_2+c_2c_1\varepsilon_3\right]\left[c_2\log_e\dfrac{c_2}{c_1}-(c_2-c_1)\right] \\
-\dfrac{(\Delta l)^2}{12(c_2-c_1)^2}\left[(8c_2-5c_1)\varepsilon_1-2(5c_2-2c_1)\varepsilon_2+(2c_2+c_1)\varepsilon_3\right] \\
+\dfrac{(\Delta l)^2}{2(c_1-c_0)^4}\left[(2c_1-c_0)c_1\varepsilon_0-2(2c_1-c_0)c_0\varepsilon_1+c_1c_0\varepsilon_2\right]\left[c_1\log_e\dfrac{c_1}{c_0}-(c_1-c_0)\right] \\
-\dfrac{(\Delta l)^2}{12(c_1-c_0)^2}\left[(8c_1-5c_0)\varepsilon_0-2(5c_1-2c_0)\varepsilon_1+(2c_1+c_0)\varepsilon_2\right]+\hat{y}_0 \\
+(2-1)\left\{\begin{array}{l}
\dfrac{(\Delta l)^2}{2(c_1-c_0)^3}\left[(2c_1-c_0)c_1\varepsilon_0-2(2c_1-c_0)c_0\varepsilon_1+c_1c_0\varepsilon_2\right]\log\dfrac{c_1}{c_0} \\
-\dfrac{(\Delta l)^2}{4(c_1-c_0)^2}\left[(5c_1-3c_0)\varepsilon_0-2(3c_1-c_0)\varepsilon_1+(c_1+c_0)\varepsilon_2\right]
\end{array}\right\} \\
\quad +2(\Delta l)\theta_0
\end{array}\right\}}_{\hat{y}_2} \\
&\quad + \underbrace{\left\{\begin{array}{l}
\dfrac{(\Delta l)^2}{2(c_2-c_1)^3}\left[(2c_2-c_1)c_2\varepsilon_1-2(2c_2-c_1)c_1\varepsilon_2+c_2c_1\varepsilon_3\right]\log_e\dfrac{c_2}{c_1} \\
-\dfrac{(\Delta l)^2}{4(c_2-c_1)^2}\left[(5c_2-3c_1)\varepsilon_1-2(3c_2-c_1)\varepsilon_2+(c_2+c_1)\varepsilon_3\right]+ \\
+\dfrac{(\Delta l)^2}{2(c_1-c_0)^3}\left[(2c_1-c_0)c_1\varepsilon_0-2(2c_1-c_0)c_0\varepsilon_1+c_1c_0\varepsilon_2\right]\log_e\dfrac{c_1}{c_0} \\
-\dfrac{(\Delta l)^2}{4(c_1-c_0)^2}\left[(5c_1-3c_0)\varepsilon_0-2(3c_1-c_0)\varepsilon_1+(c_1+c_0)\varepsilon_2\right]+(\Delta l)\theta_0
\end{array}\right\}}_{(\Delta l)\theta_2}
\end{aligned}
\tag{F6}
$$

After grouping terms, equation (F6) becomes equation (F7):

$$
\begin{aligned}
\widehat{y}_3 = &\left\{\begin{array}{l}
\dfrac{(\Delta l)^2}{2(c_3-c_2)^4}\left[(2c_3-c_2)c_3\varepsilon_2-2(2c_3-c_2)c_2\varepsilon_3+c_3c_2\varepsilon_4\right]\left[c_3\log_e\dfrac{c_3}{c_2}-(c_3-c_2)\right] \\
-\dfrac{(\Delta l)^2}{12(c_3-c_2)^2}\left[(8c_3-5c_2)\varepsilon_2-2(5c_3-2c_2)\varepsilon_3+(2c_3+c_2)\varepsilon_4\right]
\end{array}\right\} \\
&+\left\{\begin{array}{l}
\dfrac{(\Delta l)^2}{2(c_2-c_1)^4}\left[(2c_2-c_1)c_2\varepsilon_1-2(2c_2-c_1)c_1\varepsilon_2+c_2c_1\varepsilon_3\right]\left[c_2\log_e\dfrac{c_2}{c_1}-(c_2-c_1)\right] \\
-\dfrac{(\Delta l)^2}{12(c_2-c_1)^2}\left[(8c_2-5c_1)\varepsilon_1-2(5c_2-2c_1)\varepsilon_2+(2c_2+c_1)\varepsilon_3\right]
\end{array}\right\} \\
&+\left\{\begin{array}{l}
\dfrac{(\Delta l)^2}{2(c_1-c_0)^4}\left[(2c_1-c_0)c_1\varepsilon_0-2(2c_1-c_0)c_0\varepsilon_1+c_1c_0\varepsilon_2\right]\left[c_1\log_e\dfrac{c_1}{c_0}-(c_1-c_0)\right] \\
-\dfrac{(\Delta l)^2}{12(c_1-c_0)^2}\left[(8c_1-5c_0)\varepsilon_0-2(5c_1-2c_0)\varepsilon_1+(2c_1+c_0)\varepsilon_2\right]
\end{array}\right\}+\widehat{y}_0 \\
&+(3-2)\left\{\begin{array}{l}
\dfrac{(\Delta l)^2}{2(c_2-c_1)^3}\left[(2c_2-c_1)c_2\varepsilon_1-2(2c_2-c_1)c_1\varepsilon_2+c_2c_1\varepsilon_3\right]\log_e\dfrac{c_2}{c_1} \\
-\dfrac{(\Delta l)^2}{4(c_2-c_1)^2}\left[(5c_2-3c_1)\varepsilon_1-2(3c_2-c_1)\varepsilon_2+(c_2+c_1)\varepsilon_3\right]
\end{array}\right\} \\
&+(3-1)\left\{\begin{array}{l}
\dfrac{(\Delta l)^2}{2(c_1-c_0)^3}\left[(2c_1-c_0)c_1\varepsilon_0-2(2c_1-c_0)c_0\varepsilon_1+c_1c_0\varepsilon_2\right]\log_e\dfrac{c_1}{c_0} \\
-\dfrac{(\Delta l)^2}{4(c_1-c_0)^2}\left[(5c_1-3c_0)\varepsilon_0-2(3c_1-c_0)\varepsilon_1+(c_1+c_0)\varepsilon_2\right]
\end{array}\right\}+3(\Delta l)\theta_0
\end{aligned}
\qquad \text{(F7)}
$$

Observing the indicial behavior, equation (F7) can be generalized for index *i*, and the deflection, $\widehat{y}_i$, can be expressed in a generalized form with two summations (with different summation limits) as equation (F8):

$$
\begin{aligned}
\widehat{y}_i = &\underbrace{\sum_{j=1}^{i}\left\{\begin{array}{l}
\dfrac{(\Delta l)^2}{2(c_j-c_{j-1})^4}\left[(2c_j-c_{j-1})(c_j\varepsilon_{j-1}-2c_{j-1}\varepsilon_j)+c_jc_{j-1}\varepsilon_{j+1}\right]\left[c_j\log_e\dfrac{c_j}{c_{j-1}}-(c_j-c_{j-1})\right] \\
-\dfrac{(\Delta l)^2}{12(c_j-c_{j-1})^2}\left[(8c_j-5c_{j-1})\varepsilon_{j-1}-2(5c_j-2c_{j-1})\varepsilon_j+(2c_j+c_{j-1})\varepsilon_{j+1}\right]
\end{array}\right\}}_{\text{Contribution from deflection terms}}+\widehat{y}_0 \\
&+\underbrace{\sum_{j=1}^{i-1}(i-j)\left\{\begin{array}{l}
\dfrac{(\Delta l)^2}{2(c_j-c_{j-1})^3}\left[(2c_j-c_{j-1})(c_j\varepsilon_{j-1}-2c_{j-1}\varepsilon_j)+c_jc_{j-1}\varepsilon_{j+1}\right]\log_e\dfrac{c_j}{c_{j-1}} \\
-\dfrac{(\Delta l)^2}{4(c_j-c_{j-1})^2}\left[(5c_j-3c_{j-1})\varepsilon_{j-1}-2(3c_j-c_{j-1})\varepsilon_j+(c_j+c_{j-1})\varepsilon_{j+1}\right]
\end{array}\right\}}_{\text{Contributions from slope terms}}+(i)(\Delta l)\theta_0 \\
&(i=1,2,3,...,n)
\end{aligned}
\qquad \text{(F8)}
$$

Equation (F8) is the nonuniform part of equation (19c) in the text. A set of three equations {(F1), (F2), and (F8)} is then called the Improved Curved Displacement Transfer Functions for the nonuniform embedded beams.

APPENDIX G
DERIVATIONS OF IMPROVED SLOPE ANGLE AND CURVED DEFLECTION EQUATIONS IN RECURSIVE FORMS FOR UNIFORM BEAMS

Appendix G presents the details of integrations of the slope angle equation (15) and the curved deflection equation (17) for the uniform beams based on piecewise nonlinear strain representations to obtain uniform parts of equations (19a) and (19b).

Slope Equation

For the uniform embedded beam with constant depth factor, $c(x) = c$, the slope angle equation (15) for the domain $x_{i-1} \le x \le x_i$ between the two adjacent strain-sensing stations, $\{x_{i-1}, x_i\}$, becomes equation (G1):

$$\theta(x) = \underbrace{\int_{x_{i-1}}^{x} \frac{\varepsilon(x)}{c} dx}_{\text{Slope increment}} + \underbrace{\theta_{i-1}}_{\substack{\text{Slope} \\ \text{at } x_{i-1}}} \quad ; \quad (x_{i-1} \le x \le x_i) \tag{G1}$$

The nonlinear representation of strain, $\varepsilon(x)$, in the domain $x_{i-1} \le x \le x_i$ between the two adjacent strain-sensing stations, $\{x_{i-1}, x_i\}$, described by equation (13a), is duplicated below as equation (G2):

$$\varepsilon(x) = \varepsilon_{i-1} - \frac{3\varepsilon_{i-1} - 4\varepsilon_i + \varepsilon_{i+1}}{2\Delta l}(x - x_{i-1}) + \frac{\varepsilon_{i-1} - 2\varepsilon_i + \varepsilon_{i+1}}{2(\Delta l)^2}(x - x_{i-1})^2 \qquad (x_{i-1} \le x \le x_i) \tag{G2}$$

In view of equation (G2), equation (G1) can be integrated to yield equation (G3) (ref. 19):

$$\begin{aligned} \theta(x) &= \frac{1}{c}\int_{x_{i-1}}^{x} \left[\varepsilon_{i-1} - \frac{3\varepsilon_{i-1} - 4\varepsilon_i + \varepsilon_{i+1}}{2\Delta l}(x - x_{i-1}) + \frac{\varepsilon_{i-1} - 2\varepsilon_i + \varepsilon_{i+1}}{2(\Delta l)^2}(x - x_{i-1})^2 \right] dx + \theta_{i-1} \\ &= \frac{1}{c}\left[\varepsilon_{i-1}(x - x_{i-1}) - \frac{3\varepsilon_{i-1} - 4\varepsilon_i + \varepsilon_{i+1}}{4\Delta l}(x - x_{i-1})^2 + \frac{\varepsilon_{i-1} - 2\varepsilon_i + \varepsilon_{i+1}}{6(\Delta l)^2}(x - x_{i-1})^3 \right] + \theta_{i-1} \end{aligned} \qquad (x_{i-1} \le x \le x_i) \tag{G3}$$

At the strain-sensing station, x_i, one can write $x_i - x_{i-1} \equiv \Delta l$, and equation (G3) yields the slope angle, $\theta_i [\equiv \theta(x_i)]$, at the strain-sensing station, x_i, as equation (G4):

$$\theta_i = \frac{\Delta l}{c}\left[\varepsilon_{i-1} - \frac{3\varepsilon_{i-1} - 4\varepsilon_i + \varepsilon_{i+1}}{4} + \frac{\varepsilon_{i-1} - 2\varepsilon_i + \varepsilon_{i+1}}{6} \right] + \theta_{i-1} \quad ; \quad (i = 1,2,3,...,n) \tag{G4}$$

After grouping terms, equation (G4) takes on the following final form as equation (G5):

$$\theta_i = \frac{\Delta l}{12c}(5\varepsilon_{i-1} + 8\varepsilon_i - \varepsilon_{i+1}) + \theta_{i-1} \quad ; \quad (i = 1,2,3,...,n) \tag{G5}$$

Equation (G5) is the uniform part of equation (19a) in the text.

Curved Deflection Equations

For the uniform embedded beam, $[c(x) = c]$, the curved deflection, $\hat{y}(x)$, in the small domain $x_{i-1} \le x \le x_i$ between the two adjacent strain-sensing stations, $\{x_{i-1}, x_i\}$, can be obtained by integrating the slope equation (G3) [see equation (C6)] as equation (G6):

$$\hat{y}(x) = \int_{x_{i-1}}^{x} \underbrace{\left[\int_{x_{i-1}}^{x} \frac{\varepsilon(x)}{c} dx + \theta_{i-1} \right]}_{\theta(x)} dx + \hat{y}_{i-1} = \int_{x_{i-1}}^{x} \theta(x)\, dx + \hat{y}_{i-1} \quad ; \quad (x_{i-1} \le x \le x_i) \tag{G6}$$

Substituting equation (G3) into equation (G6), and carrying out integrations, one obtains equation (G7) (ref. 21):

$$\begin{aligned} \hat{y}(x) &= \frac{1}{c}\int_{x_{i-1}}^{x} \left[\varepsilon_{i-1}(x - x_{i-1}) - \frac{3\varepsilon_{i-1} - 4\varepsilon_i + \varepsilon_{i+1}}{4\Delta l}(x - x_{i-1})^2 + \frac{\varepsilon_{i-1} - 2\varepsilon_i + \varepsilon_{i+1}}{6(\Delta l)^2}(x - x_{i-1})^3 \right] dx \\ &\quad + \int_{x_{i-1}}^{x} \theta_{i-1}\, dx + \hat{y}_{i-1} \\ &= \frac{1}{c}\left[\frac{\varepsilon_{i-1}}{2}(x - x_{i-1})^2 - \frac{3\varepsilon_{i-1} - 4\varepsilon_i + e_{i+1}}{12\Delta l}(x - x_{i-1})^3 + \frac{\varepsilon_{i-1} - 2\varepsilon_i + \varepsilon_{i+1}}{24(\Delta l)^2}(x - x_{i-1})^4 \right] \\ &\quad + (x - x_{i-1})\theta_{i-1} + \hat{y}_{i-1} \\ &\qquad\qquad (x_{i-1} \le x \le x_i) \end{aligned} \tag{G7}$$

At the strain-sensing station, x_i, one can write $x_i - x_{i-1} \equiv \Delta l$, and equation (G7) gives the curved deflection, $\hat{y}_i [\equiv \hat{y}(x_i)]$, at the strain-sensing station, x_i, as equation (G8):

$$\hat{y}_i = \frac{(\Delta l)^2}{c}\left[\frac{\varepsilon_{i-1}}{2} - \frac{3\varepsilon_{i-1} - 4\varepsilon_i + \varepsilon_{i+1}}{12} + \frac{\varepsilon_{i-1} - 2\varepsilon_i + \varepsilon_{i+1}}{24} \right] + \hat{y}_{i-1} + (\Delta l)\theta_{i-1} \qquad (i = 1,2,3,...,n) \tag{G8}$$

After grouping terms, equation (G8) takes on the final form as equation (G9):

$$\hat{y}_i = \frac{(\Delta l)^2}{24c}(7\varepsilon_{i-1} + 6\varepsilon_i - \varepsilon_{i+1}) + \hat{y}_{i-1} + (\Delta l)\theta_{i-1} \quad ; \quad (i = 1,2,3,...,n) \tag{G9}$$

Equation (G9) is the uniform part of equation (19b) in the text.

APPENDIX H
DERIVATIONS OF THE IMPROVED CURVED DEFLECTION EQUATION IN SUMMATION FORM FOR UNIFORM EMBEDDED BEAMS

Appendix H is to derive the final summation form of the curved deflection equation for the uniform embedded beams using nonlinear strain representations. Equations (G5) and (G9) are duplicated below as equations (H1) and (H2), respectively.

$$\theta_i = \frac{\Delta l}{12c}\left(5\varepsilon_{i-1} + 8\varepsilon_i - \varepsilon_{i+1}\right) + \theta_{i-1} \quad ; \quad (i = 1,2,3,...,n) \tag{H1}$$

$$\hat{y}_i = \frac{(\Delta l)^2}{24c}(7\varepsilon_{i-1} + 6\varepsilon_i - \varepsilon_{i+1}) + \hat{y}_{i-1} + (\Delta l)\theta_{i-1} \quad ; \quad (i = 1,2,3,...,n) \tag{H2}$$

Equations (H1) and (H2) can be combined into a single deflection equation in summation forms as follows. Writing out equation (H2) for different indices, *i*, and making use of the indicial relationships expressed in equations (H1) and (H2), one obtains equations (H3) and (H4):

For $i = 1$:

$$\hat{y}_1 = \frac{(\Delta l)^2}{24c}(7\varepsilon_0 + 6\varepsilon_1 - \varepsilon_2) + \hat{y}_0 + (\Delta l)\theta_0 \tag{H3}$$

For $i = 2$:

$$\hat{y}_2 = \frac{(\Delta l)^2}{24c}(7\varepsilon_1 + 6\varepsilon_2 - \varepsilon_3) + \hat{y}_1 + (\Delta l)\theta_1$$

$$= \frac{(\Delta l)^2}{24c}(7\varepsilon_1 + 6\varepsilon_2 - \varepsilon_3) + \underbrace{\frac{(\Delta l)^2}{24c}(7\varepsilon_0 + 6\varepsilon_1 - \varepsilon_2) + \hat{y}_0 + (\Delta l)\theta_0}_{\hat{y}_1} \tag{H4}$$

$$+ \underbrace{\frac{(\Delta l)^2}{12c}(5\varepsilon_0 + 8\varepsilon_1 - \varepsilon_2) + (\Delta l)\theta_0}_{(\Delta l)\theta_1}$$

After grouping terms, equation (H4) becomes equations (H5) and (H6):

$$\hat{y}_2 = \frac{(\Delta l)^2}{24c}(7\varepsilon_1 + 6\varepsilon_2 - \varepsilon_3) + \frac{(\Delta l)^2}{24c}(7\varepsilon_0 + 6\varepsilon_1 - \varepsilon_2) + (2-1)\frac{(\Delta l)^2}{12c}(5\varepsilon_0 + 8\varepsilon_1 - \varepsilon_2) \tag{H5}$$
$$+ \hat{y}_0 + 2(\Delta l)\theta_0$$

For $i = 3$:

$$\hat{y}_3 = \frac{(\Delta l)^2}{24c}(7\varepsilon_2 + 6\varepsilon_3 - \varepsilon_4) + \hat{y}_2 + (\Delta l)\theta_2 = \frac{(\Delta l)^2}{24c}(7\varepsilon_2 + 6\varepsilon_3 - \varepsilon_4) +$$
$$+ \underbrace{\frac{(\Delta l)^2}{24c}(7\varepsilon_1 + 6\varepsilon_2 - \varepsilon_3) + \frac{(\Delta l)^2}{24c}(7\varepsilon_0 + 6\varepsilon_1 - \varepsilon_2) + (2-1)\frac{(\Delta l)^2}{12c}(5\varepsilon_0 + 8\varepsilon_1 - \varepsilon_2) + \hat{y}_0 + 2(\Delta l)\theta_0}_{\hat{y}_2}$$
$$\underbrace{+ \frac{(\Delta l)^2}{12c}(5\varepsilon_1 + 8\varepsilon_2 - \varepsilon_3) + \frac{(\Delta l)^2}{12c}(5\varepsilon_0 + 8\varepsilon_1 - \varepsilon_2) + (\Delta l)\theta_0}_{(\Delta l)\theta_2} \qquad \text{(H6)}$$

After grouping terms, equation (H6) becomes equation (H7):

$$\hat{y}_3 = \frac{(\Delta l)^2}{24c}(7\varepsilon_2 + 6\varepsilon_3 - \varepsilon_4) + \frac{(\Delta l)^2}{24c}(7\varepsilon_1 + 6\varepsilon_2 - \varepsilon_3) + \frac{(\Delta l)^2}{24c}(7\varepsilon_0 + 6\varepsilon_1 - \varepsilon_2)$$
$$+ (3-2)\frac{(\Delta l)^2}{12c}(5\varepsilon_1 + 8\varepsilon_2 - \varepsilon_3) + (3-1)\frac{(\Delta l)^2}{12c}(5\varepsilon_0 + 8\varepsilon_1 - \varepsilon_2) + \hat{y}_0 + 3(\Delta l)\theta_0 \qquad \text{(H7)}$$

Observing the indicial behavior, equation (H7) can be generalized for index, *i*, and the curved deflection, $\hat{y}_i$, can be expressed in a generalized form with two summations (with different summation limits) as equation (H8):

$$\hat{y}_i = \underbrace{\frac{(\Delta l)^2}{24c}\sum_{j=1}^{i}(7\varepsilon_{j-1} + 6\varepsilon_j - \varepsilon_{j+1}) + \hat{y}_0}_{\text{Contributions from deflection terms}} + \underbrace{\frac{(\Delta l)^2}{12c}\sum_{j=1}^{i-1}(i-j)(5\varepsilon_{j-1} + 8\varepsilon_j - \varepsilon_{j+1}) + (i)(\Delta l)\theta_0}_{\text{Contributions from slope terms}} \qquad \text{(H8)}$$
$$(i = 1,2,3,...,n)$$

which is the uniform part of equation (19c) in the text. A set of three equations {(H1), (H2), and (H8)} are called the Improved Curved Displacement Transfer Functions for the uniform embedded beams.

APPENDIX I
SUMMARY DATA OF LINEAR AND NONLINEAR DEFORMATION ANALYSES OF THE TAPERED CANTILEVER TUBULAR BEAM

The complete set of the strain and deflection data generated by Nastran linear and nonlinear analysis of the tapered cantilever tubular beam are listed in tables I1−I14 for different values of beam-tip load, *P*. Tables I1−I7 are for linear cases, and tables I-8−I14 are for the nonlinear cases. In the last columns of tables I1−I14, theoretically predicted deflection data are listed for comparisons.

Linear Analysis

In the Nastran linear analysis, the outputs give only vertical deflections, y_i, and zero axial displacements (that is, $u_i = 0$) (fig 6a). Note from tables I1−I7 that for linear cases, the lower and the upper surface strains at the same strain-sensing cross section have the same magnitudes. In the last columns of tables I1−I7, the data of Shifted (vertical) deflection, y_i, were calculated from the Shifted Displacement Transfer Functions [eq. (6b)] using the known depth factors, $c_i (= h_i/2)$, and lower surface strains, ε_i, listed in tables I1−I7.

Table I1. Vertical deflections, y_i, of the tapered cantilever tubular beam calculated from Nastran linear analysis and from Shifted Displacement Transfer Functions [eq. (6b)] using the known depth factors, $c_i (= h_i/2)$, and Nastran linear lower surface strains, ε_i; *P*=50 lb at the beam tip.

i	c_i, in	$\overline{\varepsilon}_i$, in/in Nastran-linear upper surface strain	ε_i, in/in Nastran-linear lower surface strain	y_i, in Nastran-linear vertical deflection	y_i, in Shifted DTF Eq. (6b)
0	4.0000	-0.00124	0.00124	0.000	0.000
1	3.8500	-0.00127	0.00127	0.036	0.036
2	3.7000	-0.00130	0.00130	0.146	0.145
3	3.5500	-0.00134	0.00134	0.335	0.335
4	3.4000	-0.00137	0.00137	0.609	0.608
5	3.2500	-0.00141	0.00141	0.973	0.973
6	3.1000	-0.00144	0.00144	1.435	1.435
7	2.9500	-0.00148	0.00148	2.002	2.002
8	2.8000	-0.00152	0.00152	2.681	2.682
9	2.6500	-0.00155	0.00155	3.482	3.484
10	2.5000	-0.00158	0.00158	4.415	4.418
11	2.3500	-0.00161	0.00161	5.490	5.494
12	2.2000	-0.00164	0.00164	6.719	6.724
13	2.0500	-0.00165	0.00165	8.116	8.122
14	1.9000	-0.00165	0.00165	9.693	9.701
15	1.7500	-0.00162	0.00162	11.464	11.475
16	1.6000	-0.00155	0.00155	13.443	13.457
17	1.4500	-0.00141	0.00141	15.637	15.655
18	1.3000	-0.00117	0.00117	18.048	18.069
19	1.1500	-0.00075	0.00075	20.658	20.679
20	1.0000	0.00000	0.00000	23.406*	23.424*

*Extremely close

Table I2. Vertical deflections, y_i, of the tapered cantilever tubular beam calculated from Nastran linear analysis and from Shifted Displacement Transfer Functions [eq. (6b)] using the known depth factors, $c_i (= h_i/2)$, and Nastran linear lower surface strains, ε_i; P=100 lb at the beam tip.

i	c_i, in	$\overline{\varepsilon}_i$, in/in Nastran-linear upper surface strain	ε_i, in/in Nastran-linear lower surface strain	y_i, in Nastran-linear vertical deflection	y_i, in Shifted DTF Eq. (6b)
0	4.0000	-0.00248	0.00248	0.000	0.000
1	3.8500	-0.00254	0.00254	0.072	0.071
2	3.7000	-0.00260	0.00260	0.292	0.291
3	3.5500	-0.00267	0.00267	0.670	0.669
4	3.4000	-0.00274	0.00274	1.218	1.216
5	3.2500	-0.00281	0.00281	1.947	1.945
6	3.1000	-0.00289	0.00289	2.871	2.868
7	2.9500	-0.00296	0.00296	4.004	4.002
8	2.8000	-0.00303	0.00303	5.362	5.361
9	2.6500	-0.00310	0.00310	6.964	6.964
10	2.5000	-0.00317	0.00317	8.830	8.830
11	2.3500	-0.00323	0.00323	10.980	10.981
12	2.2000	-0.00327	0.00327	13.439	13.442
13	2.0500	-0.00330	0.00330	16.232	16.238
14	1.9000	-0.00329	0.00329	19.386	19.395
15	1.7500	-0.00323	0.00323	22.929	22.941
16	1.6000	-0.00310	0.00310	26.886	26.901
17	1.4500	-0.00283	0.00283	31.274	31.294
18	1.3000	-0.00234	0.00234	36.097	36.120
19	1.1500	-0.00150	0.00150	41.316	41.340
20	1.0000	0.00000	0.00000	46.811*	46.828*

*Extremely close

Table I3. Vertical deflections, y_i, of the tapered cantilever tubular beam calculated from Nastran linear analysis and from Shifted Displacement Transfer Functions [eq. (6b)] using the known depth factors, $c_i(=h_i/2)$, and Nastran linear lower surface strains, ε_i; P=200 lb at the beam tip.

i	c_i, in	$\overline{\varepsilon}_i$, in/in Nastran-linear upper surface strain	ε_i, in/in Nastran-linear lower surface strain	y_i, in Nastran-linear vertical deflection	y_i, in Shifted DTF Eq. (6b)
0	4.0000	-0.00495	0.00495	0.000	0.000
1	3.8500	-0.00508	0.00508	0.143	0.142
2	3.7000	-0.00521	0.00521	0.584	0.581
3	3.5500	-0.00534	0.00534	1.340	1.338
4	3.4000	-0.00548	0.00548	2.436	2.433
5	3.2500	-0.00563	0.00563	3.894	3.890
6	3.1000	-0.00577	0.00577	5.741	5.738
7	2.9500	-0.00592	0.00592	8.007	8.005
8	2.8000	-0.00606	0.00606	10.725	10.724
9	2.6500	-0.00620	0.00620	13.929	13.930
10	2.5000	-0.00634	0.00634	17.659	17.662
11	2.3500	-0.00646	0.00646	21.960	21.966
12	2.2000	-0.00655	0.00655	26.877	26.888
13	2.0500	-0.00660	0.00660	32.463	32.480
14	1.9000	-0.00658	0.00658	38.772	38.795
15	1.7500	-0.00647	0.00647	45.858	45.889
16	1.6000	-0.00619	0.00619	53.771	53.811
17	1.4500	-0.00565	0.00565	62.549	62.599
18	1.3000	-0.00469	0.00469	72.193	72.252
19	1.1500	-0.00300	0.00300	82.631	82.692
20	1.0000	0.00000	0.00000	93.623*	93.669*

*Extremely close

Table I4. Vertical deflections, y_i, of the tapered cantilever tubular beam calculated from Nastran linear analysis and from Shifted Displacement Transfer Functions [eq. (6b)] using the known depth factors, $c_i (= h_i/2)$, and Nastran linear lower surface strains, ε_i; P=300 lb at the beam tip.

i	c_i, in	$\overline{\varepsilon}_i$, in/in Nastran-linear upper surface strain	ε_i, in/in Nastran-linear lower surface strain	y_i, in Nastran-linear vertical deflection	y_i, in Shifted DTF Eq. (6b)
0	4.0000	-0.00743	0.00743	0.000	0.000
1	3.8500	-0.00762	0.00762	0.215	0.213
2	3.7000	-0.00781	0.00781	0.875	0.872
3	3.5500	-0.00801	0.00801	2.011	2.007
4	3.4000	-0.00822	0.00822	3.654	3.649
5	3.2500	-0.00844	0.00844	5.841	5.835
6	3.1000	-0.00866	0.00866	8.612	8.607
7	2.9500	-0.00888	0.00888	12.011	12.007
8	2.8000	-0.00909	0.00909	16.087	16.085
9	2.6500	-0.00931	0.00931	20.893	20.893
10	2.5000	-0.00951	0.00951	26.489	26.493
11	2.3500	-0.00968	0.00968	32.940	32.949
12	2.2000	-0.00982	0.00982	40.316	40.332
13	2.0500	-0.00990	0.00990	48.695	48.719
14	1.9000	-0.00988	0.00988	58.158	58.191
15	1.7500	-0.00970	0.00970	68.787	68.832
16	1.6000	-0.00929	0.00929	80.657	80.716
17	1.4500	-0.00848	0.00848	93.823	93.897
18	1.3000	-0.00703	0.00703	108.290	108.378
19	1.1500	-0.00449	0.00449	123.947	124.039
20	1.0000	0.00000	0.00000	140.434*	140.502*

*Extremely close

Table I5. Vertical deflections, y_i, of the tapered cantilever tubular beam calculated from Nastran linear analysis and from Shifted Displacement Transfer Functions [eq. (6b)] using the known depth factors, $c_i (= h_i/2)$, and Nastran linear lower surface strains, ε_i; P=400 lb at the beam tip.

i	c_i, in	$\overline{\varepsilon}_i$, in/in Nastran-linear upper surface strain	ε_i, in/in Nastran-linear lower surface strain	y_i, in Nastran-linear vertical deflection	y_i, in Shifted DTF Eq. (6b)
0	4.0000	-0.00990	0.00990	0.000	0.000
1	3.8500	-0.01015	0.01015	0.287	0.284
2	3.7000	-0.01042	0.01042	1.167	1.162
3	3.5500	-0.01069	0.01069	2.681	2.674
4	3.4000	-0.01096	0.01096	4.872	4.864
5	3.2500	-0.01125	0.01125	7.788	7.780
6	3.1000	-0.01154	0.01154	11.483	11.475
7	2.9500	-0.01183	0.01183	16.015	16.008
8	2.8000	-0.01213	0.01213	21.449	21.444
9	2.6500	-0.01241	0.01241	27.858	27.855
10	2.5000	-0.01268	0.01268	35.319	35.320
11	2.3500	-0.01291	0.01291	43.919	43.927
12	2.2000	-0.01309	0.01309	53.755	53.771
13	2.0500	-0.01320	0.01320	64.927	64.953
14	1.9000	-0.01317	0.01317	77.544	77.582
15	1.7500	-0.01293	0.01293	91.715	91.769
16	1.6000	-0.01238	0.01238	107.542	107.613
17	1.4500	-0.01130	0.01130	125.097	125.185
18	1.3000	-0.00937	0.00937	144.387	144.489
19	1.1500	-0.00599	0.00599	165.263	165.367
20	1.0000	0.00000	0.00000	187.245*	187.314*

*Extremely close

Table I6. Vertical deflections, y_i, of the tapered cantilever tubular beam calculated from Nastran linear analysis and from Shifted Displacement Transfer Functions [eq. (6b)] using the known depth factors, $c_i (= h_i/2)$, and Nastran linear lower surface strains, ε_i; P=500 lb at the beam tip.

i	c_i, in	$\overline{\varepsilon}_i$, in/in Nastran-linear upper surface strain	ε_i, in/in Nastran-linear lower surface strain	y_i, in Nastran-linear vertical deflection	y_i, in Shifted DTF Eq. (6b)
0	4.0000	-0.01238	0.01238	0.000	0.000
1	3.8500	-0.01269	0.01269	0.359	0.356
2	3.7000	-0.01302	0.01302	1.459	1.453
3	3.5500	-0.01336	0.01336	3.351	3.343
4	3.4000	-0.01371	0.01371	6.089	6.080
5	3.2500	-0.01406	0.01406	9.735	9.725
6	3.1000	-0.01443	0.01443	14.353	14.344
7	2.9500	-0.01479	0.01479	20.019	20.011
8	2.8000	-0.01516	0.01516	26.812	26.807
9	2.6500	-0.01551	0.01551	34.822	34.822
10	2.5000	-0.01584	0.01584	44.148	44.154
11	2.3500	-0.01614	0.01614	54.899	54.913
12	2.2000	-0.01637	0.01637	67.193	67.217
13	2.0500	-0.01650	0.01650	81.158	81.195
14	1.9000	-0.01646	0.01646	96.930	96.982
15	1.7500	-0.01617	0.01617	114.644	114.716
16	1.6000	-0.01548	0.01548	134.428	134.522
17	1.4500	-0.01413	0.01413	156.372	156.489
18	1.3000	-0.01172	0.01172	180.483	180.621
19	1.1500	-0.00749	0.00749	206.579	206.723
20	1.0000	0.00000	0.00000	234.057*	234.161*

*Extremely close

Table I7. Vertical deflections, y_i, of the tapered cantilever tubular beam calculated from Nastran linear analysis and from Shifted Displacement Transfer Functions [eq. (6b)] using the known depth factors, $c_i(=h_i/2)$, and Nastran linear lower surface strains, ε_i; P=600 lb at the beam tip.

i	c_i, in	$\bar{\varepsilon}_i$, in/in Nastran-linear upper surface strain	ε_i, in/in Nastran-linear lower surface strain	y_i, in Nastran-linear vertical deflection	y_i, in Shifted DTF Eq. (6b)
0	4.0000	-0.01485	0.01485	0.000	0.000
1	3.8500	-0.01523	0.01523	0.430	0.427
2	3.7000	-0.01562	0.01562	1.751	1.744
3	3.5500	-0.01603	0.01603	4.021	4.011
4	3.4000	-0.01645	0.01645	7.307	7.296
5	3.2500	-0.01688	0.01688	11.682	11.669
6	3.1000	-0.01731	0.01731	17.224	17.212
7	2.9500	-0.01775	0.01775	24.022	24.012
8	2.8000	-0.01819	0.01819	32.174	32.166
9	2.6500	-0.01861	0.01861	41.786	41.784
10	2.5000	-0.01901	0.01901	52.978	52.982
11	2.3500	-0.01937	0.01937	65.879	65.891
12	2.2000	-0.01964	0.01964	80.632	80.656
13	2.0500	-0.01979	0.01979	97.390	97.429
14	1.9000	-0.01975	0.01975	116.316	116.372
15	1.7500	-0.01940	0.01940	137.573	137.651
16	1.6000	-0.01857	0.01857	161.313	161.415
17	1.4500	-0.01696	0.01696	187.646	187.773
18	1.3000	-0.01406	0.01406	216.580	216.729
19	1.1500	-0.00899	0.00899	247.894	248.047
20	1.0000	0.00000	0.00000	280.868*	280.970*

*Extremely close; beam-tip deflection = 94% of 300-in span.

Nonlinear Analysis

Tables I8−I14 list the strain and deflection outputs of Nastran nonlinear analysis. Nastran nonlinear deflection outputs have both axial and vertical displacement, $\{u_i, y_i\}$ (fig 6b). Therefore, Nastran curved deflections, $\hat{y}$, were calculated from equation (20). Note also from tables I8−I14 that the magnitudes of lower surface strains are slightly larger than the magnitudes of the associated upper surface strains because of the curved-beam effect, inducing slight axial strain components under nonlinear bending.

In the last columns of Tables I8−I14, the data of curved deflection, $\hat{y}$, were calculated from the Curved Displacement Transfer Functions [eq. (18b)] using the known depth factors, $c_i(=h_i/2)$, and the true bending strains, $(\varepsilon_i - \bar{\varepsilon}_i)/2$ [eq. (23)], for eliminating axial strains induced by curved-beam effect in nonlinear bending.

Table I8. Curved deflections, $\hat{y}_i$, of the tapered cantilever tubular beam calculated from Nastran nonlinear analysis [eq. (20)] and from Curved Displacement Transfer Functions [eq. (18b)] using the known depth factors, $c_i (= h_i/2)$, and the true bending strains, $(\varepsilon_i - \overline{\varepsilon}_i)/2$; P=50 lb at the beam tip.

i	c_i, in	x_i, in	$\overline{\varepsilon}_i$, in/in Nastran nonlinear upper surface strain	ε_i, in/in Nastran nonlinear lower surface strain	u_i, in Nastran x-disp.	y_i, in Nastran y-disp.	$\hat{y}_i$, in Nastran curved deflection Eq. (20)	$\hat{y}_i$, in Curved DTF Eq. (18b)
0	4.00	0.0	-0.00123	0.00123	0.000	0.000	0.000	0.000
1	3.85	15.0	-0.00126	0.00126	0.000	0.036	0.036	0.035
2	3.70	30.0	-0.00130	0.00130	0.000	0.145	0.145	0.144
3	3.55	45.0	-0.00133	0.00133	0.002	0.333	0.333	0.332
4	3.40	60.0	-0.00136	0.00136	0.004	0.606	0.606	0.605
5	3.25	75.0	-0.00140	0.00140	0.008	0.969	0.969	0.967
6	3.10	90.0	-0.00143	0.00143	0.016	1.428	1.428	1.427
7	2.95	105.0	-0.00147	0.00147	0.026	1.991	1.991	1.990
8	2.80	120.0	-0.00150	0.00151	0.041	2.666	2.666	2.666
9	2.65	135.0	-0.00154	0.00154	0.062	3.462	3.463	3.462
10	2.50	150.0	-0.00157	0.00157	0.091	4.388	4.389	4.390
11	2.35	165.0	-0.00160	0.00160	0.129	5.455	5.457	5.458
12	2.20	180.0	-0.00162	0.00162	0.179	6.675	6.679	6.680
13	2.05	195.0	-0.00163	0.00163	0.243	8.059	8.064	8.068
14	1.90	210.0	-0.00162	0.00163	0.324	9.621	9.629	9.634
15	1.75	225.0	-0.00159	0.00160	0.427	11.374	11.386	11.393
16	1.60	240.0	-0.00152	0.00153	0.555	13.330	13.347	13.356
17	1.45	255.0	-0.00139	0.00140	0.712	15.497	15.521	15.532
18	1.30	270.0	-0.00115	0.00116	0.902	17.875	17.909	17.921
19	1.15	285.0	-0.00073	0.00074	1.124	20.445	20.491	20.504
20	1.00	300.0	0.00001	0.00001	1.369	23.150	23.210*	23.220*

*Extremely close

Table I9. Curved deflections, $\hat{y}_i$, of the tapered cantilever tubular beam calculated from Nastran nonlinear analysis [eq. (20)] and from Curved Displacement Transfer Functions [eq. (18b)] using the known depth factors, $c_i (= h_i/2)$, and the true bending strains, $(\varepsilon_i - \overline{\varepsilon}_i)/2$; P=100 lb at the beam tip.

i	c_i, in	x_i, in	$\overline{\varepsilon}_i$, in/in Nastran nonlinear upper surface strain	ε_i, in/in Nastran nonlinear lower surface strain	u_i, in Nastran x-disp.	y_i, in Nastran y-disp.	$\hat{y}_i$, in Nastran curved deflection Eq. (20)	$\hat{y}_i$, in Curved DTF Eq. (18b)
0	4.00	0.0	-0.00243	0.00243	0.000	0.000	0.000	0.000
1	3.85	15.0	-0.00249	0.00249	0.000	0.070	0.070	0.070
2	3.70	30.0	-0.00255	0.00255	0.002	0.287	0.287	0.285
3	3.55	45.0	-0.00262	0.00262	0.006	0.658	0.658	0.656
4	3.40	60.0	-0.00268	0.00268	0.016	1.195	1.195	1.192
5	3.25	75.0	-0.00275	0.00275	0.033	1.910	1.910	1.907
6	3.10	90.0	-0.00281	0.00282	0.060	2.814	2.815	2.811
7	2.95	105.0	-0.00288	0.00288	0.101	3.922	3.924	3.920
8	2.80	120.0	-0.00294	0.00295	0.160	5.249	5.253	5.249
9	2.65	135.0	-0.00301	0.00301	0.242	6.812	6.818	6.815
10	2.50	150.0	-0.00306	0.00307	0.352	8.628	8.639	8.636
11	2.35	165.0	-0.00311	0.00312	0.498	10.718	10.735	10.733
12	2.20	180.0	-0.00315	0.00316	0.689	13.102	13.129	13.129
13	2.05	195.0	-0.00316	0.00317	0.934	15.803	15.844	15.847
14	1.90	210.0	-0.00314	0.00316	1.245	18.845	18.906	18.912
15	1.75	225.0	-0.00307	0.00309	1.637	22.249	22.338	22.350
16	1.60	240.0	-0.00293	0.00295	2.122	26.036	26.164	26.182
17	1.45	255.0	-0.00266	0.00268	2.717	30.219	30.400	30.425
18	1.30	270.0	-0.00219	0.00222	3.431	34.793	35.043	35.077
19	1.15	285.0	-0.00139	0.00143	4.264	39.722	40.059	40.099
20	1.00	300.0	0.00002	0.00002	5.184	44.896	45.337*	45.374*

*Extremely close

Table I10. Curved deflections, $\hat{y}_i$, of the tapered cantilever tubular beam calculated from Nastran nonlinear analysis [eq. (20)] and from Curved Displacement Transfer Functions [eq. (18b)] using the known depth factors, $c_i (= h_i/2)$, and the true bending strains, $(\varepsilon_i - \overline{\varepsilon}_i)/2$; P=200 lb at the beam tip.

i	c_i, in	x_i, in	$\overline{\varepsilon}_i$, in/in Nastran nonlinear upper surface strain	ε_i, in/in Nastran nonlinear lower surface strain	u_i, in Nastran x-disp.	y_i, in Nastran y-disp.	$\hat{y}_i$, in Nastran curved deflection Eq. (20)	$\hat{y}_i$, in Curved DTF Eq. (18b)
0	4.00	0.0	-0.00467	0.00467	0.000	0.000	0.000	0.000
1	3.85	15.0	-0.00477	0.00477	0.001	0.135	0.135	0.134
2	3.70	30.0	-0.00487	0.00488	0.006	0.549	0.549	0.547
3	3.55	45.0	-0.00498	0.00498	0.023	1.259	1.259	1.256
4	3.40	60.0	-0.00509	0.00509	0.058	2.284	2.285	2.282
5	3.25	75.0	-0.00519	0.00520	0.120	3.644	3.647	3.644
6	3.10	90.0	-0.00530	0.00531	0.219	5.362	5.369	5.366
7	2.95	105.0	-0.00540	0.00541	0.366	7.462	7.475	7.473
8	2.80	120.0	-0.00549	0.00551	0.577	9.968	9.993	9.993
9	2.65	135.0	-0.00558	0.00560	0.868	12.909	12.953	12.955
10	2.50	150.0	-0.00565	0.00567	1.259	16.313	16.386	16.391
11	2.35	165.0	-0.00570	0.00573	1.774	20.210	20.326	20.337
12	2.20	180.0	-0.00572	0.00575	2.440	24.633	24.813	24.831
13	2.05	195.0	-0.00569	0.00574	3.290	29.611	29.883	29.910
14	1.90	210.0	-0.00561	0.00566	4.360	35.175	35.576	35.616
15	1.75	225.0	-0.00543	0.00550	5.690	41.352	41.933	41.988
16	1.60	240.0	-0.00512	0.00520	7.323	48.159	48.983	49.060
17	1.45	255.0	-0.00460	0.00469	9.298	55.600	56.748	56.853
18	1.30	270.0	-0.00375	0.00386	11.642	63.652	65.221	65.358
19	1.15	285.0	-0.00234	0.00247	14.343	72.241	74.336	74.503
20	1.00	300.0	0.00008	0.00008	17.304	81.191	83.903*	84.082*

*Extremely close

Table I11. Curved deflections, $\hat{y}_i$, of the tapered cantilever tubular beam calculated from Nastran nonlinear analysis [eq. (20)] and from Curved Displacement Transfer Functions [eq. (18b)] using the known depth factors, $c_i (= h_i/2)$, and the true bending strains, $(\varepsilon_i - \overline{\varepsilon}_i)/2$; P=300 lb at the beam tip.

i	c_i, in	x_i, in	$\overline{\varepsilon}_i$, in/in Nastran nonlinear upper surface strain	ε_i, in/in Nastran nonlinear lower surface strain	u_i, in Nastran x-disp.	y_i, in Nastran y-disp.	$\hat{y}_i$, in Nastran curved deflection Eq. (20)	$\hat{y}_i$, in Curved DTF Eq. (18b)
0	4.00	0.0	-0.00665	0.00665	0.000	0.000	0.000	0.000
1	3.85	15.0	-0.00678	0.00678	0.001	0.193	0.193	0.191
2	3.70	30.0	-0.00691	0.00691	0.013	0.781	0.781	0.778
3	3.55	45.0	-0.00703	0.00704	0.047	1.789	1.790	1.785
4	3.40	60.0	-0.00715	0.00716	0.117	3.241	3.244	3.238
5	3.25	75.0	-0.00727	0.00728	0.241	5.164	5.172	5.166
6	3.10	90.0	-0.00737	0.00740	0.437	7.585	7.604	7.596
7	2.95	105.0	-0.00747	0.00750	0.729	10.532	10.570	10.563
8	2.80	120.0	-0.00756	0.00759	1.144	14.037	14.107	14.101
9	2.65	135.0	-0.00762	0.00766	1.713	18.130	18.251	18.248
10	2.50	150.0	-0.00766	0.00771	2.472	22.843	23.043	23.044
11	2.35	165.0	-0.00766	0.00772	3.464	28.206	28.523	28.531
12	2.20	180.0	-0.00761	0.00769	4.734	34.249	34.736	34.754
13	2.05	195.0	-0.00750	0.00759	6.338	40.999	41.728	41.759
14	1.90	210.0	-0.00731	0.00742	8.333	48.476	49.539	49.591
15	1.75	225.0	-0.00699	0.00712	10.783	56.693	58.212	58.294
16	1.60	240.0	-0.00650	0.00665	13.750	65.651	67.779	67.900
17	1.45	255.0	-0.00576	0.00594	17.288	75.329	78.255	78.425
18	1.30	270.0	-0.00462	0.00484	21.426	85.675	89.617	89.846
19	1.15	285.0	-0.00283	0.00309	26.133	96.589	101.780	102.065
20	1.00	300.0	0.00015	0.00015	31.246	107.872	114.508*	114.820*

*Extremely close

Table I12. Curved deflections, $\hat{y}_i$, of the tapered cantilever tubular beam calculated from Nastran nonlinear analysis [eq. (20)] and from Curved Displacement Transfer Functions [eq. (18b)] using the known depth factors, $c_i (= h_i/2)$, and the true bending strains, $(\varepsilon_i - \overline{\varepsilon}_i)/2$; P=400 lb at the beam tip.

i	c_i, in	x_i, in	$\overline{\varepsilon}_i$, in/in Nastran nonlinear upper surface strain	ε_i, in/in Nastran nonlinear lower surface strain	u_i, in Nastran x-disp.	y_i, in Nastran y-disp.	$\hat{y}_i$, in Nastran curved deflection Eq. (20)	$\hat{y}_i$, in Curved DTF Eq. (18b)
0	4.00	0.0	-0.00843	0.00843	0.000	0.000	0.000	0.000
1	3.85	15.0	-0.00857	0.00857	0.002	0.244	0.244	0.241
2	3.70	30.0	-0.00870	0.00870	0.020	0.988	0.988	0.984
3	3.55	45.0	-0.00882	0.00883	0.074	2.260	2.262	2.255
4	3.40	60.0	-0.00893	0.00895	0.186	4.088	4.094	4.086
5	3.25	75.0	-0.00903	0.00906	0.381	6.502	6.519	6.509
6	3.10	90.0	-0.00911	0.00915	0.690	9.531	9.568	9.558
7	2.95	105.0	-0.00918	0.00923	1.147	13.205	13.280	13.270
8	2.80	120.0	-0.00922	0.00928	1.791	17.555	17.692	17.684
9	2.65	135.0	-0.00923	0.00930	2.668	22.610	22.845	22.841
10	2.50	150.0	-0.00919	0.00928	3.829	28.398	28.783	28.785
11	2.35	165.0	-0.00911	0.00922	5.331	34.943	35.549	35.559
12	2.20	180.0	-0.00897	0.00909	7.238	42.264	43.186	43.211
13	2.05	195.0	-0.00874	0.00888	9.619	50.376	51.740	51.785
14	1.90	210.0	-0.00841	0.00858	12.548	59.282	61.251	61.325
15	1.75	225.0	-0.00793	0.00814	16.098	68.974	71.753	71.868
16	1.60	240.0	-0.00728	0.00751	20.339	79.429	83.273	83.441
17	1.45	255.0	-0.00635	0.00663	25.326	90.600	95.812	96.048
18	1.30	270.0	-0.00502	0.00534	31.077	102.412	109.336	109.649
19	1.15	285.0	-0.00302	0.00340	37.538	114.747	123.743	124.125
20	1.00	300.0	0.00022	0.00022	44.496	127.413	138.776*	139.187*

*Extremely close

Table I13. Curved deflections, $\hat{y}_i$, of the tapered cantilever tubular beam calculated from Nastran nonlinear analysis [eq. (20)] and from Curved Displacement Transfer Functions [eq. (18b)] using the known depth factors, $c_i (= h_i/2)$, and the true bending strains, $(\varepsilon_i - \overline{\varepsilon}_i)/2$; P=500 lb at the beam tip.

i	c_i, in	x_i, in	$\overline{\varepsilon}_i$, in/in Nastran nonlinear upper surface strain	ε_i, in/in Nastran nonlinear lower surface strain	u_i, in Nastran x-disp.	y_i, in Nastran y-disp.	$\hat{y}_i$, in Nastran curved deflection Eq. (20)	$\hat{y}_i$, in Curved DTF Eq. (18b)
0	4.00	0.0	-0.01005	0.01005	0.000	0.000	0.000	0.000
1	3.85	15.0	-0.01018	0.01019	0.003	0.291	0.291	0.288
2	3.70	30.0	-0.01030	0.01031	0.029	1.176	1.177	1.170
3	3.55	45.0	-0.01040	0.01042	0.105	2.685	2.688	2.680
4	3.40	60.0	-0.01049	0.01052	0.262	4.849	4.860	4.849
5	3.25	75.0	-0.01055	0.01059	0.534	7.698	7.726	7.714
6	3.10	90.0	-0.01059	0.01065	0.963	11.261	11.323	11.310
7	2.95	105.0	-0.01060	0.01067	1.594	15.568	15.690	15.678
8	2.80	120.0	-0.01058	0.01066	2.479	20.644	20.867	20.856
9	2.65	135.0	-0.01051	0.01061	3.674	26.514	26.894	26.887
10	2.50	150.0	-0.01038	0.01051	5.245	33.198	33.816	33.815
11	2.35	165.0	-0.01019	0.01034	7.259	40.708	41.672	41.682
12	2.20	180.0	-0.00993	0.01010	9.792	49.052	50.505	50.532
13	2.05	195.0	-0.00957	0.00977	12.922	58.225	60.353	60.404
14	1.90	210.0	-0.00909	0.00933	16.729	68.213	71.251	71.336
15	1.75	225.0	-0.00847	0.00875	21.288	78.986	83.225	83.356
16	1.60	240.0	-0.00765	0.00798	26.667	90.496	96.286	96.480
17	1.45	255.0	-0.00658	0.00696	32.909	102.677	110.428	110.695
18	1.30	270.0	-0.00512	0.00556	40.018	115.437	125.603	125.950
19	1.15	285.0	-0.00302	0.00353	47.913	128.652	141.694	142.107
20	1.00	300.0	0.00030	0.00030	56.353	142.146	158.439*	158.866*

*Extremely close

Table I14. Curved deflections, $\hat{y}_i$, of the tapered cantilever tubular beam calculated from Nastran nonlinear analysis [eq. (20)] and from Curved Displacement Transfer Functions [eq. (18b)] using the known depth factors, $c_i (= h_i/2)$, and the true bending strains, $(\varepsilon_i - \overline{\varepsilon}_i)/2$; P=600 lb at beam tip.

i	c_i, in	x_i, in	$\overline{\varepsilon}_i$, in/in Nastran nonlinear upper surface strain	ε_i, in/in Nastran nonlinear lower surface strain	u_i, in Nastran x-disp.	y_i, in Nastran y-disp.	$\hat{y}_i$, in Nastran curved deflection Eq. (20)	$\hat{y}_i$, in Curved DTF Eq. (18b)
0	4.00	0.0	-0.01154	0.01155	0.000	0.000	0.000	0.000
1	3.85	15.0	-0.01166	0.01167	0.004	0.334	0.334	0.330
2	3.70	30.0	-0.01175	0.01177	0.038	1.348	1.349	1.342
3	3.55	45.0	-0.01182	0.01185	0.137	3.074	3.079	3.069
4	3.40	60.0	-0.01187	0.01191	0.342	5.543	5.559	5.545
5	3.25	75.0	-0.01189	0.01195	0.695	8.783	8.824	8.809
6	3.10	90.0	-0.01187	0.01194	1.249	12.824	12.915	12.898
7	2.95	105.0	-0.01181	0.01190	2.059	17.689	17.868	17.851
8	2.80	120.0	-0.01170	0.01182	3.188	23.399	23.724	23.708
9	2.65	135.0	-0.01154	0.01168	4.703	29.971	30.522	30.509
10	2.50	150.0	-0.01131	0.01148	6.678	37.412	38.301	38.296
11	2.35	165.0	-0.01100	0.01120	9.191	45.725	47.100	47.107
12	2.20	180.0	-0.01061	0.01084	12.322	54.901	56.955	56.980
13	2.05	195.0	-0.01011	0.01038	16.154	64.917	67.897	67.949
14	1.90	210.0	-0.00949	0.00980	20.765	75.740	79.950	80.040
15	1.75	225.0	-0.00873	0.00909	26.227	87.320	93.131	93.271
16	1.60	240.0	-0.00778	0.00819	32.597	99.593	107.442	107.643
17	1.45	255.0	-0.00658	0.00706	39.905	112.474	122.860	123.132
18	1.30	270.0	-0.00504	0.00559	48.133	125.863	139.326	139.668
19	1.15	285.0	-0.00291	0.00355	57.183	139.637	156.715	157.104
20	1.00	300.0	0.00037	0.00037	66.792	153.640	174.763*	175.138*

* Extremely close; beam-tip deflection = 58% of 300-in span.

REFERENCES

1. Ko, William L., W. L. Richards, and Van T. Tran, *Displacement Theories for In-Flight Deformed Shape Predictions of Aerospace Structures*, NASA/TP-2007-214612, October 2007.

2. Ko, William L., *Collection of Memoranda on Applications of Ko Displacement Theory to Deformed Shape Predictions of Aerospace Structures*, NASA/BR-119, April 2008.

3. Ko, William L., and W. Lance Richards, *Method for Real-Time Structure Shape-Sensing*, U.S. Patent No. 7,520,176, issued April 21, 2009.

4. Ko, William L., and Van Tran Fleischer, *Further Development of Ko Displacement Theory for Deformed Shape Predictions of Non-Uniform Aerospace Structures*, NASA/TP-2009-214643, September 2009.

5. Ko, William L., and Van Tran Fleischer, *Methods for In-Flight Wing Shape Predictions of Highly Flexible Aerospace Structures: Formulation of Ko Displacement Theory*, NASA/TP-2010-214656, August 2010.

6. Ko, William L., and Van Tran Fleischer, *First and Second Order Displacement Transfer Functions for Structure Shape Calculations Using Analytically Predicted Surface Strains*, NASA/TP-2012-215976, March 2012.

7. Ko, William L., and Van Tran Fleischer, *Improved Displacement Transfer Functions for Structure Deformed Shape Predictions Using Discreetly Distributed Surface Strains*, NASA/TP-2012-216060, November 2012.

8. Ko, William L. and Van Tran Fleischer, *Extension of Ko Straight-Beam Displacement Theory to Deformed Shape Predictions of Slender Curved Structures*, NASA/TP-2011-214567, April 2011.

9. Ko, William L., and Van Tran Fleischer, *Large-Deformation Displacement Transfer Functions for Shape Predictions of Highly Flexible Slender Aerospace Structures*, NASA/TP-2013-216550, November 2013.

10. Ko, William L., W. L. Richards, and Van Tran Fleischer, *Applications of Ko Displacement Theory to the Deformed Shape Predictions of Doubly Tapered Ikhana Wing*, NASA/TP-2009-214652, November 2009.

11. Jutte, Christine, William L. Ko, Craig Stephens, John Bakalyar, Lance Richards, and Allen Parker, *Deformed Shape Calculations of a Full-Scale Wing Using Fiber Optic Strain Data from a Ground Loads Test*, NASA/TP-2011-215975, November 2011.

12. Richards, W. Lance, and William L. Ko, *Process for Using Surface Strain Measurements to Obtain Operational Loads for Complex Structures*, U.S. Patent No. 7,715,994, issued, May 11, 2010.

13. Ko, William L. and Van Tran Fleischer, *Method for Estimating Operational Loads on Aerospace Structures Using Span-wisely Distributed Surface Strains*, NASA TP/2013-216518, April 2013.

14. Kopmaz, Osman, and Omer Gundogdu, "On the Curvature of an Euler-Bernoulli Beam," International Journal of Mechanical Engineering Education, Vol. 31, No. 2, p. 132-142, 2004.

15. Hodges, Dewey H., “Proper Definition of Curvature in Nonlinear Beam Kinematics,” *AIAA Journal*, Vol. 22, No. 12, pp. 1825-1827, December 1984.

16. Monasa, Frank, and Gilbert Lewis, “Large Deformations of Point Loaded Cantilevers with Nonlinear Behavior,” *Journal of Applied Mathematics and Physics* (ZAMP), Vol. 34, No. 1, pp. 124-130, January 1983.

17. Ohtsuki, Atsumi, “Analysis of the Characteristics of Fishing Rods Based on the Large-Deformation Theory,” *Materials and Science in Sports*, TMS, pp. 162-170, 2001.

18. *MSC. NASTRAN 2005 Quick Reference Guide*: The MacNeal Schwendler Corporation, Newport Beach, California, 2005.

19. Hodgeman, Charles D., *Standard Mathematical Tables*, 7th edition, Chemical Rubber Publishing Co. Cleveland, Ohio, 1957.